

Characterisation of Spectral and Angular Effects on Photovoltaic Modules for Energy Rating



Loughborough
University

by

Husyira Al Husna Binti Mohd Nasim

Doctoral Thesis

Submitted in partial of fulfilment of the requirements for the award of
Doctor of Philosophy of Loughborough University

June 2018

© Husyira Al Husna Binti Mohd Nasim 2018



**Certificate of Originality
Thesis Access Conditions and Deposit Agreement**

Students should consult the guidance notes on the electronic thesis deposit and the access conditions in the University's Code of Practice on Research Degree Programmes

Author: Husyira Al Husna Binti Mohd Nasim

Title: Characterisation of Spectral and Angular Effect of Photovoltaic Modules for Energy Rating Method

I, Husyira Al Husna Binti Mohd Nasim – D2-1 Villa Duta Condos, Bukit Antarabangsa, 68000 Ampang Malaysia, "the Depositor", would like to deposit "Characterisation of Spectral and Angular Effect of Photovoltaic Modules for Energy Rating Method", hereafter referred to as the "Work", once it has successfully been examined in Loughborough University Institutional Repository

Status of access OPEN / ~~RESTRICTED~~ / ~~CONFIDENTIAL~~

Moratorium Period.....N/A.....years, ending...../.....20.....

Status of access approved by (CAPITALS).....*T.R. BETTS*.....

Supervisor (Signature).....*TRBett*.....

School of: Wolfson School of Mechanical, Electrical and Manufacturing Engineering

Author's Declaration *I confirm the following:*

CERTIFICATE OF ORIGINALITY

This is to certify that I am responsible for the work submitted in this thesis, that the original work is my own except as specified in acknowledgements or in footnotes, and that neither the thesis nor the original work therein has been submitted to this or any other institution for a degree

NON-EXCLUSIVE RIGHTS

The licence rights granted to Loughborough University Institutional Repository through this agreement are entirely non-exclusive and royalty free. I am free to publish the Work in its present version or future versions elsewhere. I agree that Loughborough University Institutional Repository administrators or any third party with whom Loughborough University Institutional Repository has an agreement to do so may, without changing content, convert the Work to any medium or format for the purpose of future preservation and accessibility.

DEPOSIT IN LOUGHBOROUGH UNIVERSITY INSTITUTIONAL REPOSITORY

I understand that open access work deposited in Loughborough University Institutional Repository will be accessible to a wide variety of people and institutions - including automated agents - via the World Wide Web. An electronic copy of my thesis may also be included in the British Library Electronic Theses On-line System (EThOS). I understand that once the Work is deposited, a citation to the Work will always remain visible. Removal of the Work can be made after discussion with Loughborough University Institutional Repository, who shall make best efforts to ensure removal of the Work from any third party with whom Loughborough University Institutional Repository has an agreement. Restricted or Confidential access material will not be available on the World Wide Web until the moratorium period has expired.


- That I am the author of the Work and have the authority to make this agreement and to hereby give Loughborough University Institutional Repository administrators the right to make available the Work in the way described above.

- That I have exercised reasonable care to ensure that the Work is original, and does not to the best of my knowledge break any UK law or infringe any third party's copyright or other Intellectual Property Right. I have read the University's guidance on third party copyright material in theses.
- The administrators of Loughborough University Institutional Repository do not hold any obligation to take legal action on behalf of the Depositor, or other rights holders, in the event of breach of Intellectual Property Rights, or any other right, in the material deposited.

The statement below shall apply to ALL copies:

This copy has been supplied on the understanding that it is copyright material and that no quotation from the thesis may be published without proper acknowledgement.

Restricted/confidential work: All access and any copying shall be strictly subject to written permission from the University Dean of School and any external sponsor, if any.

Author's signature..........Date.....4/6/2018.....

user's declaration: for signature during any Moratorium period (Not Open work):			
<i>I undertake to uphold the above conditions:</i>			
Date	Name (CAPITALS)	Signature	Address

Abstract

This thesis presents work aimed at the development of practical and simplified methods for advanced characterisation of PV modules while reducing energy yield estimation uncertainties, focusing on the spectral and angular effects.

In this work, practical characterisation method to measure the spectral response (SR) curve of PV modules have been developed based on the polychromatic method. Improvement of the method have been achieved through the development of new measurement setup and detail evaluation of the polychromatic fitting algorithm. Set of coloured plate with unique transmission profiles supplemented with a smaller number of optical bandwidth filters used in the measurement setup resulted in high throughput irradiance (the lowest is measured at 150 W/m^2). High uniformity of the throughput irradiance over the measurement plane contribute to low uncertainty in the measurement of short-circuit current where the highest estimated uncertainty lays within the uncertainty margin for the STC measurement, at 2.5%. Measurement of optical/electrical of device under test with associated uncertainty are combined with the fitting algorithm through the Monte-carlo simulation method. The uncertainty in the final determination of SR characteristic gave the value of 7%, with about $\pm 10\%$ agreement between the SR curves obtained through the polychromatic method to the conventional monochromatic method.

The measurement of angular response developed in this method employed the indoor measurement setup with the additional turn table attachment. The evaluation of divergent light of the non-ideal light source and the accuracy in angle adjustment of the turn table have been quantified and incorporated into the angular response measurement as uncertainties. Partial illumination method are applied for a reliable extraction of operating current in the measurement of PV modules with the uncertainty estimated at 1%. 4% variation in the measurement of angular dependency of various PV devices at high tilt angle have been realised which translate to about 1.5% difference in the simulated annual energy performance. The application of the same simulator in the development of spectral and angular response measurement in this work creates the potential for the angle-dependent spectral response characterisation on module scale. This have been realised through a simulation.

Low uncertainty in energy yield is important as this indicate the risk in the investment of PV project. Detail evaluation with accuracy and uncertainty analysis of the works to be described will further improve the uncertainty in the measurement of spectral and angular response of PV modules, hence better accuracy in the assessment of energy yield can be achieved.

Acknowledgements

Many of the spectral and angular response measurements presented in Chapter 4 & 5 have been performed as part of the measurement intercomparison campaign in the EURAMET project “PhotoClass”. I would like to acknowledge the measurement results provided by other participants in this campaign, JRC-ESTI, Fraunhofer and PTB, which have been used in the validation of the measurement methods developed in this work.

I would like to recognise the contribution of Martin Bliss in the development of the automated measurement setup of both spectral and angular response in the Pasan facility which have greatly improved the time efficiency of the measurement process. Also for the many useful discussions that have taken place on the uncertainty analysis of the measurement setup.

Special thanks to Alex Smith for his assistance in the measurement of irradiance uniformity of the Pasan illumination and also for his advice on techniques to perform I-V measurements using the Pasan system. Thanks also to Blago Mihaylov for his contribution in the calibration of spectroradiometer.

Deep gratitude to Tom Betts and Ralph Gottschalg for their supervision at every stage throughout the development of this work. In particular, special thanks to Tom Betts with whom I had many fruitful discussions which have led to the completion of this thesis, for his words of support and encouragement during the writing-up of this thesis, and also for introducing me to the world of programming with Delphi.

A large thank you goes to the members of the Applied PV group in particular and other members of CREST for making my journey as PhD student exciting and fulfilling. I would like to extend my gratitude to friends outside this circle for their kind support and fun times spent together and also to my main sponsor, MARA for funding my PhD study.

Finally, thank you to my husband, Yuta for his endless support morally, emotionally and financially even from afar throughout every stage of this journey. Also special thanks to Umi, Buya, and all family members in my home country for their understanding and kind words which help me to stay calm even at rough times.

Table of contents

1	INTRODUCTION	1
1.1	RESEARCH BACKGROUND.....	1
1.2	THESIS STRUCTURE	3
2	PHOTOVOLTAIC DEVICE PERFORMANCE RATING.....	5
2.1	CHARACTERISTIC OF PHOTOVOLTAIC DEVICES	5
2.2	PHOTOVOLTAIC DEVICE PERFORMANCE IN REAL ENVIRONMENTS.....	10
2.3	PERFORMANCE RATING OF PHOTOVOLTAIC DEVICE	15
2.4	UNCERTAINTY CONSIDERATION IN ENERGY RATING ASSESSMENT.....	26
2.5	CONCLUSIONS	29
3	EVALUATION OF METHOD FOR SPECTRAL RESPONSE MEASUREMENT OF LARGE AREA PHOTOVOLTAIC MODULES	30
3.1	INTRODUCTION.....	31
3.2	POLYCHROMATIC METHOD FOR THE MEASUREMENT OF LARGE AREA DEVICE	36
3.3	EVALUATION OF THE POLYCHROMATIC METHOD MEASUREMENT SETUP	40
3.4	ELECTRICAL AND OPTICAL MEASUREMENT OF POLYCHROMATIC METHOD.....	46
3.5	CONCLUSIONS	51
4	SPECTRAL RESPONSE MEASUREMENT OF FULL SIZE PHOTOVOLTAIC MODULES.....	53
4.1	INTRODUCTION.....	54
4.2	SPECTRAL RESPONSE MODEL	55
4.3	VALIDATION OF POLYCHROMATIC SPECTRAL RESPONSE MEASUREMENT	62
4.4	DETERMINATION OF SPECTRAL RESPONSE CURVE.....	69
4.5	OPTIMISATION OF THE POLYCHROMATIC SPECTRAL RESPONSE METHOD.....	71
4.6	CONCLUSIONS	74
5	OPTICAL ANGULAR RESPONSE MEASUREMENTS OF FULL SIZE PHOTOVOLTAIC MODULES	76
5.1	INTRODUCTION.....	78
5.2	EVALUATION OF ANGULAR RESPONSE MEASUREMENT SETUP.....	87

5.3	ANGULAR RESPONSE MEASUREMENT OF CELL AREA PV DEVICES	95
5.4	PARTIAL ILLUMINATION METHOD IN I-V CURVE MEASUREMENT OF PHOTOVOLTAIC MODULES	98
5.5	ANGLE-DEPENDENT SPECTRAL RESPONSE MEASUREMENTS OF PHOTOVOLTAIC DEVICES	102
5.6	CONCLUSIONS	105
6	THESIS CONCLUSIONS	107
6.1	SPECTRAL RESPONSE CHARACTERISATION	107
6.2	ANGULAR RESPONSE CHARACTERISATION	109
6.3	POTENTIAL FUTURE RESEARCH	111
	PUBLICATIONS AND ACHIEVEMENT	I
	REFERENCES	II

List of figures

Figure 1. 1. Graph of global instalment capacity of PV technology [1].	1
Figure 1. 2. Simplified flowchart that describes the assessment of PV energy rating method as addressed in IEC 61853.	2
Figure 2. 1. Efficiency chart of PV technologies plotted by the National Renewable Energy Laboratory (NREL) [10, 11].	5
Figure 2. 2. Equivalent circuit of diode model representing electrical behaviour of an ideal PV device.	8
Figure 2. 3. Schematic diagram showing the current-voltage generation of PV device.	8
Figure 2. 4. Equivalent circuit of PV device showing the inclusion of series and shunt resistance.	9
Figure 2. 5. World map of global horizontal irradiation from the 2017 The World Bank, Solar resource data, Solargis [19].	10
Figure 2. 6. Spectral irradiance of sun radiation at varying AM values [20] (left) and illustration of AM (right).	11
Figure 2. 7. I-V curve shift due to irradiance and temperature effect.	12
Figure 2. 8. Typical spectral response characteristics of various PV technologies [22].	13
Figure 2. 9. Seasonal sun path geometry with respect to a point on earth at a high latitude.	14
Figure 2. 10. I-V curve performance of shaded and un-shaded solar cells in series (left) and parallel (right) connection.	15
Figure 2. 11. Schematic image of the standard power rating method of a PV module.	16
Figure 2. 12. Factors that influence the determination of energy yield.	18
Figure 2. 13. Performance surface method developed in ESTI [27].	20
Figure 2. 14. Consideration of environmental influences on outdoor performance of a PV module.	20
Figure 2. 15. Power measurement points in the G-T matrix.	21
Figure 2. 16. Angular response measurement of PV module.	22
Figure 2. 17. Typical spectral response (SR) curve of c-Si PV device over varying wavelength value.	23
Figure 2. 18. Simplified flow chart showing the assessment of PV energy rating method.	27
Figure 3. 1. Block diagram illustrating the measurement setup in DSR method.	33
Figure 3. 2. Figures showing the SR measurement setup using pulse light solar simulator with interference filter (left) and photograph of a unit of filter as used in SUPSI (right) [56].	34
Figure 3. 3. Schematic image of partial illumination SR measurement method of a full size PV module (left) and photograph of SR measurement apparatus at TUV Rheinland, Cologne [58] (right).	35
Figure 3. 4. Schematic image of SR polychromatic measurement for small areas [48].	36
Figure 3. 5. Bell-shaped graph of Gaussian function.	37
Figure 3. 6. Simplified flow chart showing the elements in polychromatic measurement method.	37

Figure 3. 7. Simplified flow chart illustrating the steps in constructing the model for fitting the polychromatic measurement data.	39
Figure 3. 8. Schematic of the Pasan 3B simulator in CREST showing Xenon lamps and measurement plane of the facility.	40
Figure 3. 9. Transmission profile of polychromatic broadband filters and a small number of colour band filters used in the polychromatic measurement setup.	42
Figure 3. 10. Photographs of polychromatic filters used in the Pasan simulator (top left), Xenon light bulbs with filters (right) and without (bottom left).	43
Figure 3. 11. Schematic image of non-uniformity measurement setup with an array of diode lays horizontally across the measurement plane and reference photodiode fix at one place (left). Result of non-uniformity measurement of unfiltered Pasan irradiance (right).	44
Figure 3. 12. Measurement of throughput irradiance non-uniformity of polychromatic filters over 2x2m measurement plane.	45
Figure 3. 13. Schematic of the polychromatic measurement setup using the Pasan 3B facility (plan view).	46
Figure 3. 14. Schematic of measurement plane showing the difference in the occupied area by a full size module and reference cell.	48
Figure 3. 15. Spectral measurement of throughput irradiance of all filters in the measurement setup.	49
Figure 3. 16. Spectrally resolved measurement of unfiltered Pasan with corresponding total uncertainty per pixel array.	50
Figure 3. 17. Blue dotted graph shows the relative difference in spectral measurement of filter F3 and red dotted graph shows the measurement of F10 against the spectral the unfiltered Pasan.	50
Figure 4. 1. Flow-chart of SR polychromatic measurement method.	53
Figure 4. 2. Uncertainty envelope of the spectral measurement of the Pasan simulator irradiance.	54
Figure 4. 3. Examples of random walks generated from 3 (left) and 250 (right) iterations.	55
Figure 4. 4. The evolution of regression analysis using different Gaussian models to fit the measured SR points of a c-Si device (top). The graph shows the improvement of difference between the Gaussian models to the measurement of SR of the device at individual points as the number of Gaussians in the sum increases (bottom).	56
Figure 4. 5. Result comparison between 50 modelled SR curves generated through the MC simulation and the measured SR of a c-Si device.	57
Figure 4. 6. Example of step functions showing a segment of horizontal line (left) and multiple segments (right). Replication of curvy graph by the increased steps in the step function (bottom).	58
Figure 4. 7. Comparison of regression analysis results using step (left) and Gaussian summation (right) functions as the SR model fit to measured SR data points.	59

Figure 4. 8. Light transmittance profile of the combined artificial edge filters	60
Figure 4. 9. Calculated spectral irradiance distribution used in the simulation based on the transmission profile as shown in Figure 4. 8	61
Figure 4. 10. Relative difference between the output $SR_{\lambda, mod}$ of different numbers of segments and the calibration SR	62
Figure 4. 11. Photograph of the reference cell used in the polychromatic measurement method	62
Figure 4. 12. Comparison of SR measurement obtained by the polychromatic method and the DSR method for unfiltered c-Si Device A (left) and filtered c-Si Device B (right)	63
Figure 4. 13. Throughput spectral measurement (top) and the ideal case of spectral measurement data (bottom)	64
Figure 4. 14. Top Image shows the set of transmission profiles used in the current measurement setup. Bottom graph shows the improvement of spectral variability in the NIR region by the addition of 2 artificial filters in the mix (red dotted lines)	65
Figure 4. 15. Relative difference between the output $SR_{\lambda, mod}$ using different sets of filters for device A (top) and device B (bottom)	66
Figure 4. 16. Photograph of large area devices used in the validation of the polychromatic method; (a) non-encapsulated IBC c-Si cell, (b) encapsulated mono c-Si cell, (c) 6 series module of IBC cells	67
Figure 4. 17. SR measurement comparison between various labs with different measurement facilities of a bare PV cell (top), encapsulated PV cell (bottom left) and 6 series cells mini-module (bottom right)	68
Figure 4. 18. Wavelength-by-wavelength comparison between SR measurement by PTB and Hermite interpolation curve of polychromatic measurement points of a single encapsulated cell, and 6-cell mini-module	69
Figure 4. 19. Photographs of the commercial PV modules used here in the polychromatic SR determination.	70
Figure 4. 20. SR curve result obtained by the polychromatic measurement method of mono-si (left) and back contact (right) modules	71
Figure 4. 21. Comparison of uncertainty in polychromatic SR of various large area devices	72
Figure 4. 22. Comparison of simulation polychromatic SR results with the calibration SR using 18 segments (left) and 36 segments (right) in the step function and an optimised set of irradiance filters (top)	73
Figure 5. 1. Schematic of optimal orientation angle of a PV module operating outdoors and seasonal sun path geometry with respect to a point on earth at a latitude of about 50° N	76
Figure 5. 2 Schematic of an ideal measurement setup for the angular response characterisation of PV modules	80
Figure 5. 3. Photograph of two-axis tracker for outdoor angular response characterisation of PV modules as used by Sandia National Laboratories [95]	83

Figure 5. 4. Photograph of pyranometer with diffuser attachment for the measurement of diffuse in-plane irradiance reported in [82].	84
Figure 5. 5. Schematic of setup configuration for angular response measurement of a tilted PV module with 3 bypass diodes (left) and the resulting measured I-V characteristic (right).	86
Figure 5. 6. Photograph of the angular response measurement setup and schematic image of Pasan 3B simulator at CREST.	88
Figure 5. 7. Image of the black tube used in the evaluation of angular distribution of Pasan illumination.	89
Figure 5. 8. Schematic showing the measurement setup used for evaluation of the angular distribution variability of the Pasan light source (a,b,c) and the $I_{sc\theta}$ measurement results from a small-area reference cell at various positions within the measurement plane (d).	89
Figure 5. 9. Schematic of the approximation of Xe lamps as an extended light source (top) and the geometrical relationship of angle distributions of divergent light incident on the DUT.	90
Figure 5. 10. Schematic showing the ideal condition when the DUT is aligned with the rotating pivot point (top) and the condition when there is displacement in the alignment (bottom).	91
Figure 5. 11. Photograph of Xe lamps from the DUT point of view (left) and rotation stage with DUT fixed on it from the Xe lamps point of view.	92
Figure 5. 12. Photograph of rotation stage before (left) and after (right) the beams are covered using black matte cloth to reduce background light effect.	93
Figure 5. 13. Photograph of the rotation stage attachment in tilted position around the pivot point axis with DUT attached.	94
Figure 5. 14. Photograph of samples used for the angular response measurements using the Pasan facility; (a) Non-encapsulated back contact cell, (b) Encapsulated CIGS module, (c) Encapsulated c-Si cell, (d) Encapsulated c-Si reference cell.	95
Figure 5. 15. Measurement results of the encapsulated PV devices and Fresnel mode.	96
Figure 5. 16. Variability of angular response characteristics of encapsulated PV devices of different technologies.	96
Figure 5. 17. Graph of Fresnel model of different refractive index.	97
Figure 5. 18. Comparison of angular response of encapsulated/non-encapsulated c-Si (left) and back contact (right) devices.	98
Figure 5. 19. Plan view of the orientation of a module in respect to the centre point of the Xe lamps in the Pasan facility at CREST.	99
Figure 5. 20. Schematic of the 6 series-connected cells module in the validation of the algorithm for photocurrent extraction using the mismatch theory (top left) and graphs of I-V measurements showing the flow of the algorithm (1)-(3).	100

<i>Figure 5. 21. Comparison of normalised short-circuit current measurements taken directly at the target cell's terminals to that extracted from an I-V measurement taken at the module's terminals.</i>	<i>101</i>
<i>Figure 5. 22. Photograph of a PV module mounted on the rotation stage for I-V curve measurements with (right) and without (left) opaque tape applied to target cell.....</i>	<i>101</i>
<i>Figure 5. 23. Transmittance of mono-Si and back contact modules against varying tilt angle in the measurement of angular response using the modified Pasan solar simulator.</i>	<i>102</i>
<i>Figure 5. 24. Image of the angular spectral response curve of various PV devices determined using the DSR method with rotation table as developed by PTB (left) [103] and FhG (right) [102].</i>	<i>103</i>
<i>Figure 5. 25. Spectral response at normal incidence and broadband angular response of two full size modules determined using the polychromatic method and partial illumination method respectively.</i>	<i>104</i>
<i>Figure 5. 26. Simulation result of angle-dependent spectral response curves of mono-Si and back contact modules (top) and the ratio of the shift in spectral response curve at varying angle to the normal position (bottom).</i>	<i>105</i>

List of tables

<i>Table 2. 1. Climatic data set defined in IEC 61853-4 draft [42].</i>	<i>25</i>
<i>Table 3. 1. List of materials and throughput irradiance level of the selected filters</i>	<i>42</i>
<i>Table 3. 2. Source of uncertainty in indoor solar simulator measurements.</i>	<i>47</i>
<i>Table 4. 1 Information of PV modules used in the polychromatic measurement method.</i>	<i>70</i>
<i>Table 5. 1. List of devices used in the angular response measurement.</i>	<i>95</i>

Glossary

AIST

Refer to the National Institute of Advanced Industrial Science and Technology of Japan.

Aoi

Abbreviation for angle-of-incidence which defines that an incident line or ray makes with a perpendicular to the surface at the point of incidence.

Avantes

A spectroradiometer manufacturer.

Black body

A theoretical body which absorbs all incident radiation with zero reflection and transmission.

Broad-bandwidth filters

A type of bandpass filters that selectively transmit a broad portion of spectrum.

CCD

Refer to the charge-coupled device which is a type of electronic sensor.

Cd-Te

Abbreviation for cadmium telluride, a type of thin-film technology formed from cadmium and tellurium used in PV device.

Cosine response

A terminology that describe the loss in incident irradiation following the cosine law of an optical instrument.

DSC

Abbreviation for dye-sensitized solar cell, a type of organic-based PV technology.

EURAMET

Abbreviation for the European Association of National Metrology Institutes, an organisation that support the development of measurement infrastructure through a series of schemes.

FhG-ISE

Abbreviation for the Fraunhofer Institute for Solar Energy Systems, based in Germany.

GaAs

Refer to a compound of elements gallium and arsenic.

Goniometric stage

Device used to rotate an object precisely within a small angular range.

IEC

Abbreviation for the International Electrotechnical Commissions, a standard and conformity assessment body for all electrical, electronic and related technology.

ARC

Abbreviation for anti-reflective coating which is a type of optical coating applied to the surface of optical elements such as glass and lenses to reduce reflection.

ASHRAE

Abbreviation for the American Society of Heating, Refrigerating, and Air-conditioning Engineers. An ASHRAE model is a terminology that refer to an analytical model commonly used for quickly model a reflection loss of optical element.

Bypass diode

A type of diode that is used in photovoltaic devices to prevent the occurrence of the damaging over-heating condition due to the shading effect.

CIGS

A type of thin-film technology formed from copper indium gallium selenide used in PV device.

Concentrator PV

A PV technology that incorporates the element of light concentration through the application of fresnel lens.

CREST

Abbreviation for the Centre for renewable energy systems and technology, referring to a department in Loughborough University

DUT

Abbreviation for device under test.

Edge filters

Type of optical filters that transmit the edge portion of spectrum on short or long wavelength region.

EKO MS-700

A spectroradiometer model that commonly used to measure spectral distribution of sunlight.

Flat-plate PV

Refer to PV array of module that consists of flat solar panels.

Goodness-of-fit

A statistical model describing the well fitness of a set of observations to its theoretical value.

G-T matrix

A matrix of electrical performance of PV devices under a wide range of irradiance and temperature, acquired through the performance measurement of the device.

Interference filters

A type of optical filters that reflect one or more spectral bands and transmit others while maintaining zero coefficients of absorption.

JRC-ESTI

Abbreviation for the European Solar Test Installation - European Commission, a PV test laboratory based in Italy.

Lock-in system

A type of system that can extract a signal with a known lock phase from an extremely noisy environment.

mc-Si

Abbreviation for multi crystalline-silicon technology.

Monte-carlo simulation

A probabilistic simulation to predict possible outcomes from varying inputs of a system.

Narrow-bandwidth filters

A type of bandpass filters that selectively transmit a narrow portion of spectrum.

NIR

Refer to near-infrared, indicating the spectrum of light corresponding to the long wavelength region.

Pasan

Refer to the commonly used short-pulsed solar simulator for power output measurement of commercial size PV modules.

Polynomial fitting

A type of statistical analysis that evaluate the relationship between variables in a model based on nth degree polynomial.

Pyranometer

An optical instrument for measuring solar irradiance.

Sandia

Refer to the Sandia National Laboratories of research and development based in the US.

SNR

Refer to the ratio of strength of an electrical or other signal carrying information to that of unwanted interference or noise.

STC

A standardised condition for the power output measurement of photovoltaic devices.

UV

Refer to ultraviolet, indicating the spectrum of light corresponding to the short wavelength region.

LCOE

Abbreviation for the levelised cost of electricity, which describes the net present value of the unit-cost of electricity over the lifetime of generating asset.

Monochromatic method

A method to measure the photoresponse of optical devices using a sequence of monochromatic illumination.

NREL

Abbreviation for the National Renewable Energy Laboratory, a federal laboratory formed to facilitate research, development, commercialisation and deployment of renewable energy and efficiency technologies, based in the US.

OSC

Refer to organic solar cell, a type of PV technology that uses organic electronics.

Polychromatic method

A method to measure the photoresponse of optical devices using a sequence of polychromatic broadband illumination.

PTB

A national metrology institute of Germany.

Pyrheliometer

An optical instrument for measuring the direct beam of solar irradiance.

Short-pass filters

Type of optical filters that transmit the edge portion of spectrum on short wavelength region.

Solar elevation

Refer to the altitude of the sun and the angle between horizon and the centre of sun.

TUV Rheinland

Refer to the company that provides technical service for testing, inspection, certification, consultation and training worldwide.

1/r² law

The inverse-squared law is a physical law that defines that specified physical quantity or intensity is inversely proportional to the square of the distance from the source of that physical quantity.

1 Introduction

1.1 Research background

1.1.1 The significance of energy yield

The photovoltaic (PV) effect is a phenomenon that describes the excitation (energy increase) of electrons in a material by exposure to light, while a PV device refers to a device that utilises sunlight to generate electrical current in a silent and clean process, without moving parts. PV technology has emerged as one of the significant renewable power generator technologies with a total capacity of 303GW having been installed worldwide by 2016 [1]. The expansion of installed capacity in recent years has been driven by the improved cost competitiveness and technical performance of the technology.

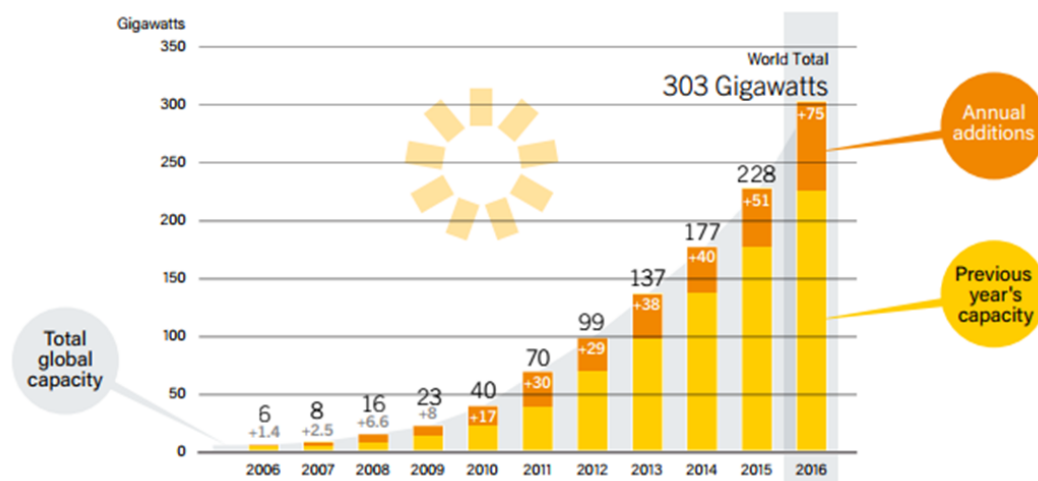


Figure 1. 1. Graph of global instalment capacity of PV technology [1].

In PV projects, a significant contribution to the instalment cost is the cost of PV modules, about 42% in the case of utility-scale PV projects [2]. The development of a PV project requires the assessment of technical aspects to determine the plant design and to estimate energy yield. Energy yield is a prediction of energy output of the PV system for the full lifetime of the project, taking into account the environmental conditions at the project site and the performance of the PV modules and other system components. Since revenue is driven by energy yield, low uncertainty in its prediction is a key factor to develop an optimally balanced system in terms of cost and performance for specific site.

The uncertainty in energy yield is determined by the uncertainties in the environmental data such as the in-plane irradiance, ambient temperature, wind speed, soiling rate, etc, in the module and inverter characterisation, and in changes to system performance due to ageing over several years of operation.

Time series evaluation is performed using simulation software to calculate the output of a PV module using the information of rated output of the module, before simulation of DC array effects and DC-AC conversion (in the case of grid-connected systems). At the module level, the convention is to rate the power output of PV module under standard test conditions (STC) in kW and model differences under real operating conditions through the use of temperature coefficients and sometimes characteristics measured at different irradiance levels. The lack of detailed information of PV module performance due to the single-point power rating increases uncertainty in the models of energy yield.

1.1.2 Development of an energy based rating method

An energy-based rating method is under development by the IEC to enable a more comprehensive performance comparator of PV modules. The method is established under IEC 61853, consisting of 4 parts where the different aspects in energy rating calculation are outlined. Parts 1 and 2 are currently public and detail the procedure for performance measurement of PV modules under irradiance and temperature conditions beyond STC and the characterisation of PV module under further environmental conditions (spectrum and angle of incidence), respectively. Part 3 will be the methodology of energy rating assessment while part 4 will describe the reference climatic data that are to be used in the calculation of energy rating. Parts 3 and 4 are still in closed draft form.

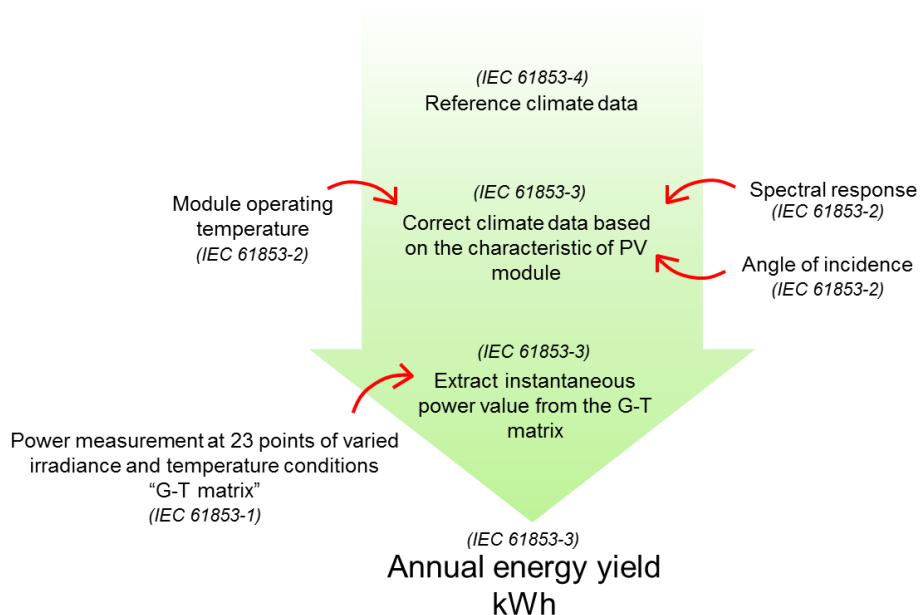


Figure 1. 2. Simplified flowchart that describes the assessment of PV energy rating method as addressed in IEC 61853.

The subject of practicality and validity of the energy rating method (IEC 61853) have been the subject of debate among PV researchers [3, 4, 5, 6, 7]. Unlike estimation of the true operational energy yield,

the accuracy in the energy rating method depends only on the uncertainty in measurement of PV modules, i.e. measurement of power under various irradiance and temperature, and measurement of characteristics of the modules under varying environmental factors while the tabulated standard meteorological data are treated as free from uncertainty. Research regarding the irradiance-temperature characteristics has been conducted intensively, yet little attention has been paid to the spectral and angular response characteristics. Although the characterisation method of spectral response (SR) and angular response have been standardised (IEC 61853-2), due to the limitation of measurement apparatus, the access to such measurements at full size module scale is restricted to only a handful of labs worldwide. Therefore, it is the aim of this thesis to provide comprehensive information of these characteristics by the development of practical characterisation methods to assist in the practical adoption of the energy rating standard.

1.2 Thesis structure

Chapter 2 of this thesis will discuss the fundamental knowledge of the performance of PV devices, influence of environmental conditions on PV performance and methods to rate PV performance. Background of energy rating methods and issues associated with the determination of a reliable energy rating will also be addressed in this chapter.

Development of practical characterisation methods for SR and angular response of PV modules is the central work of this thesis. The SR characterisation method developed here builds on the novel polychromatic method [8] considering the low technical requirements of the measurement setup which enables the measurement of large area PV device to take place in more common pulse type solar simulators. Chapter 3 explores the methods that are available for the measurement of SR characteristics of PV devices and discusses the advantages that the polychromatic method has. Evaluation of the measurement setup with uncertainty analysis is also described in this chapter.

Detailed analysis of SR determination of large area PV devices will be presented in Chapter 4. Uncertainty propagation using Monte-Carlo simulation in the polychromatic method will be explained in detail. Through the robust analytical process, uncertainty contributions in the method are identified and validation of the polychromatic method against the conventional SR measurement method is performed. Suggestions for the optimisation of the method conclude the chapter.

Angular response measurement methods for PV modules usually employ an outdoor measurement setup to benefit from the uniformity of the sun's light. However, uncertainty in detectors used to monitor

the direct/diffuse radiation ratio of sunlight heavily influence the accuracy in the angular response characteristic. Discussion of current methods for angular response measurement will be detailed in Chapter 5. An indoor measurement technique based on a non-destructive method [9] is applied employing the solar simulator facility in CREST. Analysis of the suitability and the accuracy of the measurement setup and the determination of angular response characteristic of PV modules is also presented. Chapter 5 concludes with discussion of the feasibility of the measurement of angle dependent spectral responsivity of PV modules using the combination of the practical SR and angular response methods presented in this thesis.

Finally, conclusions and recommendations for future work to further optimise the SR and angular response measurement methods of full size PV modules will draw this thesis to a close.

2 Photovoltaic device performance rating

A practical energy rating method for PV modules which is founded on the conventional power rating method has been developed by PV experts in the IEC and by consultation. The attempt is motivated by the urgency of assessing detailed information on how a module will perform under real environmental conditions to reduce the investment risk in PV projects. This method is detailed in the IEC 61853, consisting of 4 parts. The standardisation of this method is an ongoing process with half of the parts already published. Nevertheless, debate regarding the applicability of the IEC 61853 as a standard method still continue, largely due to the increased technical (and financial) burden of the characterisation methods. In this chapter, discussion focusing on the importance of PV energy rating and existing methods is presented. Fundamental background knowledge of PV including the varying performance behaviour of PV devices in real environments and PV characterisation methods are also reviewed.

2.1 Characteristic of photovoltaic devices

2.1.1 Overview of photovoltaic technologies

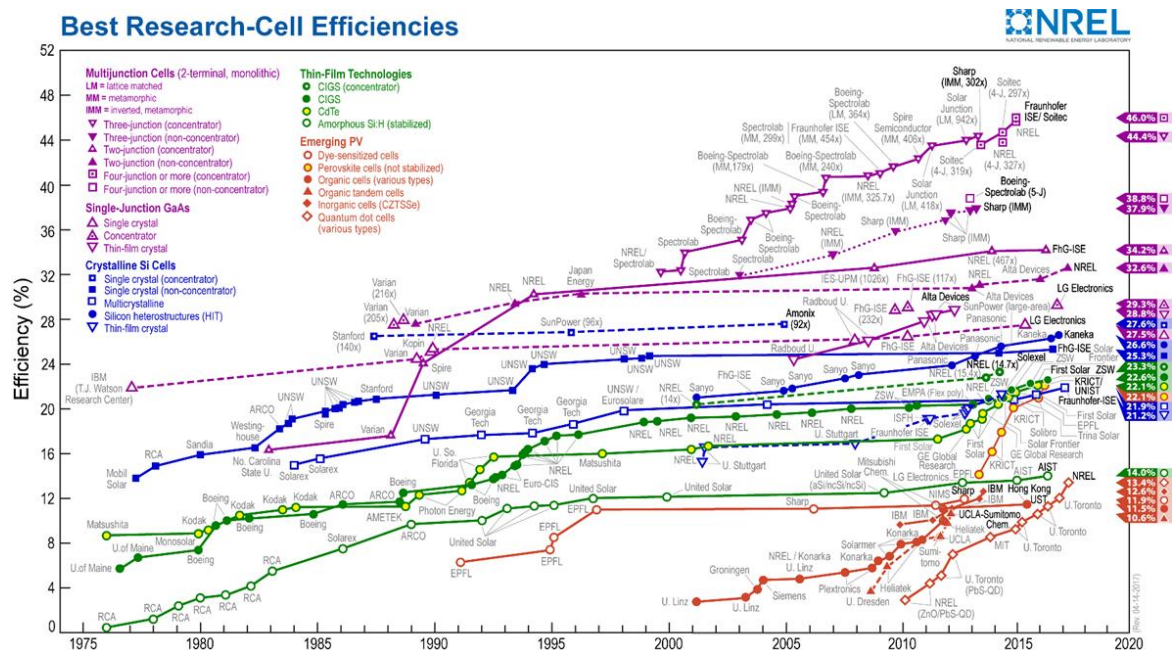


Figure 2. 1. Efficiency chart of PV technologies plotted by the National Renewable Energy Laboratory (NREL) [10, 11].

Figure 2. 1 shows the efficiency development curves of various PV technologies under research from 1975 up to now, provided by NREL. Over this period, there were many new types of PV cells and

continual improvement to efficiencies being developed, indicating the advancement in knowledge and experience among PV researchers. The development of PV technologies has passed many significant milestones since first discovered back in 1839 [12]. The technology manipulates the photoelectric effect within a semi-conductor, with charge carriers generated by incident light to create a practical solar cell. Crystalline-silicon (c-Si) has been used as the main material in the production of solar cells due to its abundance and also its superior efficiency to most other semi-conductors. As research on solar cell technology progresses, PV researchers have experimented with and sometimes commercialised materials that have potential in PV applications, such as the thin-film technologies [13].

The rated efficiency measurement of PV devices in cell-scale as can be seen in Figure 2. 1 is performed by calibration laboratories in accordance with the standard procedure under the standard test condition (STC). As can be seen from the graph, the highest rated power under the STC is recorded by the multi-junction technology with the efficiency higher than 45%. The highest efficiency under the category of c-Si technology is demonstrated at 26.6%. However, as the size of PV devices increases, the efficiency will go down by some percentages due to several factors such as the series resistance from the cells interconnections.

For commercial PV modules, cost, efficiency, lifetime durability and performance stability over time are the main considerations. To date, flat-plate silicon based PV technology is still the market share leader thanks to this. Efficiency of modules is dictated by the rated power (W_p) per square metre. An HIT modified mono c-Si module manufactured by Kaneka holds the record for the highest research module efficiency of $24.4 \pm 0.5\%$ [14, 15], with the best production modules a few percent below this.

High efficiency c-Si based cells require a difficult and energy-hungry manufacturing process, which increases the total production cost [16]. CdTe, CIGS and amorphous silicon modules are the main 3 thin-film technologies that have a relatively significant share in the PV market. The use of thin-film solar cells in PV panels has the advantage of reduced manufacturing costs, yet the efficiency is still behind c-Si modules by about 4% lower record efficiency [14]. For this reason and some others relating to installation costs, the market share taken of thin film based PV panels is still lower than that of c-Si modules (around 4.9%) [17].

The largest contribution to the capital cost of a PV project is mostly the cost of the PV modules [18]. Currently there are many new promising materials and advanced cell architectures being developed to further increase the efficiency of modules while reducing the manufacturing cost. These have led to the emergence of new PV technologies which offer improved rated efficiency. Application of high efficiency

PV panels contribute to the improved installation area efficiency as less panels will be sufficient to meet power demand by the consumer.

In real environments, the output generation of PV devices is influenced by many environmental factors, beyond that of specified under the standard test condition (STC). The estimation of energy yield of PV system takes into account both characteristic of the modules and weather condition of the location where the system is to be installed. Due to the wide range of variability of the environmental condition such as in-plane irradiance, ambient temperature, spectral irradiance and sun angular factor, the information of rated efficiency alone is insufficient to make an accurate estimation of energy delivery of PV system, hence pose a high risk in the return of investment. On account of this, a standard rating method that details the influence of environmental factors on the output performance of PV modules has been established.

2.1.2 Characteristic of photovoltaic devices

Current-voltage characteristic: I-V curve

The basic operational performance of a PV device is evaluated by measurement of the current and voltage generated within the device when light is incident on its surface. This is influenced by several factors such as material of the cell and operating environment, hence the current-voltage characteristic (I-V curve) is used to describe the behaviour of a PV device under different conditions.

Under no illumination, the behaviour of a PV device is similar to a diode, therefore a diode-based equivalent circuit can be used to describe it (Figure 2. 2). The dark current (I_d) generated in this condition can be written as in Eq. 2. 1.

$$I_d = I_0 \left\{ \exp\left(\frac{qV}{nkT}\right) - 1 \right\} \quad \text{Eq. 2. 1}$$

I_0 : diode saturation q : electron charge V : voltage
 n : identity factor (diode) k : Boltzmann constant T : temperature (kelvin)

When illuminated, energy from the photon excites electrons into the conduction band, allowing current to flow. Some of this current is lost through electron-hole recombination (I_d) and the remainder is used to power an external circuit. This is called the photocurrent, I_{ph} . Current-voltage relation flowing in the PV device at this time is described in Eq. 2. 2.

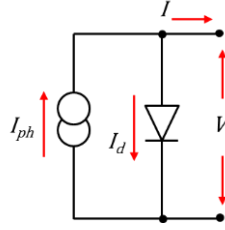


Figure 2. 2. Equivalent circuit of diode model representing electrical behaviour of an ideal PV device.

$$I = I_{ph} - I_0 \left\{ \exp \left(\frac{qV}{nkT} \right) - 1 \right\} \quad \text{Eq. 2. 2}$$

The electrical properties of a PV device can be interpreted from I-V curve measurement as it holds a detailed description of its solar energy conversion ability and efficiency. Photocurrent generation performance of PV devices is measured as short-circuit current, I_{sc} when voltage is at 0 V. It is primarily affected by the intensity of incident light for a linear device. As illustrated in Figure 2. 3, open-circuit voltage, V_{oc} is the voltage of the device when there is no current flowing. As described in Eq. 2. 3, the value of V_{oc} is influenced by temperature and shifts logarithmically with the I_{sc} . The maximum useful output of a PV device is measured at the maximum power point, P_{mp} . It is the point on the IV curve where the product of current and voltage reaches its maximum. At this point, the current and voltage are called I_{mp} and V_{mp} respectively.

$$V_{oc} = \frac{nkT}{q} \ln \left\{ \frac{I_{ph}}{I_d} + 1 \right\} \quad \text{Eq. 2. 3}$$

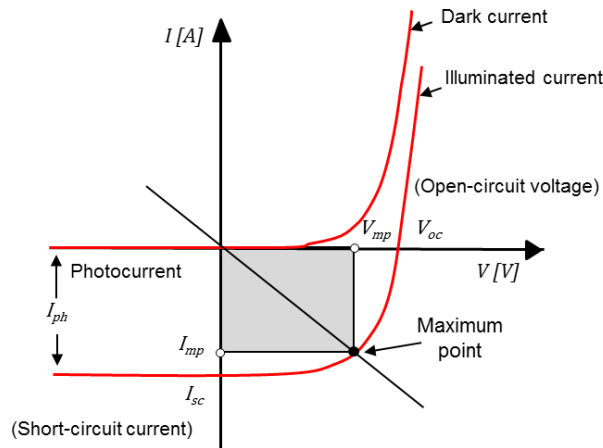


Figure 2. 3. Schematic diagram showing the current-voltage generation of PV device.

Other useful performance parameter of PV devices that can be determined from I-V curve measurements is the fill factor (FF) and efficiency (η) which describe the ratio of output power to input power (from incident light).

Under a controlled environment, the PV device I-V curve and efficiency are affected by the series and shunt resistance (R_s, R_{sh}) within the device itself (Eq. 2. 4). These are called the parasitic resistances (Figure 2. 4). R_s is the lumped contributions of path resistance from metal contacts, interconnections, cable connects, and the resistance of the semiconductor itself, while R_{sh} is caused by imperfections in the device, eg: from the manufacturing process that allows current to leak across the junction. High series resistance reduces the efficiency of the device, by reducing the voltage at maximum power point. R_{sh} has the opposite effect on the I-V curve where a good quality device has a very high R_{sh} value, maintaining high current at the maximum power point.

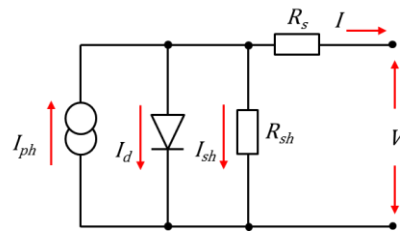


Figure 2. 4. Equivalent circuit of PV device showing the inclusion of series and shunt resistance.

$$I = I_{ph} - I_0 \left\{ \exp \left[\frac{q(V + IR_s)}{nkT} \right] - 1 \right\} - \frac{V + IR_s}{R_{sh}} \quad \text{Eq. 2. 4}$$

In real environments, the irradiance from sunlight is consistently changing mostly due to the change in spectral distribution and sun position, hence the shift in the power output of PV devices operating outdoor. Incident spectral irradiance, E_λ on PV device influence the generation of I_{ph} as expressed in Eq. 2. 5.

$$I_{ph} = A \cdot \int E_\lambda \times SR_\lambda \cdot d_\lambda \quad \text{Eq. 2. 5}$$

Where A is the area of PV device, and SR_λ is the spectral response characteristic of the device. The constant shift of sun position throughout the day also introduce the angular effect on the generation of I_{ph} . The next section will discuss the subject of solar radiation and the performance of PV devices in real environments under the influence of spectral and angular effect.

2.2 Photovoltaic device performance in real environments

Factors that influence the efficiency of PV devices operating outdoor are solar irradiance, temperature, spectral irradiance and angle of incidence. This section will give an overview of the environmental conditions and how the different components of solar radiation effect the performance parameters of PV devices.

2.2.1 Solar radiation

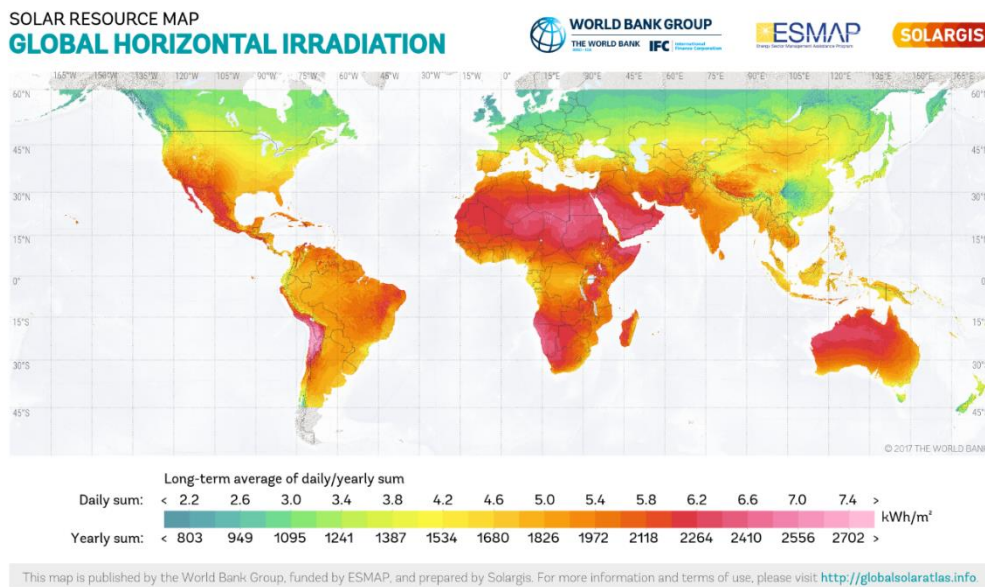


Figure 2. 5. World map of global horizontal irradiation from the 2017 The World Bank, Solar resource data, Solargis [19].

The intensity of solar radiation (Figure 2. 5) is governed by the sun position and the weather (mostly attenuation by cloud cover). The position of sun relative to a location is mostly influenced by the latitude, date and time. Solar radiation from the sun travels a distance of approximately 150 million km and reaches the earth in the form of electromagnetic waves. The spectral distribution of this radiation is similar to that of black body radiation at about 6000K. When the radiation enters the earth's atmosphere, it experiences attenuation due to the scattering, reflection, and absorption by molecules that varies by different wavelengths before it reaches ground level. These atmospheric attenuation processes vary with time and atmosphere composition, hence there is variation in the spectral distribution of sunlight and this affects device current generation (Eq. 2. 5).

Sunlight consists of two broad components, direct and diffuse. Direct irradiance is that coming straight from the sun, while diffuse is the scattered radiation with variation of angular distribution. The diffuse

component generally has lower intensity compared to the direct one, except under conditions of high cloudiness or very steep angle of incidence to the collector plane. The parameter that describes the relative thickness of the earth's atmosphere that sunlight travels through is called the air mass (AM) – Figure 2. 6. The relationship between AM value and sun elevation (h) can be expressed using Eq. 2. 6.

$$AM = \frac{1}{\sin h} \quad \text{Eq. 2. 6}$$

The AM value is location, date and time dependent, for example, high latitude locations (further than 23.45° from the equator) will always have air mass value higher than 1 and experience greater variation in spectral irradiance throughout the year, while locations close to the equator have lower dependency on this factor. The ratio of direct/diffuse components changes with the shift of sun position where maximum portion of direct irradiance on a surface is achieved when the sun is perpendicular. At this condition, sun elevation is the smallest thus less pronounced radiation attenuation. As the sun moves from this position, elevation will increase, hence the decreased in solar irradiance and increased in the distance between sun and earth's surface.

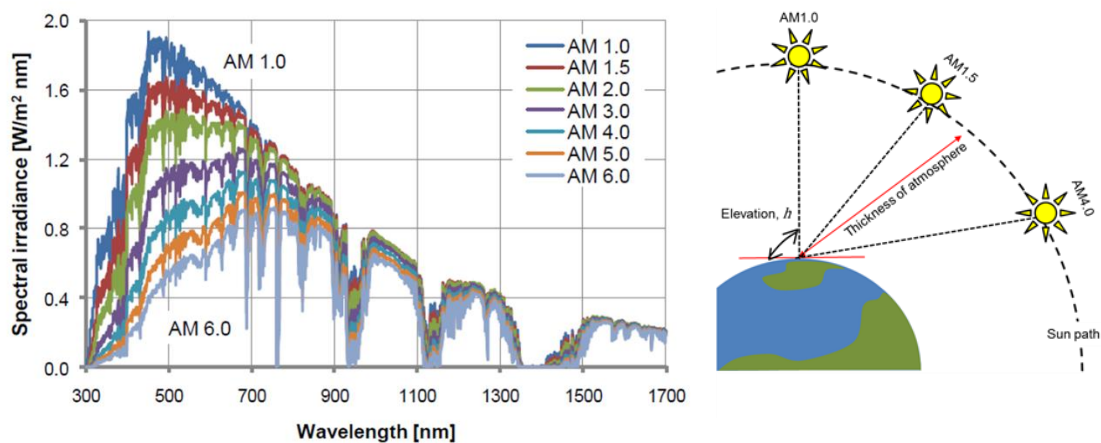


Figure 2. 6. Spectral irradiance of sun radiation at varying AM values [20] (left) and illustration of AM (right).

As the AM increase the spectral distribution of solar radiation will be shifted especially at short wavelength region (Figure 2. 6). Variation of spectral irradiance due to attenuation (both AM and cloudiness) and sun angle contribute to the constant change in the output of PV devices operating outdoor. The following section will discuss the effect of varying spectral irradiance and angle of irradiance on the output performance of PV panels in real environments.

2.2.2 Effect of environmental factors on photovoltaic performance parameters.

Irradiance and temperature effects

The usable current due to the generation of I_{ph} that is through the PV device when the circuit is shorted is called the short-circuit current, I_{sc} . From Eq. 2. 3, it is understood that I_{sc} has a logarithmic effect on V_{oc} thus, increasing I_{sc} will also cause a slight increase in V_{oc} . Effect of varying irradiance and temperature on the I-V curve is illustrated in Figure 2. 7.

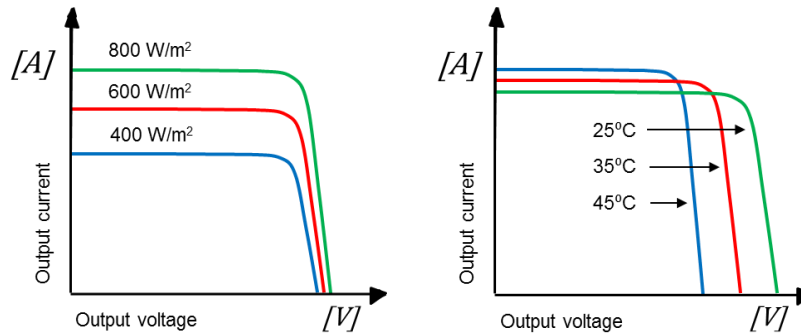


Figure 2. 7. I-V curve shift due to irradiance and temperature effect.

In general, the efficiency, η of the PV device will decrease when there is low irradiance, but there is an exception for some PV technologies that have a large series resistance, for which the efficiency will be affected negatively at high irradiance by the R_s voltage drop. For concentrator PV technologies, the incident irradiance is magnified by the use of lenses by as much as 1000 suns. This significantly increases its efficiency, resulting in reduced area requirement of PV cell within one module. However, since the electrical generation of this technology only utilises direct sunlight, an additional mechanical system is needed to keep tracking the sun and hence complicates the system. This is some of the reasons why the conventional flat-plate PV technology is still preferred by many over concentrator types despite its high efficiency – 38.9% module efficiency recorded on February 2016 [21].

Spectral and angular effects

The generation of electron-hole pairs in a PV device is determined by its band gap, material absorption properties and incident spectral irradiance. Incident photons of energy that is lower than the band gap energy will not be utilised by the device for current generation. The energy of photon is inversely proportional to the wavelength, λ which indicate that the shorter the wavelength, the more energetic the photon and vice versa. This can be expressed as in Eq. 2. 7, using Planck's constant (h) and speed of light (c).

$$E = \frac{hc}{\lambda} \quad \text{Eq. 2. 7}$$

High energy incident photons are absorbed by the material while low energy incident photons cannot be used for photogeneration as the material will be transparent to such photons. The effectiveness of photogeneration in a PV device can be described using the external quantum efficiency (EQE) characteristic, which is the ratio of the number of electrons delivered to an external circuit to the number of incident photons. The EQE of a PV device depends on the technology. Silicon-based material has a band gap of about 1.1 eV, which indicates a cut-off at long wavelength. Material with lower band gap than this will have a cut-off at shorter wavelength.

The spectral response (SR) parameter is similar to the EQE. While EQE define the efficiency of output electron per number of incident photon, the SR represent the ratio of generated photocurrent to the power of incident irradiance. Therefore, SR is usually used to calculate for the generation of short-circuit current at known incident spectral irradiance (Eq. 2. 5).The typical SR characteristic of PV devices of different technologies is shown in Figure 2. 8.

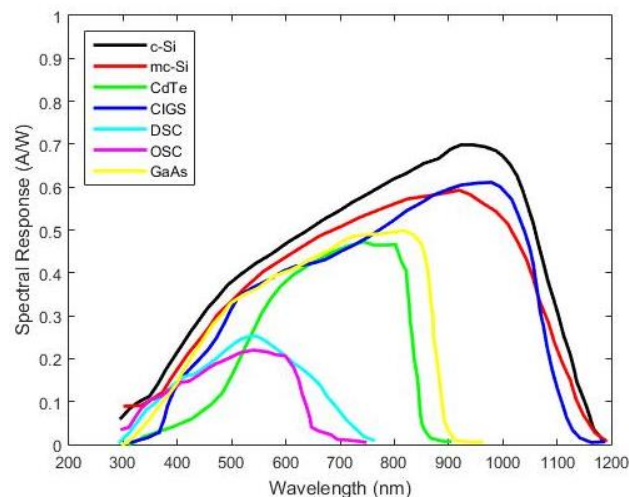


Figure 2. 8. Typical spectral response characteristics of various PV technologies [22].

The usable wavelength for photogeneration of PV devices are vary depending on its material. The typical silicon-based devices have a broad SR characteristic ranging from 300 nm to 1200 nm (Figure 2. 8). The combination of SR characteristic and the constant shift in spectral distribution in real environments (Figure 2. 6) influence the variation in the output performance of PV devices (Eq. 2. 5).

The angular response characteristic of PV devices is influenced by the angular factor of sun position as this is what determines the amount of energy incident on the device. The tilt angle of PV modules orientation outdoor is decided through the calculation of solar elevation for maximum incident power, mainly from the direct component of solar radiation. The sun angle constantly shift throughout the

season (Figure 2. 9). Location with higher latitude will experience more variation in angle-of-incidence (AoI) as the sun path shifted throughout the season. Maximum irradiance incidence on PV devices at normal angle with respect to the collector plane and decreases as the sun angle increases. The AoI effect does not include the cosine effect but is the additional loss due to reflection at different incidence angles as the reflected radiation does not contribute to the generation of I_{ph} (this is affected by the incident spectral irradiance).

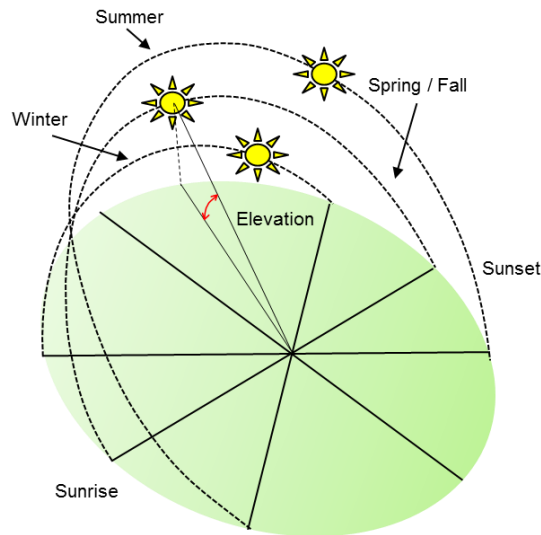


Figure 2. 9. Seasonal sun path geometry with respect to a point on earth at a high latitude.

It was reported that the AoI effect have a significant impact on the performance of PV modules operating in real environment at steep AoI of above 60° as only about 10% of the solar radiation is incident on the modules [23]. For the encapsulated PV modules, this effect depends on the optical property of the front glass used in the encapsulation. Analytical model is usually applied to account for the reflectance loss of PV modules in the estimation of output power of the module under scrutinise via modelling such as the PVsyst [24]. The quantification of this effect is by the light transmittance at the air/glass interface at various angles which can be performed both indoor and outdoor. Characterisation of AoI effect of PV devices is only recently standardised [25].

Mismatch effect

Mismatch occurs when one (or more) cell of a series connection experience different condition than the other cells, for example due to shading. The total I-V curve performance of a PV module is influenced by the total number of cells in the module which are interconnected electrically in series and in parallel. Under real operating environments, partial shading of any cells in the module by trees, dirt, neighbouring buildings and so on will have an impact on the overall performance of the PV module. This is because the current output of the PV module with series connection is limited by the least performing cell within

the module. According to Kirchhoff's law, current through each element which is connected in series will be constrained to be the same. Similarly, the voltage in a parallel connection of cells is forced to be the same.

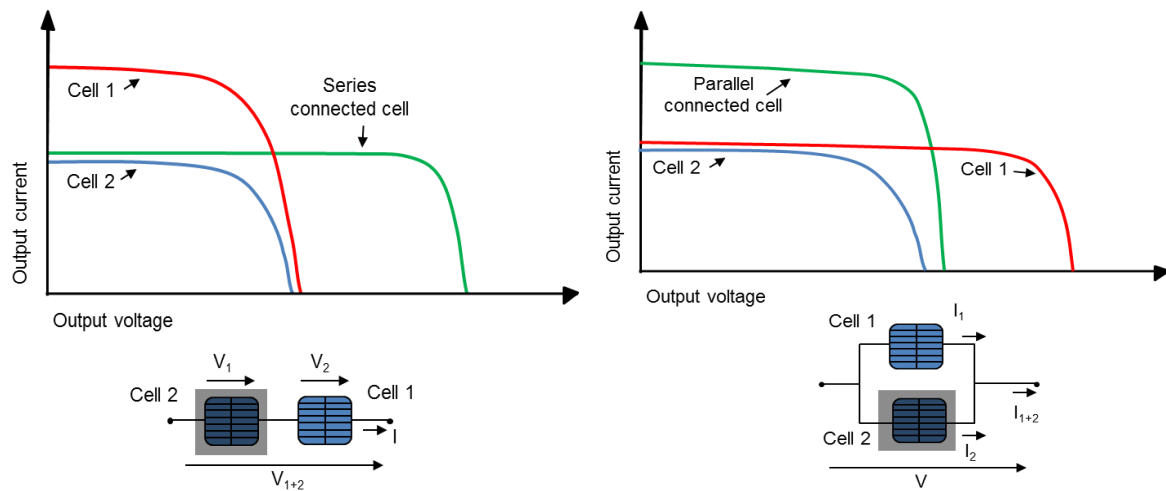


Figure 2. 10. I-V curve performance of shaded and un-shaded solar cells in series (left) and parallel (right) connection.

As illustrated in Figure 2. 10, in the case of shaded and un-shaded cells within a module, the former produces a lower current output than the latter. This leads to hot spot heating due to the low current output cell being pushed into reverse bias and causing a dissipation of power. The larger the number of cells connected in series, the larger reverse bias across the shaded cell that occurs. To prevent destruction, a bypass diode is connected across a number of series connected cells. A typical commercial PV module will have 3-4 bypass diodes in it. The series connected orientation of cells in the module makes the indoor characterisation of modules more challenging. Having a high uniformity of incident irradiance across the module area is a strict requirement.

2.3 Performance rating of photovoltaic device

2.3.1 Power rating of photovoltaic devices

Power rating method

Solar cells are conventionally rated in terms of efficiency under STC while PV modules typically have a nameplate rating of output power under STC, also called the peak power (W_p). The STC describes the incidence broadband irradiance to be $1000\text{W}/\text{m}^2$ with spectral irradiance match to the AM 1.5 reference spectrum and operating cell temperature of 25°C . The power-based rating method is adequate to serve as a basis for comparison of peak performance between various technologies but gives very little information on the actual energy delivery performance of PV modules in operation. Real environmental conditions rarely match STC thus W_p is seldom generated by the module [26]. PV researchers have

been endeavouring to find a rating method that will minimise the difference between customer's expectations and actual energy delivery of PV modules. [26, 27]

Nominal operating cell temperature (NOCT) is a rating method designed to provide information about the likely operating temperature of a PV module in realistic conditions. It is the temperature that the module reaches under environmental conditions of 20°C ambient temperature, 1000W/m² broadband irradiance and <1ms⁻¹ wind speed [28]. This condition is considered to be more realistic of actual operating conditions of PV modules on site because it means that the module will result in lower power rating under NOCT compared to STC. The conditions for NOCT were developed based on the analysis of a long term utility scale solar farm monitoring project [29]. However, the inconsistency of NOCT measurements carried out by different performance measuring labs or the manufacturer, results in variability in the reported NOCT value due to changeability in irradiance which is location dependent [30, 31].

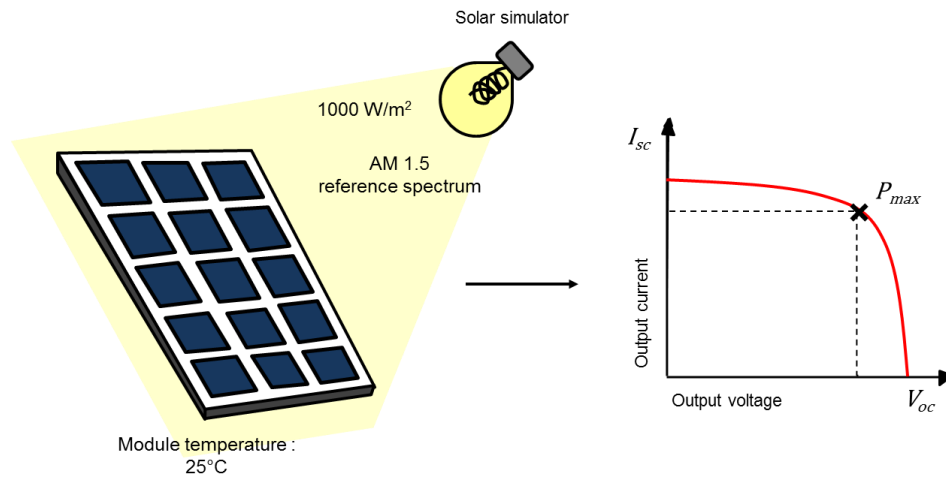


Figure 2. 11. Schematic image of the standard power rating method of a PV module.

Power measurements of full size PV modules under STC are commonly performed indoors using a flash tester (Figure 2. 11). In this method, the P_{max} value is extracted from the I-V characteristic measured by the flasher. The IEC 60904 series is established to serve as a guideline for STC measurement method. Due to the limitations of spectral distribution of the light source not matching the reference spectrum AM1.5, application of a spectral mismatch factor (MMF) correction to the I-V curve measurement is required [32]. The MMF can be calculated using the equation below.

$$MMF = \frac{\int E_{\lambda} \cdot SR_{DUT_{\lambda}} d\lambda}{\int E_{0_{\lambda}} \cdot SR_{DUT_{\lambda}} d\lambda} \cdot \frac{\int E_{0_{\lambda}} \cdot SR_{ref_{\lambda}} d\lambda}{\int E_{\lambda} \cdot SR_{ref_{\lambda}} d\lambda} \quad \text{Eq. 2. 8}$$

Where E_λ is the spectral distribution of the simulator, $E_{0\lambda}$ is the reference spectrum at AM1.5, $SR_{DUT\lambda}$ is the spectral response of device under test (DUT) and $SR_{ref\lambda}$ is the spectral response of the reference device used for measuring irradiance.

Uniformity of illumination is a crucial aspect in the measurement. For a valid measurement, the specification of the instrument used as a light source has to be within the requirements described in IEC 60904-9 [33]. The performance requirement is a 3 letter classification which describes the quality of spectral irradiance match, irradiance non-uniformity on test plane, and temporal stability of the light source. A calibrated reference device is used for calibration of the instrument. This is important in the determination of uncertainty which will reflect the procedure to measure the I-V curve of the PV module in regard to the specification of the light source as outlined in IEC 60904-1 [34]. Module maximum power (P_{max}) is extracted from the forward bias sweep I-V curve measurement, although methods for P_{max} extraction vary.

Rated power and price of PV modules are the driving factors in deciding which technology to select before the implementation of a system. Having detailed information regarding the performance characteristics of a PV module will enable more accurate energy yield modelling thus raising confidence in the investors funding a PV project. Although it is well understood that the return on investment in PV projects is dependent on the energy yield, the complexity, high cost, and the time consuming nature of the assessment push the consideration of energy yield into second place when designing a PV plant. The assessment requires long term performance monitoring in the climate of interest, but recent studies have demonstrated that a reliable energy yield estimation is possible using long term climatic data and comprehensive characteristics of PV modules of interest [35].

Energy-based performance rating of photovoltaic devices

Energy yield of PV modules is defined in watt hours (Wh). Energy yield as a comparator between different PV technologies is more comprehensive than the power rating method as it describes the energy delivery of PV technologies under realistic operating conditions. Energy yield provides information on annual revenue of PV systems, and is used in calculating the levelised cost of electricity (LCOE) of the system [2]. Choosing a capable PV technology for a specific location will lead to surplus in revenue over the total operating period of the system. Current energy yield assessment has a large uncertainty margin due to the limited availability of sufficient performance information of PV modules. Each percentage rise in uncertainty results in significant investment uncertainty with regard to capital expenditure, therefore high uncertainty in energy yield will increase the risk in investment, which in turn increases the cost of financing PV projects. With this in mind, there are many efforts being made by

experts and researchers in PV to suggest a model that can be used to predict energy yield of PV modules reliably over the years of operation.

Estimating the energy delivery of a PV module is a very challenging task [36]. There are many environmental variables that have to be taken into account that influence the yield. Long term recorded environmental data is necessary to characterise the climatic conditions of the location. These include the annual in-plane irradiance, monthly average ambient temperature, seasonal variation of spectral distribution, wind and soil condition of the site. This information is then combined with the pre-measured characteristics of the PV module of interest. Instantaneous direct current yield Y_{DC} of the module under specific environmental conditions is calculated using Eq. 2. 9 [6].

$$Y_{DC} = G_{POA} \cdot \eta_{STC} \cdot A_{module} \cdot f \quad \text{Eq. 2. 9}$$

Where G_{POA} is in plane irradiance incident on the modules, η_{STC} is the rated efficiency of the module at STC as provided in the nameplate, A_{module} is the size of the module and f includes the factors that influence the efficiency from STC under real environments. Figure 2. 12 illustrates the inputs that are required in the assessment of energy yield.

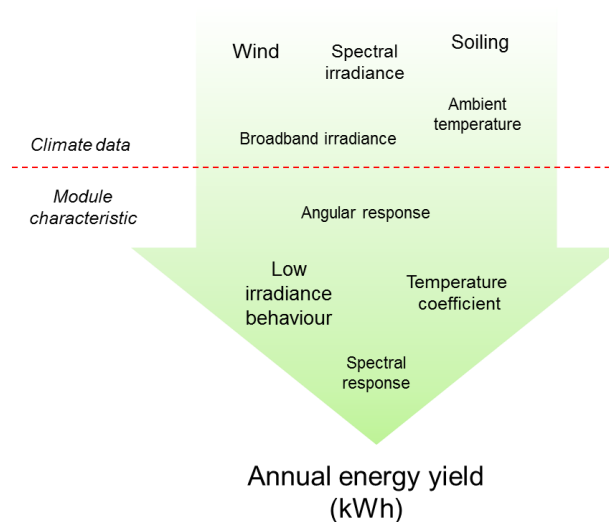


Figure 2. 12. Factors that influence the determination of energy yield.

Module performance ratio (MPR) is another indicator that is generally used to describe the performance of different PV technologies under outdoor conditions. MPR is a dimensionless index and is the ratio of actual energy output of module under real operation to the rated nominal output (P_{STC}). In other words, MPR is a method to quantify the loss in efficiency of a module outdoors compared to its STC value. Nominal output is the energy that would have been delivered by the module if it were operating at its

rated efficiency but under real irradiation data. For the calculation of annual MPR, annual in-plane irradiation (H_{POA}) is used (Eq. 2. 9).

$$MPR = \frac{Y_{DC}}{P_{STC}} \cdot \frac{1000Wm^{-2}}{H_{POA}} \quad \text{Eq. 2. 10}$$

MPR is useful to elaborate the driving factors in performance of different technologies without accounting for the size of the module [35, 6]. For this reason, MPR is suitable to be used as an indicator to compare the efficiency of different technologies under climates of interest.

2.3.2 Energy rating method

Overview of energy rating method

An indicator to quickly compare the energy delivery performance of PV devices has long been demanded by both PV system consumers and designers. Driven by this motivation, there have been several attempts made by experienced PV institutions such as the National Renewable Energy Laboratory (NREL) and Sandia National Laboratories to develop a performance model of PV modules accounting for varying operating conditions as a function of irradiance and temperature [37, 38]. The idea is to have a more comprehensive rating method than the single-value STC power rating so that the performance of a PV module on different types of site can be predicted, for comparison with other modules.

The performance surface, commonly known as the “G-T matrix”, approach was developed by the European Solar Test Installation (ESTI) [27]. The method incorporates power rating under several different operating conditions to determine the performance surface of a PV module as a function of in-plane irradiance and module temperature. The hourly in-plane irradiance data is obtained through the available weather data and is used for the estimation of module temperature (T_{MOD}) as expressed in Eq. 2. 11 [27],

$$T_{MOD} = \left(\frac{NOCT - 20^{\circ}C + 2^{\circ}C}{800} \right) G + T_{AMB} - 2^{\circ}C \quad \text{Eq. 2. 11}$$

Where T_{AMB} is the hourly ambient temperature – from the available weather data, and $NOCT$ is the nominal operating cell temperature of the PV technology. It have been realised through analytical evaluation of outdoor PV performance carried out by ESTI that T_{MOD} is about 2°C colder than T_{AMB} , hence the extra 2°C in the equation.

The idea of the G-T matrix approach is to have a reference power surface from which the annual energy yield of a PV module can be predicted based on input data of hourly irradiation and ambient temperature. These are the meteorological data that are typically obtainable from meteorological monitoring networks. Due to the direct measured inputs and straightforward logic of the method, it has been adopted as the first part of the IEC 61853 energy rating standard.

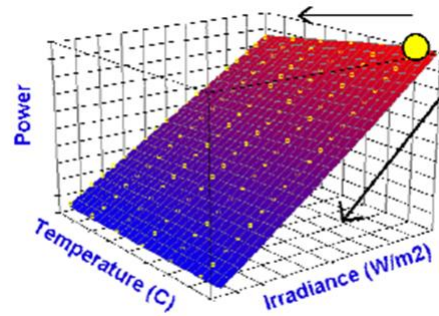


Figure 2. 13. Performance surface method developed in ESTI [27].

The energy rating method is formulated to take into account environmental influences on the performance of the PV module outdoors. Seasonal variation of solar angles and air mass will affect the in-plane irradiance incident on the PV module. Further variation in irradiance due to cloud cover and in module operating temperature due to irradiance, wind conditions and mounting orientation will also have an impact on the instantaneous power output of PV modules operating outdoors. For standardisation, a set of reference weather data for a number of locations representative of differing climates will be required. Considering these aspects, the committee which is responsible for the standardisation of energy rating method has divided the IEC 61853 series into 4 parts. Having a standard for energy rating method not only will serve its purpose as a PV performance index, it will also allow for a uniform reporting from various PV performance measuring laboratories to be achieved.

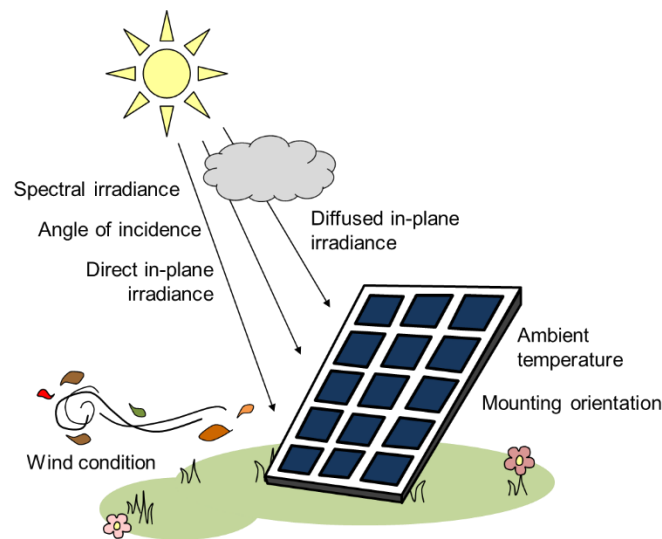


Figure 2. 14. Consideration of environmental influences on outdoor performance of a PV module.

IEC 61853 series

Energy rating is quite similar to energy yield prediction, where both weather data and module characteristics are combined for the estimation of energy delivery. The difference between the two is that energy yield prediction uses a set of weather data of a specific location which have been measured for a long period of time, while energy rating utilises reference weather data sets. As mentioned previously, energy yield assessment is a complicated task and can be very costly due to the long term measured weather data requirement. For this reason, energy rating as an indicator for comparing different technologies at a location of interest (with a similar climate to one of the reference data sets) is a significant improvement over the STC power rating method.

The first two parts of the IEC 61853 standard provide the guidelines and requirements on how to extract all the relevant characteristics of a PV module. Power measurement under 23 points of varying irradiance and temperature is described in **IEC 61853-1** [39]. The range of irradiance and module temperature for the power measurements is 100-1100 Wm^{-2} and 15-75°C, respectively. The performance surface obtained through this measurement is essential in the energy rating method as it will be referred to for the determination of instantaneous power at given G and T values. Module conditions and measurement setup requirements for both indoor and outdoor measurement methods are outlined in this part. The specified density of G-T matrix is designed to provide sufficient performance information of a PV module to enable reliable extraction of power values in between points within the matrix region.

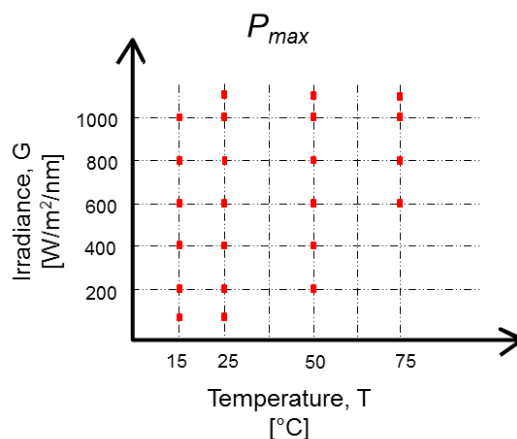


Figure 2. 15. Power measurement points in the G-T matrix

Under real environmental conditions, the in-plane irradiance incident on the PV module (which is responsible for short-circuit current generation) is affected by the AoI and spectrum, while voltage performance of PV modules is dictated largely by the operating temperature of the module, with a secondary dependence on irradiance. The various environmental factors combine with respective

module response characteristics to determine instantaneous power output of a PV module operating in a real environment. Characterisation methods for the effects of Aoi and spectrum are described in **IEC 61853-2** [25].

PV modules are conventionally installed at a fixed tilt which means the angle of incident light is constantly changing throughout the day and the year, as the sun changes position. The Aoi determines both the fractions of direct and diffuse irradiance incident on a PV module and the loss of incident energy due to reflection. This latter characteristic varies from module to module as it depends on the type of glass used on top of the device and various anti-reflection coatings or texturing that may be applied to different layers within the module. The angular response characteristics of PV modules are measured as the function of light transmittance to the photoactive layer ($\tau(\theta)$), where θ is the angle of incidence with respect to the module plane normal. It is determined experimentally through measurements of the short-circuit current at different rotation angles of the PV device, which are then normalised and corrected to remove the geometric cosine loss effect:

$$\tau(\theta) = I_{sc}(\theta) / (\cos(\theta)I_{sc}(0)) \quad \text{Eq. 2. 12}$$

Standardised procedures and requirements for the measurement of the angular response characteristic of a PV device have only been made available recently and included in the IEC 61853 series. For a full size module, $\tau(\theta)$ of the module under test is given at various angles from -80° to $+80^\circ$.

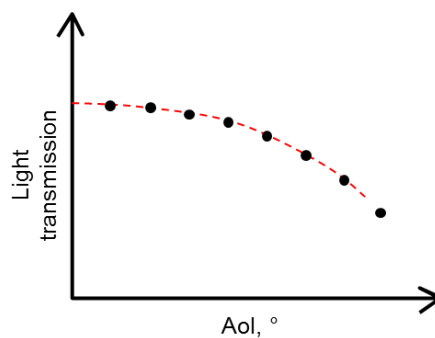


Figure 2. 16. Angular response measurement of PV module

The angular response characteristic of PV module will then be used to correct the in-plane irradiance data from the standardised weather data (this will be detailed under IEC 618534), as well as for the correction of direct/diffuse components.

The AM value, sun angle and cloudiness governs the spectral distribution of sunlight and hence increases/decreases the effective irradiance usable by the PV module for the generation of I_{ph} . To account for this effect in the estimation of power, the spectral response characteristic of the PV module is required. The conventional procedure to measure spectral responsivity of PV devices, what is later referred to in this thesis as the monochromatic method, has previously been standardised and can be found in the series of standards for power rating, part 8 (IEC 60904-8) [40]. The same procedure has been adopted for the **IEC 61853-2**. The method utilises sequential illumination with monochromatic irradiance at specific wavelengths and corresponding measurement of the photocurrent of the device under test.

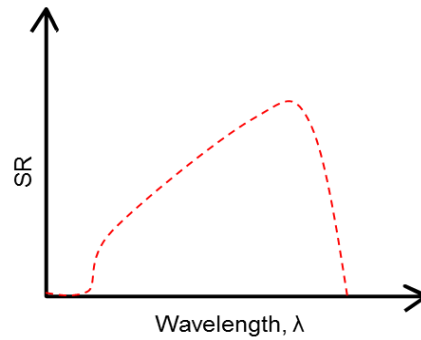


Figure 2. 17. Typical spectral response (SR) curve of c-Si PV device over varying wavelength value

The usable spectral in the generation of I_{ph} varies across technologies as discussed previously. Incident spectral irradiance will be corrected for using the measured SR characteristic of PV modules, denoted as spectral correction factor, C as written in the equation below.

$$C = \frac{1000 \int_{\lambda_{max}}^{\lambda_{min}} SR(\lambda) E_{corr,AOI}(\lambda) d\lambda}{G_{corr,AOI} \int_{\lambda_{max}}^{\lambda_{min}} SR(\lambda) E_{STC}(\lambda) d\lambda} \quad \text{Eq. 2. 13}$$

C is basically the ratio between the current generation of PV devices under STC to that of under spectrally resolved irradiance data as available in the weather data. Here 1000 and E_{STC} are the irradiance and reference spectral irradiance as defined in the STC respectively, while $G_{corr,AOI}$ and $E_{corr,AOI}$ are the angularly corrected in-plane irradiance and spectral irradiance data from the weather data sheet. $SR(\lambda)$ is the measured SR characteristic of the modules. C is then used to modify the in-plane irradiance value, $G_{corr,AOI}$, and noted as G_{eff} for the look up of power output from the G-T matrix.

The voltage of a PV module is affected by module operating temperature (T_{mod}). Environmental factors such as in-plane irradiance, ambient temperature and wind speed affect the operating temperature of

modules in real environments. The module temperature can also be affected by the orientation of the module and the type of mounting structure used. Characterisation of the relationship between these factors on the performance of the PV module is necessary to determine the module temperature for energy rating assessments. T_{mod} can be calculated using the equation as below [41].

$$T_{mod} = T_{amb} + \frac{G_{POA}}{u_0 + u_1 v} \quad \text{Eq. 2. 14}$$

Where T_{amb} is the ambient temperature, G_{POA} is the spectrally corrected in-plane irradiance value, v is the wind speed and u_0 , u_1 are referred to as the Faiman coefficients. The determination of these coefficients is achieved by using linear regression analysis based on the measurement of module temperature at varying irradiances and wind speed conditions. The procedures and evaluation method for this measurement are also described in the **IEC 61853-2**.

The guidance to perform the energy rating from start to finish is described in part 3 of the **IEC 61853** series (not a published standard yet). Draft of this document has been acquired through one of the committee, restricted for internal use. Although this is subjected to further amendment, the current **IEC 61853-3** draft lists the relevant equations and instructions to perform energy rating assessment, including the calculation of correction factors with regard to angular and spectral effects on in-plane irradiance data and also module operating temperature from ambient temperature values. Extraction of the instantaneous output power values corresponding to the given G , T values from the G-T matrix obtained from IEC 62853-1 uses a bilinear interpolation method. For $G_1 < G < G_2$ and $T_1 < T < T_2$, calculation of $P(G, T)$ is as follows:

$$\frac{P(G, T_1)}{G} = \frac{P(G_1, T_1)}{G} + \frac{G - G_1}{G_2 - G_1} \cdot (P(G_2, T_1) - P(G_1, T_1))/G \quad \text{Eq. 2. 15}$$

$$\frac{P(G, T_2)}{G} = \frac{P(G_1, T_2)}{G} + \frac{G - G_1}{G_2 - G_1} \cdot (P(G_2, T_2) - P(G_1, T_2))/G \quad \text{Eq. 2. 16}$$

and,

$$\frac{P(G, T)}{G} = \frac{T_2 - T}{T_2 - T_1} \cdot \frac{P(G, T_2)}{G} + \frac{T - T_1}{T_2 - T_1} \cdot \frac{P(G, T_1)}{G} \quad \text{Eq. 2. 17}$$

In cases where the variables G , T are outside the matrix region, linear extrapolation should be used. In the case of $T > T_{max}$,

$$\frac{P(G, T_{max})}{G} = \frac{P(G_1, T_{max})}{G} + \frac{G - G_1}{G_2 - G_1} \cdot (P(G_2, T_{max}) - P(G_1, T_{max}))/G \quad \text{Eq. 2. 18}$$

$$\frac{P(G, T_{max-1})}{G} = \frac{P(G_1, T_{max-1})}{G} + \frac{G - G_1}{G_2 - G_1} \cdot (P(G_2, T_{max-1}) - P(G_1, T_{max-1}))/G \quad \text{Eq. 2. 19}$$

and,

$$\frac{P(G, T)}{G} = \frac{P(G, T_{max-1})}{G} + \frac{T - T_{max-1}}{T_{max} - T_{max-1}} \cdot (P(G, T_{max}) - P(G, T_{max-1}))/G \quad \text{Eq. 2. 20}$$

While for the case of $G > G_{max}$ and $T > T_{max}$,

$$\frac{P(G, T_{max})}{G} = \frac{P(G_{max-1}, T_{max})}{G} + \frac{G - G_{max-1}}{G_{max} - G_{max-1}} \cdot \frac{P(G_{max}, T_{max}) - P(G_{max-1}, T_{max})}{G} \quad \text{Eq. 2. 21}$$

$$\frac{P(G_{max}, T)}{G} = \frac{P(G_{max}, T_{max-1})}{G} + \frac{T - T_{max-1}}{T_{max} - T_{max-1}} \cdot (P(G_{max}, T_{max}) - P(G_{max}, T_{max-1}))/G \quad \text{Eq. 2. 22}$$

and,

$$\frac{P(G, T)}{G} = \frac{P(G, T_{max})}{G} + \frac{P(G_{max}, T)}{G} - \frac{P(G_{max}, T_{max})}{G} \quad \text{Eq. 2. 23}$$

The last part of the IEC 61853 series, **IEC 61853-4** is also not a published standard and have been acquired together with IEC 61853-3 for internal use. The climatic data used for the calculation of energy yield in the standardised energy rating method is selected from the standard data set of 6 different locations listed in the **IEC 61853-4**. The location selected for the list covers a wide range of climate conditions. The data set provides hourly values of climatic data over one full year which consists of ambient temperature, different types of in-plane and horizontal irradiance (global/direct/diffuse), wind speed, sun elevation and also spectrally resolved irradiance data. Table 2. 1 shows the locations that are selected for the standard weather data.

Table 2. 1. Climatic data set defined in IEC 61853-4 draft [42].

Location	Latitude	Longitude	Climate type
Gabon	1°S	11°E	Tropical humid
Arizona, United States	33°30'N	112°W	Subtropical arid
Saga, Japan	33°22'N	130°30'E	Subtropical coastal
Glasgow, Scotland	56°N	4°W	Temperate coastal
Tibet, China	34°	83°E	High elevation
Alberta, Canada	57°N	112°W	Temperature continental

2.4 Uncertainty consideration in energy rating assessment

2.4.1 Propagation of uncertainty

Uncertainty in measurement defines the range of possible values attributed to the measured quantity due to the random effects in the measurement. The information of measurement uncertainty is particularly important to indicate the level of confidence that the measured value actually lies within the uncertainty margin. The uncertainty arises from many sources such as repeatability, calibration and environment. Calculating the total uncertainty resulting from all sources involves the estimation in the contribution from various sources before evaluation of how will these combine to give a standard uncertainty. Method for the propagation of standard uncertainty can be found in the “Guide to the expression of uncertainty in measurement” handbook (GUM) [43]. The expression in measurement result (Y) can be written such as:

$$Y = x + U_c(y) \quad \text{Eq. 2. 24}$$

Where $U_c(y)$ is the combined uncertainties. There are 2 types of uncertainties, i.e. type A and type B. The former is uncertainty estimated by statistical analysis of repeated measurement and the latter is estimated by any other available information, such as the calibration of the instruments, systematic errors, etc. The estimation of uncertainty type A is made by making assumption regarding the shape of the distribution of the measurement values. The distribution of measurement values is generally assumed to be normal. However, in some cases rectangular distribution is assumed which indicate that there is zero possibility of having any value within certain limits.

The expression of uncertainty of measurement is by taking the combined uncertainty ($U_c(y)$), both type A and type B which calculated using the following equation:

$$U_c(y) = \sqrt{\sum_{i=1}^n (c_i)^2 u^2(x_i)} \quad \text{Eq. 2. 25}$$

Where c_i is the sensitivity coefficient, $u(x_i)$ is the standard uncertainty, and n is the number of uncertainty sources. The sensitivity coefficient c_i is the ratio for change in the measurement result per unit change input and this is necessary in the expression of uncertainty as this describe how the inputs contribute to the combined uncertainty. The calculation of standard uncertainty on the other hand requires the uncertainty values to be divided by divisor – determined by the shape of distribution assumed earlier.

2.4.2 Uncertainty in energy rating assessment

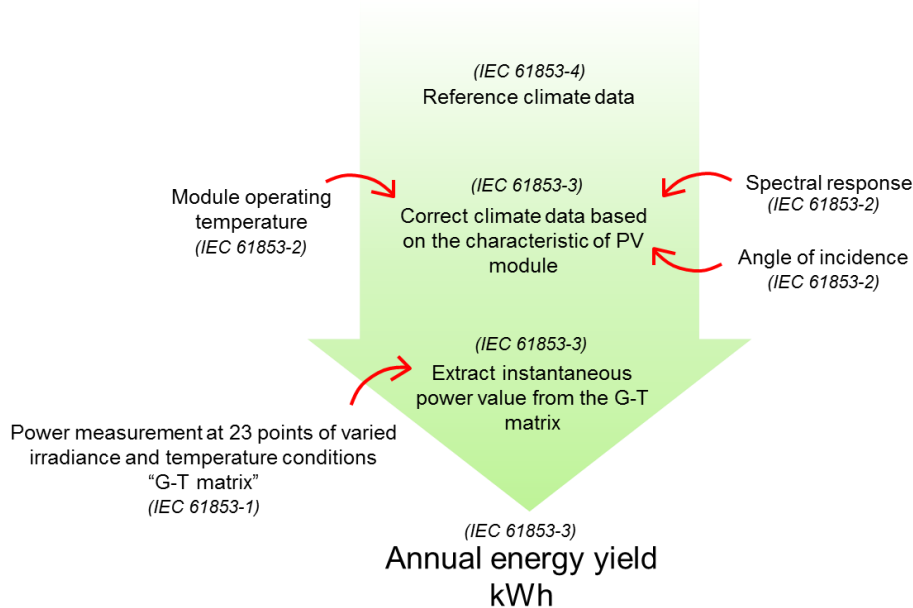


Figure 2. 18. Simplified flow chart showing the assessment of PV energy rating method.

In PV energy rating, the accuracy of the calculation is determined by the uncertainty associated with all the contributing characteristics measurements of the PV module i.e. low irradiance behaviour, temperature dependency, spectral and angular effects. For this reason, the uncertainties associated with the measurement of such characteristics are required to facilitate the uncertainty propagation to the final energy rating assessment.

Figure 2. 18 shows a simplified flow chart illustrating the process of the IEC energy rating method. The process begins with reference weather data selection of the location that has the most similar climatic conditions to the location of interest. Both climatic data and the characteristics of the module are combined to derive the annual energy yield using the calculation models prescribed in the IEC 61853-3. Correction factors due to environmental effects are applied to the climatic data and finally the corrected in-plane irradiance and module temperature at each hour are used to extract power values from the G-T matrix.

The uncertainty in PV module energy performance calculations entirely depends on the accuracy of power measurement at varying G-T (IEC 61853-1) and PV characteristic measurements (IEC 61853-2) as the reference weather data set prescribed in the IEC 61853-4 has no associated uncertainty. MPR value is usually used to evaluate the output performance of PV modules using the available weather

data for performance comparison between modules due to its practicality which is less complicated than the energy yield assessment. Recent research of the uncertainty contribution to MPR evaluation due to the various characterising measurements was estimated at 2% for one site [7].

The predominant influence is reported to be from the uncertainty in the G-T matrix measurement and determination of module operating temperature. Variability in the power measurement affects the MPR value by 0.5-1.3% depending on the location while in the determination of coefficients u_0 and u_1 (Eq. 2. 14), the effect on MPR is considerably large at 1%. In another report, power measurement uncertainty at low irradiance for a c-Si module is reported to be more than 2% [44]. Therefore for locations at higher latitudes where irradiance level is usually low, MPR evaluation will be highly affected by the uncertainty in the measurement of the low irradiance behaviour of the module under test. For an indoor measurement setup, the major uncertainty contribution is due to spectral MMF correction. The MMF correction (Eq. 2. 8) requires information of spectral response of the module under test. Deviation of temperature from STC shifts the spectral response curve of the module, therefore the lack of availability of spectral response data of PV modules at varying temperatures leads to an increase in uncertainty in MMF correction.

The second largest contribution to the MPR evaluation is from the angle of incidence effect on the module performance. The measurement procedure to perform such measurements has been recently included in the IEC 61853 series as a standard, but uncertainty analyses on the method have not yet been reported. For this reason, some researchers have made a rough estimation of the effect of angle of incidence in MPR evaluation at 1% [6]. The estimation is based on data analyses of the outdoor PV module performance where variation between 2-3% is observed depending on the latitude of the location where the module is installed. This variation is caused by the combination of the availability of direct in-plane irradiance at the location and the losses in direct irradiance at higher angles of incidence due to the module reflection characteristics. However, due to module-to-module variation in angle of incidence characteristics, measurement of the module under test with associated uncertainty and its influence on MPR evaluation still requires further investigation.

In [7], uncertainty contributions in spectral effects are derived from the value of the variability in multiple spectral response measurements which is less than 0.04%. Another report assumed that the uncertainty in spectral response measurements is uniform across the wavelength range, with uncertainty values of 2-5% [45]. However, the propagation of uncertainty in the measurement of spectral response into MPR is quite complicated as the correlations between neighbouring wavelengths have to be taken into consideration. To do this, uncertainty at each point in the spectral response curve is required and then randomisation methods as suggested in [46] can be applied. Although the method

for spectral response measurements is standardised and already established for a small area device, there are only a handful of PV labs that are equipped with the facilities to perform the measurement on full sized modules reliably. As yet the uncertainty analyses on such measurements is not being reported.

2.5 Conclusions

The impracticality of the current power rating at STC has become more apparent with increased global installation of utility scale PV systems. High uncertainty in the one-point value of power rating method increases the investment risk in PV projects. PV researchers have been working on finding a practical way to rate the performance of PV modules on an energy basis for over a decade to enable access to more comprehensive information on the energy delivery of PV module in real environments.

An amount of research regarding the evaluation and validation of energy rating methods as described in the IEC 61853 has been conducted. A fairly good understanding of the effect of environmental factors on the evaluation of energy rating calculations has also been achieved through this research. However, due to the limitation of facilities in PV laboratories with regard to the characterisation of optical effects of full size PV modules, rough estimations are often made when accounting for the effect of angular and spectral responses on the MPR evaluation. The focus of this thesis is to provide the missing relevant information of the contributions of spectral response and angle of incidence characteristics of PV modules to the uncertainty of the PV energy rating calculation.

Measurement of the spectral response curve of a large area PV module in its entirety is a challenging task. The conventional spectral response measurement methods utilise monochromatic sources to illuminate the device under test to measure the photo-current of the device at specific wavelengths. High uncertainty in photocurrent measurement due to low incident irradiance on the module under test is a major challenge in the monochromatic method. The problem is even more pronounced in the application to large area devices, due to lower irradiances and signal-to-noise ratio (SNR) in the current measurement. As a result, most performance measuring PV labs exclude uncertainty analysis of measurements from their reporting. In the following chapter, an alternative method to measure the spectral response curves of full size PV modules with uncertainty analysis will be presented.

The standard procedure for measurement of the angle of incidence characteristic is only recently available and has been included in the IEC 61853 series. The measurement method is reviewed and validated using the short pulsed solar simulator facility in CREST. This will be presented in this thesis together with the uncertainty analysis on the method.

3 Evaluation of method for spectral response measurement of large area photovoltaic modules

Photocurrent generation within a PV device is governed by its wavelength-dependent absorption efficiency, which is quantified with external quantum efficiency (EQE). The usable wavelength range for current generation varies depending on the technology. Crystalline silicon based devices can absorb a broader wavelength range in comparison to the typical thin-film devices due to the relatively lower band gap energy (Figure 2. 8). While the EQE is useful in the evaluation of a solar cell, the spectral response ($SR(\lambda)$), more directly measured and in convenient units, is more often used to describe the fraction of usable irradiance of each wavelength that is converted into current (A/W). It is used in the calculation of I_{SC} , produced by a device under a given incident spectral irradiance ($E(\lambda)$), as shown in the Eq. 2. 5.

The SR of a PV module is required for the energy yield calculation under varying environmental conditions over a period of time to account for the effect of constant shift of the solar spectrum due to the attenuation solar radiation. As discussed previously, as AM increases, the irradiance at short wavelengths is attenuated more than at longer wavelengths (Figure 2. 6). In the calculation of energy yield, the SR characteristic of modules under scrutiny will be used to correct the measured in-plane incident spectral irradiance data ($E(\lambda)$), since only a certain fraction will be utilised in the I_{SC} generation (Eq. 2. 5) [7].

The SR characteristic of a PV device can also be influenced by physical factors apart from the semiconductor material, i.e. type of glass used in encapsulation, and though less significant, module-to-module variation in SR arises. It is common to utilise a 'typical SR curve' for the technology of interest in the absence of SR measurement data for energy yield calculation of PV modules [45]. However, this can add to uncertainty in the G_{eff} (usable irradiance in photocurrent generation as discussed in 2.3.2), thus increased in uncertainty in the energy yield calculation overall.

To obtain the SR characteristic, the convention is to measure it by the monochromatic method. This method utilises monochromatic illumination which is produced using a monochromator for the measurement of photocurrent at a sequence of specific wavelengths. The procedure to perform this measurement has been standardised and is documented in the IEC 60904-8 [40, 6]. The monochromator can be made of filters or the grating type. A combination of bias lighting and phase lock-in system is usually applied to enable a reliable photocurrent measurement due to the low irradiance intensity of the monochromatic light and resulting current signal [47].

Typical uncertainty in SR measurement is reported at 2-3% for small area c-Si technology devices using the standard monochromatic measurement setup [46]. Measurements by the Physikalisch-Technische Bundesanstalt (PTB) however, have demonstrated a record measurement uncertainty of 2x2cm reference cells, reported at 1% maximum in the visible light range and less than 5% in the ultraviolet (UV) and near infra-red (NIR) regions [46]. Measurement of spectral responsivity of small area PV devices (individual cells) is well established, but that is not the case for large area devices (modules). Currently, the capability to measure SR of full size PV devices is limited to only a few labs worldwide. This is mostly due to the complexity and high uncertainty in the measurement setup.

This chapter addresses the subject of SR characterisation methods for large area PV devices to provide reliable input to a PV energy rating method. A review of characterisation methods employing standard and non-standard methods is presented below. The development of a reliable SR measurement method for large area PV devices, based on a previously introduced novel polychromatic method [48] will be described. Unlike the conventional method, the application of monochromatic illumination is not necessary, only a set of broadband filters and a spectroradiometer are used in the polychromatic measurement setup. The simplicity in the setup allows for the method to be applied to SR characterisation of large area PV devices. For the illumination of large area PV modules, the Pasaan 3B pulsed light solar simulator available in CREST is used as the light source. A detailed discussion with regards to the technical evaluation of this measurement setup is presented in this chapter.

3.1 Introduction

3.1.1 Overview of spectral response measurement of photovoltaic devices

Technical requirements for spectral response measurement of PV devices

The SR is determined by measuring the photoresponse (as I_{SC}) of the device under sequential illumination by a series of specific wavelengths of light. For reliable measurement, there are considerations to be taken into account in the measurement setup. For measurement setups based on the monochromatic method these factors are:

- 1) Narrow bandwidth.

The conventional DSR measurement method requires the monochromatic bandwidths to be as narrow as possible, i.e. within 20 nm, to reduce error in defining the wavelengths corresponding to the current signal measurements [49].

2) High irradiance intensity.

High intensity of incident irradiance is also important to generate more charge carriers in the device for a reliable I_{SC} measurement, i.e.: to have the device operate in a linear regime and have a reasonable measurement signal-to-noise ratio.

3) High wavelength resolution.

The wavelength resolution of the measurement system is required to be fine enough to capture any detail in the SR of the device under test to avoid over- or underestimation of the spectral photocurrent sum (i.e. short-circuit current). An interpolation approach is usually applied in SR measurements for technologies with a smooth SR curve (such as c-Si).

4) High irradiance uniformity.

Another significant consideration is the uniformity of illumination over the area of the DUT. Results obtained from a measurement that has poor irradiance uniformity can be misleading due to any non-linear behaviour in lateral charge conduction and poor spatial uniformity of I_{SC} generation across the DUT.

The standard method to measure the SR characteristic of a PV device is based on the Differential Spectral Responsivity (DSR) method. This method was first implemented in the PTB for the calibration of reference solar cells (2x2 cm) [50, 51]. Many other research into the SR measurement of PV devices has also been reported by many researchers with the aim to improve the practicality and accuracy of the measurements. A review of such a measurement methods is presented in the following section.

Standard procedure for spectral response measurement

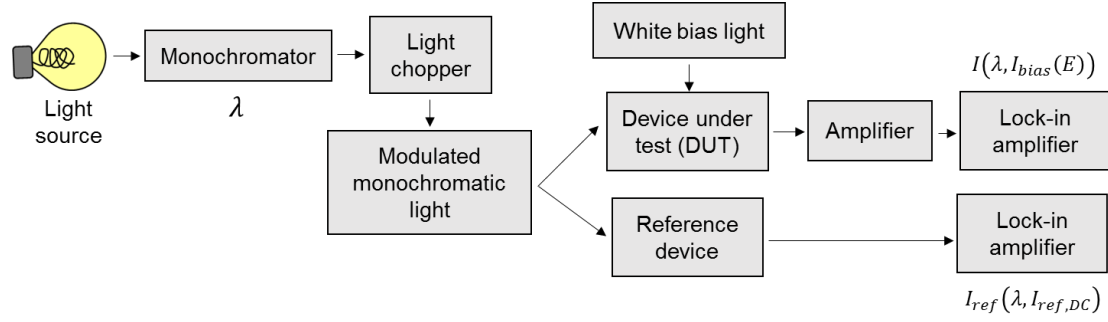


Figure 3. 1. Block diagram illustrating the measurement setup in DSR method.

Figure 3. 1 shows the block diagram of the DSR measurement setup. In this method, the monochromatic light (E_λ) is modulated by the light chopper at a selected frequency while constant white bias light is applied to boost the intensity of incident light and have the device under test operate in a linear region. A reference device with known SR is used to monitor the intensity of the monochromatic light. The I_{SC} measurement of the DUT is amplified and the component contributed by the monochromatic light is extracted from the modulated signal using the information of frequency set earlier. The calculation of SR at wavelength, λ is as below.

$$SR(\lambda, I_{bias}(E)) = \frac{I(\lambda, I_{bias}(E))}{I_{ref}(\lambda, I_{ref,DC})} \cdot SR_{ref}(\lambda, I_{ref,DC}) \quad \text{Eq. 3. 1}$$

Where $SR(\lambda, I_{bias}(E))$ is the SR of the DUT, $I(\lambda, I_{bias}(E))$ and $I_{ref}(\lambda, I_{ref,DC})$ are the short-circuit current measurements of the DUT and the reference device respectively, and $SR_{ref}(\lambda, I_{ref,DC})$ is the spectral response of reference device.

Some PV labs have developed advanced apparatus to increase the accuracy in SR measurement aiming for a better calibration of PV devices. Currently, there are two major labs that employ a high precision tuneable laser-based DSR system: PTB [52] and the Fraunhofer Institute for Solar Energy System (FhG-ISE) [53]. The advantage of using the laser-based system is that a very narrow-bandwidth monochromatic illumination with high intensity can be achieved, but it requires a significant amount of investment.

Another unique measurement approach, the LED-based system, has also been developed by the US National Institute of Standards and Technology (NIST). The measurement setup uses high powered LED arrays and light guides for full illumination of the monochromatic beam on the DUT [54]. The system

has the advantage of providing high wavelength resolution but the bulky setup restricts its application to small area devices.

While the DSR method can be applied for measurement of solar cells without major complications, its application to large area devices is very challenging with much stricter considerations to be taken into account, as described in the following.

Spectral response measurement of large area photovoltaic devices

Currently there are 2 methods reported for the SR measurement of full size PV modules: the filter-based full illumination method and grating-based partial illumination method. The former usually employs a pulsed light solar simulator facility with a set of narrow-bandwidth filters to illuminate DUT with monochromatic light (Figure 3. 2). The measurement setup of this system is rather simple compared to the DSR method because there is neither white bias lighting nor lock-in techniques applied in the measurement because: 1) high irradiance illumination projected onto the measurement plane and 2) it is impractical to install light chopper in front of the relatively large area light source – 39cm × 39 cm. Research regarding this technique has been conducted in a number of PV labs such as the European Solar Test Installation (JRC-ESTI), the University of Applied Sciences and Arts of Southern Switzerland (SUPSI), and the Solar Energy Research Institute of Singapore (SERIS) [55, 56, 57].



Figure 3. 2. Figures showing the SR measurement setup using pulse light solar simulator with interference filter (left) and photograph of a unit of filter as used in SUPSI (right) [56].

The concern with regard to the filter-based measurement method of large area devices is that the narrow-bandwidth filters used in the system significantly reduce the intensity of throughput irradiance, hence the increase in the non-uniformity of the illumination over the area of DUT. Low SNR in the

measurement contributes to high uncertainty in the output I_{SC} . To minimise this effect, a rather broad bandwidth quasi-monochromatic filter is used, e.g. 50 nm as reported in [55] and [57].

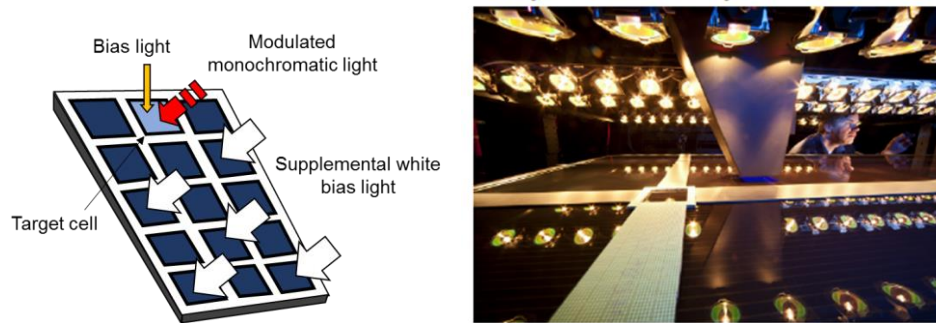


Figure 3. 3. Schematic image of partial illumination SR measurement method of a full size PV module (left) and photograph of SR measurement apparatus at TUV Rheinland, Cologne [58] (right).

The partial illumination method on the other hand, employs a more complex system where chopped monochromatic light illuminates a target cell within the module while having uniform supplemental white bias light illuminating the entire module other than the cell (Figure 3. 3). The intensity of the monochromatic light has to be low enough relative to the illumination of the other cells to create the required current-limiting mismatch condition of the target cell. This method was developed and first implemented by the National Institute of Advanced Industrial Science and Technology of Japan (AIST) [59]. Since the system employs a steady state light source, thin film modules which often have a dependency on time-varying elements can also be measured. Nevertheless, the uncertainty of this measurement is not reported. TUV Rheinland of Germany have also adopted this method in their facility [58].

Despite having the requirements and procedures to perform SR characterisation of PV modules detailed in the IEC 60904-8 [40], practical challenges with implementing such measurements and the associated unknown or high uncertainty persist. As discussed previously, having a high irradiance intensity incident on the DUT for the measurement of SR characteristic is crucial to avoid errors due to low absolute signal and low SNR which contribute to uncertainty in the I_{SC} measurement. The application of narrow band-width filters severely limits the intensity of the throughput irradiance, hence the additional lock-in techniques incorporated in such measurements on small areas. Such techniques are difficult to scale up to module area steady state solar simulators due to beam sizes, and impossible to implement in the far more common pulsed light types. On account of this, a practical SR measurement method based on a polychromatic method is further developed in this research. The method is also a filter-based method except instead of narrow-bandwidth filters, broadband filters are equipped in the measurement setup. The application of such filters allows for the throughput of high intensity over the entire area of PV modules, hence the increased SNR in the I_{SC} measurement.

3.2 Polychromatic method for the measurement of large area device

3.2.1 Overview of the polychromatic measurement method

Concept of polychromatic measurement

The polychromatic method was first developed in CREST as an alternative SR measurement method applied to small area PV devices [48]. The idea is to maximise the irradiance incident on the DUT so that a reliable I_{sc} measurement can be extracted without the application of supplemental bias lighting or lock-in technique, utilising broadband filters. The measurement setup of this method employs a set of polychromatic filters with variation of cut-off wavelength for the measurement of short-circuit current ($I_{sc, filters}$) of DUT under different throughput irradiance spectra ($E_{\lambda, filters}$), each of which is measured concurrently with the device current. A schematic image of the original measurement setup is shown in Figure 3. 4.

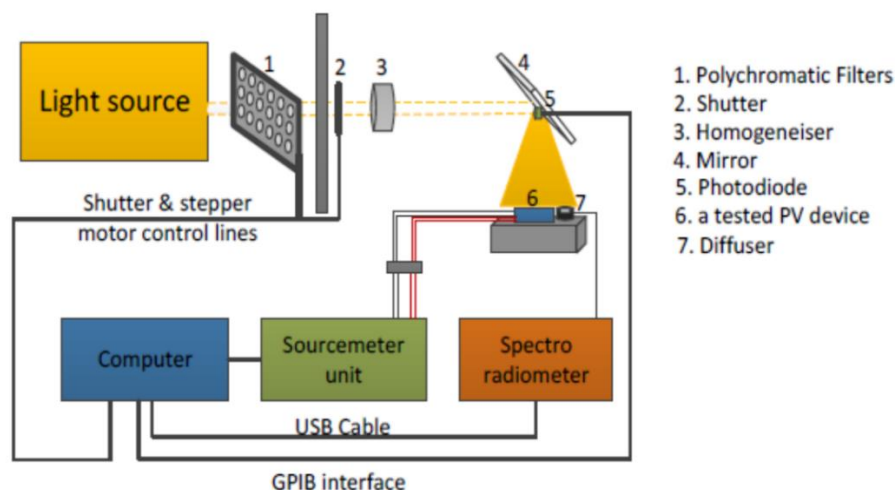


Figure 3. 4. Schematic image of SR polychromatic measurement for small areas [48].

The determination of spectral responsivity of a DUT by this method is through SR curve modelling using the information of $I_{sc, filters} - E_{\lambda, filters}$, obtained through measurement. Research on SR curve modelling of PV devices is not new. A few modelling approaches that utilise either empirical or physical models can be found in the literature [60, 20, 61]. The early development work of the polychromatic method employed the former approach where the non-linear Gaussian summation (Eq. 3. 2) function is used to model the SR curve of DUT [62]:

$$SR_{\lambda, mod} = \sum_{i=1}^N h_i \cdot \left[- \left(\frac{\lambda - c_i}{2w_i} \right)^2 \right] \quad \text{Eq. 3. 2}$$

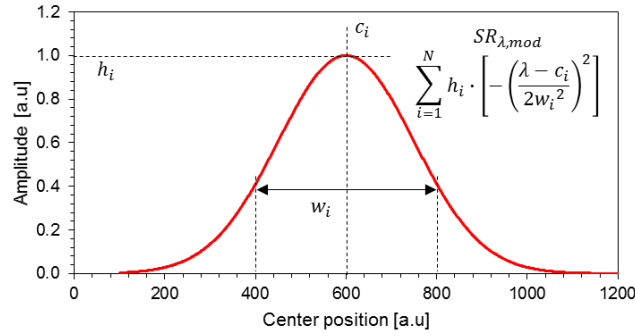


Figure 3. 5. Bell-shaped graph of Gaussian function.

Where N is the number of Gaussians and h , c_i , w_i are the parameters of the model. A fitting algorithm is developed to fit the Gaussian summation model to the current and spectral information of the measurements by iteratively tuning the parameters. In this method, $SR_{\lambda, mod}$ with fitted parameters will be regarded as a representation of the SR characteristic of the DUT. The simplified flow chart visualising the overall process of the polychromatic method is shown in Figure 3. 6 .

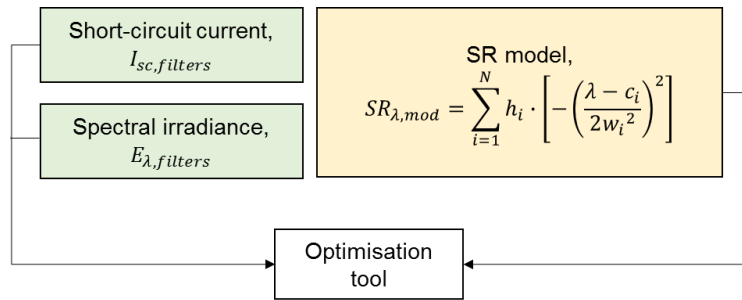


Figure 3. 6. Simplified flow chart showing the elements in polychromatic measurement method.

3.2.2 Polychromatic data fitting algorithm

Development of optimisation program

The fitting of polychromatic measurements ($I_{sc, filters} - E_{\lambda, filters}$) into $SR_{\lambda, mod}$ is performed using a gradient-based optimisation tool, the Levenberg-Marquadt (LM) method. Gradient method describes an algorithm which converges parameter values iteratively along the gradient of pre-defined function. This is often used in numerical computing to solve problems of minimisation/maximisation of an error function. The most common application of this method is in regression analysis which is an analysis to predict the relationship between variables of functions. Curve fitting is an example of this analysis where the variables in a curve function are optimised to minimise the difference between a set of measured data points and the curve. The difference value may be defined as the sum squared error (R) parameter in the minimisation problem and is used as indication to decide whether the fitting is successful, also known as goodness-of-fit parameter.

The polychromatic fitting algorithm is similar to the curve fitting method in which the difference between measurement data and modelled function is to be minimised. The LM algorithm is selected due to its stability in parameter convergence in minimal time [63, 64]. The incorporation of $I_{sc, filters} - E_{\lambda, filters}$ and $SR_{\lambda, mod}$ in the LM algorithm is implemented using the Delphi programming language to automate the fitting process. The source of this algorithm is adopted from the Numerical Recipes textbook [64]. The construction of parameter R in the polychromatic fitting algorithm utilises all the input data i.e. $I_{sc, filters} - E_{\lambda, filters}$, $SR_{\lambda, mod}$, and starting parameter values. This will be detailed in the following.

3.2.3 Optimisation of objective function

In general, each optimisation process is unique. The first step in the process is to construct an appropriate model that addresses the optimisation problem [65]. The model is a mathematical expression containing the objective, variables and sometimes constraints of the problems. The next step is to identify the type of problem as this will determine which optimisation algorithm is to be used, for example the linear/non-linear least square algorithm, evolution strategies, genetic algorithm and so on. Finally, an optimiser is selected based on the problems defined earlier. Currently there are many optimisers to choose from as this is a common feature embedded in mathematical based software such as Microsoft Excel and MATLAB.

The objective in the polychromatic fitting method is to model the SR characteristic of PV devices using the $SR_{\lambda, mod}$ based on the information of $I_{sc, filters} - E_{\lambda, filters}$ of the DUT. It is understood from Eq. 2. 5 that the integration of wavelength functions E_{λ} and SR_{λ} will give the value of generated current (I_{sc}). Similarly, the integration of $E_{\lambda, filters}$ and $SR_{\lambda, mod}$ will produce the corresponding calculated short-circuit current ($I_{mod, filters}$), at incident $E_{\lambda, filters}$:

$$I_{mod, filters} = device\ area \times \int_{\lambda_{min}}^{\lambda_{max}} E_{\lambda, filters} \cdot SR_{\lambda, mod} d\lambda \quad \text{Eq. 3. 3}$$

Theoretically, if the $SR_{\lambda, mod}$ is an exact match to the actual SR characteristic of the DUT, at given $E_{\lambda, filters}$, the values of $I_{mod, filters}$ will be the same as $I_{sc, filters}$ for all filters used in the polychromatic measurements, at least to within measurement uncertainty. The evaluation of this condition can be performed using the sum squared error (R) as a goodness-of-fit indicator, where in an ideal condition, $R = 0$. In this case, R can be written as,

$$R = \sum (I_{sc, filters} - I_{mod, filters})^2 \quad \text{Eq. 3. 4}$$

From Eq. 3. 2, R can be expressed as,

$$R = \sum \left[I_{sc, filters} - \left(device\ area \times \int_{\lambda_{min}}^{\lambda_{max}} E_{\lambda, filters} \cdot SR_{\lambda, mod} d\lambda \right) \right]^2 \quad \text{Eq. 3. 5}$$

In [48], the expression of R is,

$$R = \sum \left[I_{sc, filters} - \left(device\ area \times \int_{\lambda_{min}}^{\lambda_{max}} E_{\lambda, filters} \cdot \sum_{i=1}^N a_i \cdot \left[-\left(\frac{\lambda - b_i}{2c_i^2} \right)^2 \right] d\lambda \right) \right]^2 \quad \text{Eq. 3. 6}$$

To achieve the objectives in polychromatic fitting, R is minimised. Taking Eq. 3. 5 as the objective model, optimisation of R is performed ($R \approx 0$). Commonly, the iterative gradient method with parameter x is applied to solve a minimisation problem (Eq. 3. 7).

$$\min_{x \in \mathbb{R}} R(x) \quad \text{Eq. 3. 7}$$

Where in this case, the parameter is referred to those of $SR_{\lambda, mod}$. The flow of this algorithm is demonstrated in Figure 3. 7.

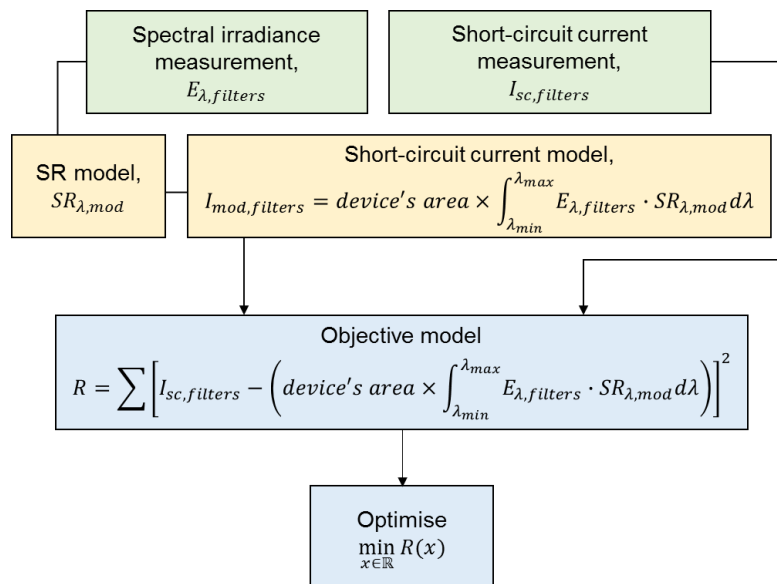


Figure 3. 7. Simplified flow chart illustrating the steps in constructing the model for fitting the polychromatic measurement data.

3.3 Evaluation of the polychromatic method measurement setup

The polychromatic measurement method for small area PV devices employs a steady state solar simulator as a light source with an array of very thin polychromatic broadband filters of polymeric materials, each placed in a small filter holder [48]. To be able to measure the photoresponse of large area devices, a short-pulse solar simulator is used (Pasan 3B). As for the filtering of the light source, the application of the same set of filters as [48] with the high intensity flash light results in physical damage to the filters, adversely affecting the measurement plane non-uniformity. To avoid this issue, a replacement set of hard plate broadband filters have been carefully selected to be used in the simulator to produce the required diversity in spectral irradiance. The throughput spectral irradiance, $E_{\lambda, filters}$ projected onto the measurement plane is evaluated using a spectroradiometer. Accuracy in the current measurement of the DUT under polychromatic illumination, $I_{sc, filters}$ is evaluated and the effect of the filters on the irradiance uniformity and spectral measurement is investigated. The objective of this evaluation is to identify the sources of uncertainty in the polychromatic SR characterisation method at large scale. The measurement uncertainty is incorporated in the fitting algorithm for the determination of the SR characteristic using a Monte-Carlo simulation method. This will be detailed in the following chapter.

3.3.1 Pasan 3B simulator as light source

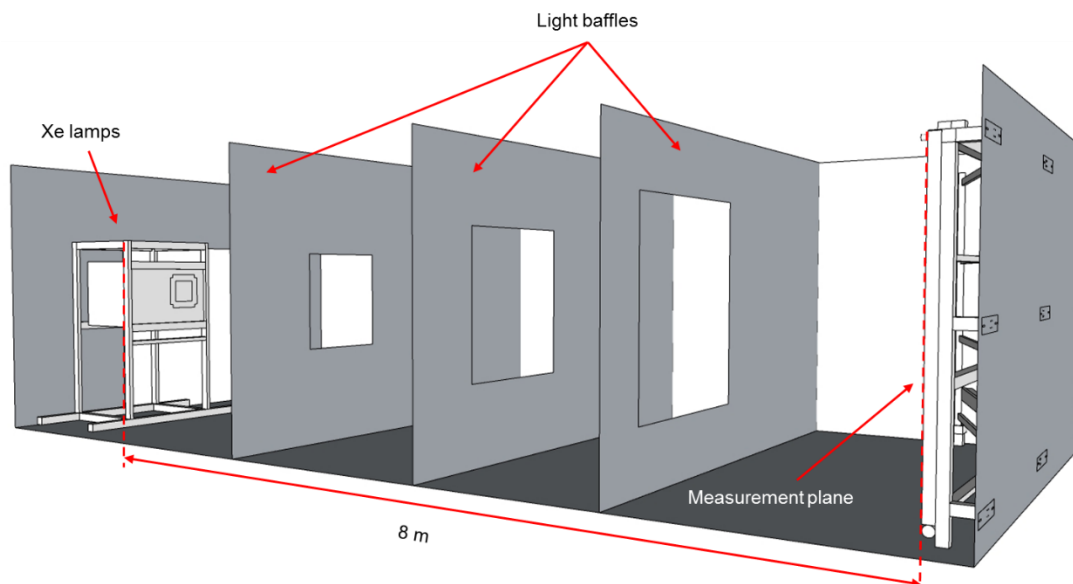


Figure 3. 8. Schematic of the Pasan 3B simulator in CREST showing Xenon lamps and measurement plane of the facility.

Measurement of I-V characteristics of full size PV modules using a flash or short-pulsed solar simulator is common in the PV industry and in research laboratories. In such a system, the uniformity of the

projected illumination across the measurement plane is high, to meet solar simulator classification (IEC 60904-9) [33]. For the Pasan 3B simulator as used in CREST, the non-uniformity is less than 2% over a measurement area of 2x2 m. The optical quality falls into class AAA for spectral match to the AM 1.5 reference spectrum, non-uniformity of irradiance and temporal stability. The system measures I-V characteristics of commercial PV modules within an uncertainty of 2.5% at STC. It is equipped with a filter cassette to house up to 20 filters and filter shifting system adjacent to the main light source. Neutral density mesh filters are installed in the system as standard to measure the performance of PV modules at varying irradiance. A monitor cell is fixed in the measurement plane to monitor the irradiance level. A schematic of this facility is shown in Figure 3. 8.

The development of the polychromatic measurement method to full size PV modules described in the following has taken place using the Pasan 3B solar simulator facility. At 8 m distance, the simulator can project an irradiance exceeding 1000W/m² which indicates that the output intensity near the lamps is very high. The paper-like polymeric material filters as used in [48] are not suitable to be employed in the Pasan system because of the lack of robustness in extreme conditions (i.e. abrupt increase/decrease in irradiance) which has historically resulted in rapid damage to the filters. For this reason, having a high physical and optical durability is a requirement in choosing the material of the replacement polychromatic filters.

3.3.2 Broadband filter selection

One of the drawbacks of employing narrow-band filters with large simulator such as the short-pulsed simulator is that the uniformity of the throughput illumination will be severely affected. The evaluation of broadband filters includes the aspect of light transmittance profile and its effect on the non-uniformity of the throughput irradiance on the measurement plane.

Light transmittance

To create a variation of spectral distributions, 15 polychromatic broadband filters including a small number of colour band filters have been carefully selected based on their transmission profiles. Each filter in the set has a unique light transmittance to maximise the variation of spectral irradiance throughout the usable wavelength range of typical PV modules from the UV to the NIR. Throughput total irradiance of the selected filters is measured by the (c-Si) monitor cell. The light transmittance profile of the filters with corresponding irradiance is shown in Figure 3. 9 and Table 3. 1 respectively.

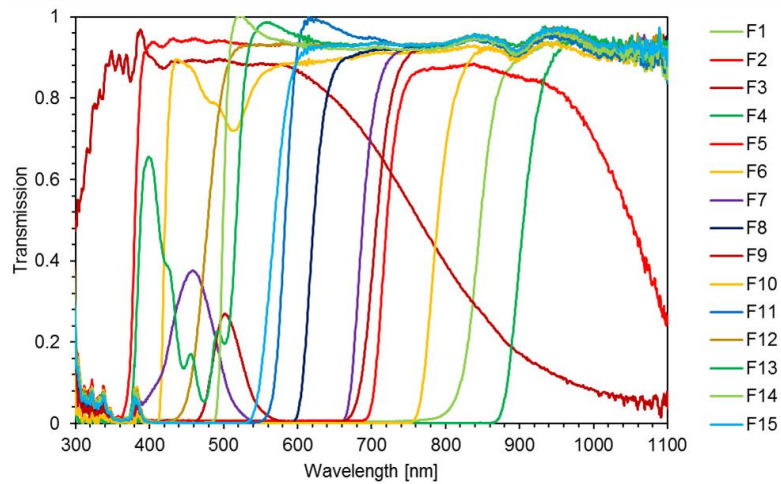


Figure 3. 9. Transmission profile of polychromatic broadband filters and a small number of colour band filters used in the polychromatic measurement setup.

Table 3. 1. List of materials and throughput irradiance level of the selected filters

Filters	Material / manufacturer	Measured throughput irradiance [W/m ²]
F1	Glass / Schott	228
F2	Glass / Schott	376
F3	Glass / Schott	577
F4	Plastic / Clarex	150
F5	Plastic / Perspex	933
F6	Plastic / Perspex	867
F7	Plastic / Perspex	521
F8	Plastic / Perspex	618
F9	Plastic / Perspex	481
F10	Plastic / Perspex	310
F11	Plastic / Perspex	705
F12	Plastic / Perspex	866
F13	Plastic / Perspex	846
F14	Plastic / Perspex	838
F15	Plastic / Perspex	724

In general, optical filters are made of glass. An optical glass filter is expensive due to the delicate manufacturing process for a precise cut-on/cut-off wavelength, customised to specific application. Expanding the filter to the size of the aperture of the light bulbs in the Pasan system (36x8cm per light bulb, Figure 3. 10) can be very costly. The polychromatic filters used here are made of cheap thermoplastic material which cost only about £5 per 40x40cm piece (apart from the colour band filters which are glass). This adds an economical advantage to the polychromatic method over the

conventional monochromatic method where a piece of narrow-bandwidth filter can cost up to £300 per 5×5cm. Coloured plastic sheets used in this work have a minimum thickness of 3mm and are sturdy, so can be fitted in the filter cassette in one piece. The glass filters on the other hand, are more fragile and smaller in area, therefore framing is necessary to install them in the cassette slots (Figure 3. 10).

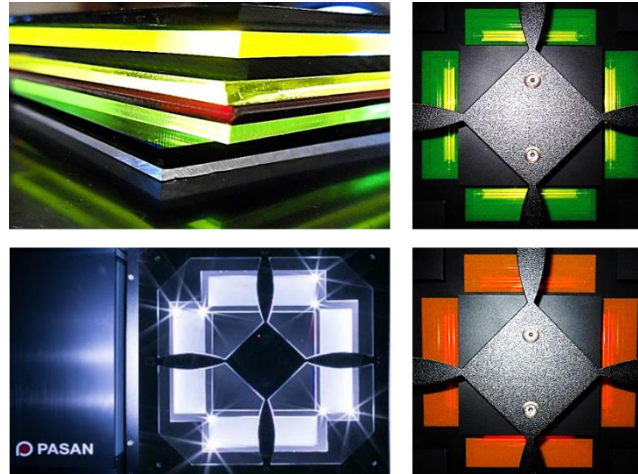


Figure 3. 10. Photographs of polychromatic filters used in the Pasan simulator (top left), Xenon light bulbs with filters (right) and without (bottom left).

3.3.3 Irradiance non-uniformity

The throughput irradiance of the selected filters varies from as low as 150 W/m² to 933 W/m² (Table 3. 1). To investigate the effect of inserting these additional filters into the light path on the uniformity of irradiance in the measurement plane, non-uniformity measurement is carried out in accordance with the IEC 60904-9 [33] for each filter.

$$Non - uniformity \{ \% \} = \left[\frac{max\ irradiance - min\ irradiance}{max\ irradiance + min\ irradiance} \right] \times 100 \quad Eq. 3. 8$$

A linear array of 11 photodiodes, attached to a movable beam is laid horizontally across the measurement plane (Figure 3. 11). The sensors were calibrated under natural sunlight prior to the measurement. The bar is raised vertically up the measurement plane (2m) in 0.1m steps after each flash to create an irradiance map of 400 points. The non-uniformity of the unfiltered CREST Pasan light source is determined in this way as 1.54%. The uniformity map of this measurement shows an almost symmetrical pattern where the irradiance is lower in the central region of the measurement plane (top-bottom) and higher at the edges of the plane (Figure 3. 11).

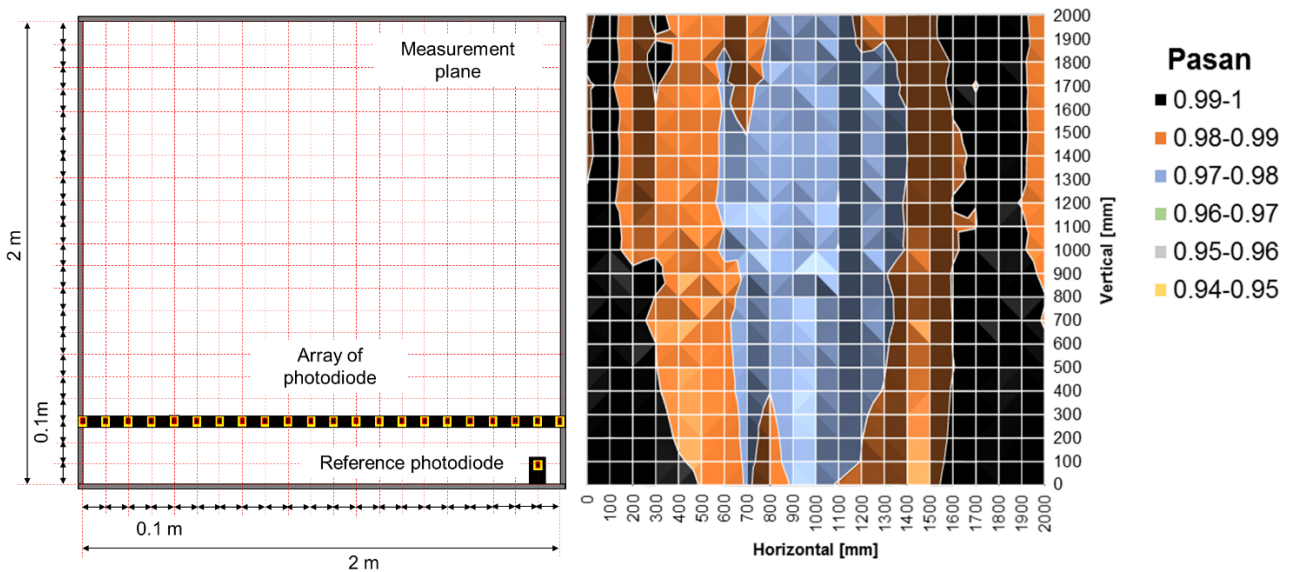


Figure 3. 11. Schematic image of non-uniformity measurement setup with an array of diode lays horizontally across the measurement plane and reference photodiode fix at one place (left). Result of non-uniformity measurement of unfiltered Pasan irradiance (right).

Figure 3. 12 shows the uniformity maps of the throughput irradiance of all the filters. The most noticeable result is from the measurement of F4 where low irradiance is observed across most of all points while the pattern of the map still follows the trend from the measurement of the unfiltered Pasan light source. This corresponds to the lowest throughput irradiance measured from the set of selected filters (Table 3. 1). Non-uniformity of F4 over the whole measurement plane is 3% which indicates a 1.46% increase in the non-uniformity in the filtered Pasan system.

Other significant results are from the measurements of F1, F2, and F3 of the glass material. The trend in the uniformity maps for these filters shows a very similar pattern, yet different to the map of the unfiltered Pasan light source. The measured irradiance is mostly low on the left side of the measurement plane and increases gradually as it shifts to the right edge. The non-uniformity of these filters are measured at 2.62%, 2.55% and 2.71% for F1, F2, and F3, respectively, which is about 1% higher than that of the unfiltered light. Other uniformity maps generally show very similar pattern to Figure 3. 11 with non-uniformity ranging from 1.4% to 1.68%. This indicates that the non-uniformity of the throughput irradiance is hardly affected.

From this measurement, it can be concluded that the trend in the uniformity depends on the filter material rather than the throughput irradiance level or the spectral transmittance profile of the filters. Although high non-uniformity over the whole plane is observed in the measurement of F4, the uniformity map actually shows a significant difference only at the extreme corners of the measurement plane which

covers about 1.4% of the 2x2m region. By taking these corners out of the picture, the non-uniformity can be improved by 0.3% even though this means that the measurement area will be reduced. However, this reduction of area will not affect the measurement of even full typical size (1x1.6m) PV modules as the remaining area can still comfortably accommodate them. The effect of irradiance non-uniformity on the $I_{sc, filters}$ measurements will be discussed in the following section.

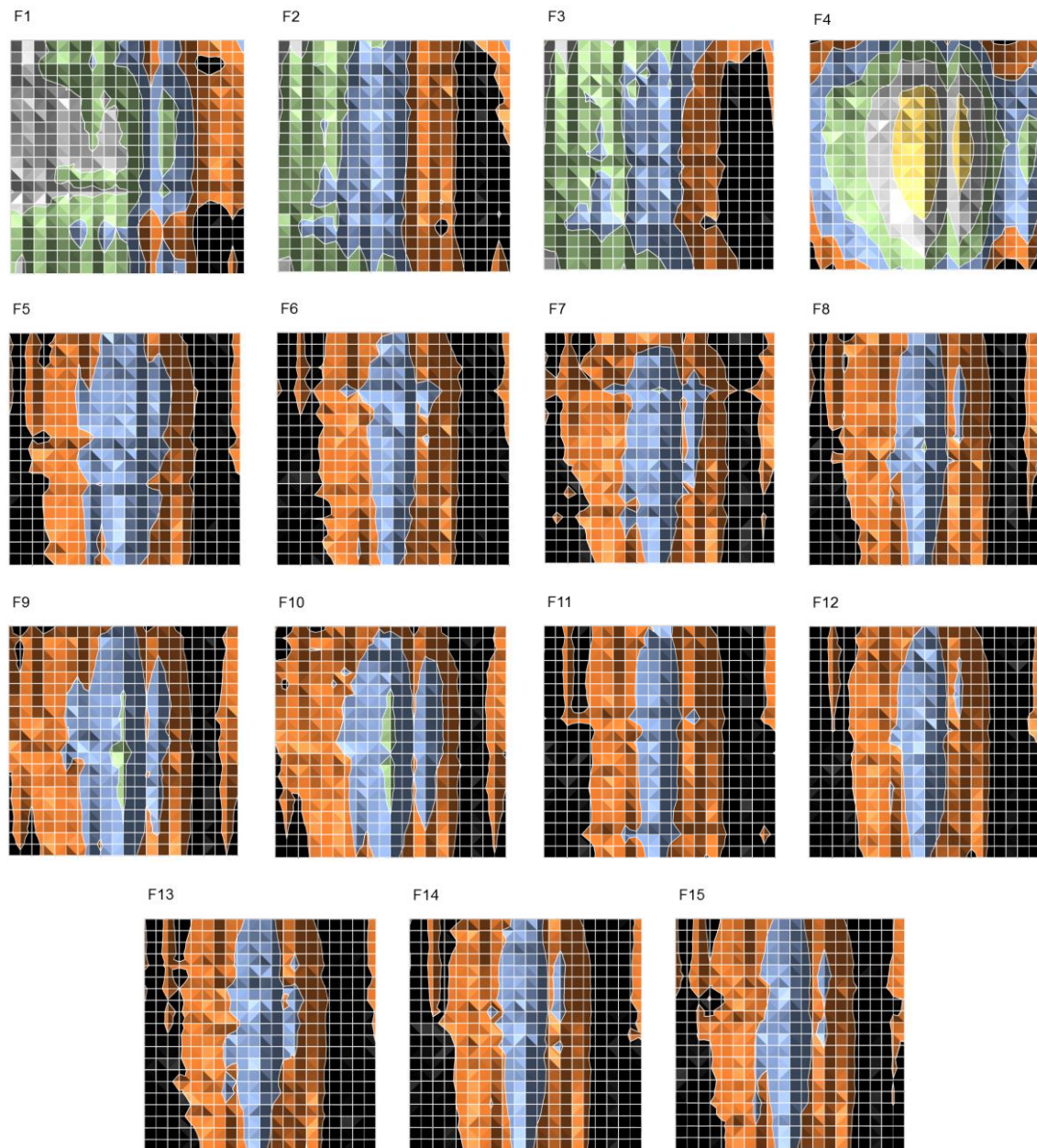


Figure 3. 12. Measurement of throughput irradiance non-uniformity of polychromatic filters over 2x2m measurement plane.

3.4 Electrical and optical measurement of polychromatic method

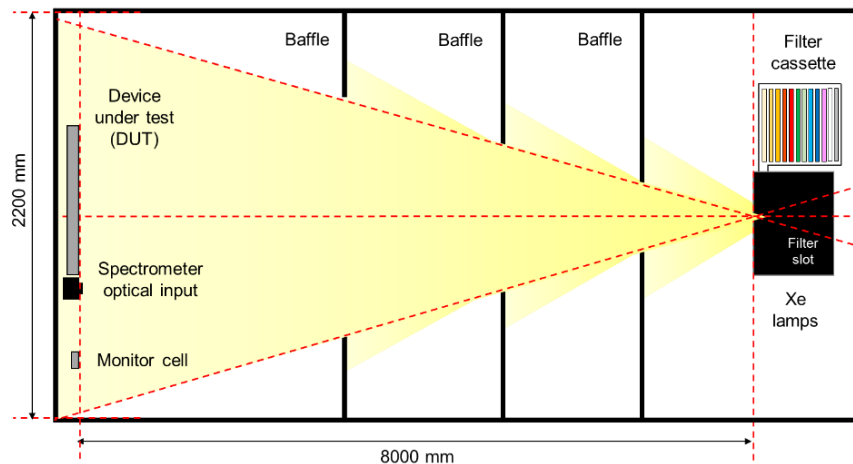


Figure 3. 13. Schematic of the polychromatic measurement setup using the Pasan 3B facility (plan view).

The measurement of $E_{\lambda, filters}$ with corresponding $I_{sc, filters}$ of the DUT is performed simultaneously for each filter in automated mode (Figure 3. 13), in which the filters are positioned by motors in turn, the simulator triggered and measurements of both I-V curve and spectral irradiance are taken. The $I_{sc, filters}$ is extracted from the I-V curve measured by the Pasan system while the $E_{\lambda, filters}$ is measured using an Avantes CCD array spectroradiometer. Prior to the measurement, 16 consecutive flashes are triggered as a warm-up to stabilise the temperature of the light bulbs. This is necessary in order to reduce the error due to flash-to-flash variation, as a result of non-uniform spectral behaviour against temperature of the four individual lamps in the simulator [50]. Incorporating this procedure improves the repeatability in current measurement by up to 0.4% depending on the technology of DUT [66]. The $I_{sc, filters}$ - $E_{\lambda, filters}$ measurements of each filter are averages of measurements over 4 flashes.

3.4.1 Short-circuit current measurement

Source of uncertainty in indoor solar simulator measurements in STC

The estimation of uncertainty in the electrical parameters measurement of PV modules such as the P_{max} , I_{sc} and V_{oc} using indoor solar simulator takes into account the contribution in the calibration of reference cell (RC) in the setup. The uncertainty in the measurement of module performance using large area solar simulator such as the standard short-pulsed simulator has higher uncertainty compared to the small area one due to the application of reference cell and also the high non-uniformity of the projected illumination over the wide measurement plane of 2x2m. Source of uncertainty in indoor simulator measurements in STC are [66]:

Table 3. 2. Source of uncertainty in indoor solar simulator measurements.

Uncertainty sources in the STC
<p>In Irradiance intensity: RC calibration RC drift Irradiance non-uniformity at the target Temporal change in irradiance Difference in reflections between DUT and RC Orientation of DUT and RC Position of DUT and RC</p>
<p>In junction temperature: Temperature sensor calibration Imperfect data acquisition of temperature measurement Difference between position of sensor and junction Temperature non-uniformity Temperature drift during measurement</p>
<p>In irradiance spectrum: Mismatch factor Filter deterioration and lamp aging Non-uniformity of spectral irradiance Temporal change of spectrum</p>
Uncertainty in I-V data acquisition (DAQ)
Offset and range Series resistance due to connectors and packaging Room temperature effect on measuring equipment Shunt resistors calibration and temperature effect Parameter extraction uncertainty
Uncertainty sources in measurement area
Area definition Reflection Measurement resolution Edge interpretation
Variation of repeat measurements

Uncertainty in short-circuit current measurement under polychromatic irradiance

Standard uncertainty in the measurement of $I_{sc, filters}$ using the Pasan system have been evaluated. Calibration of Pasan system contribute to about 0.12% uncertainty in the measurement of $I_{sc, filters}$, while temperature effect contribute to 0.039% uncertainty per °C. The extraction of parameter I_{sc} from the I-V curve sweep of Pasan system contribute to the uncertainty in $I_{sc, filters}$ by 0.05% due to fitting error and uncertainty due to repeatability of measurement with the system is evaluated at 0.23%. Uncertainty caused by non-uniformity effect is filter-dependent thus it is calculated separately for each filter.

For standard I-V measurement under STC, the uncertainty in I_{sc} is mostly affected by the irradiance non-uniformity and MMF correction due to the discrepancy in the Pasan and reference spectra. The

MMF correction is irrelevant in the polychromatic method, therefore the predominant uncertainty contribution in the measurement of $I_{sc, filters}$ is from the irradiance non-uniformity effect. The propagation of standard uncertainty of $I_{sc, filters}$ measurement ($u_{I_{sc, filters}}$) is in accordance with the GUM handbook as described in 2.4.1. For the measurement of full size PV modules the calculated $u_{I_{sc, filters}}$ is ranging from 1.5% to 2.5%. This is corresponding to the lowest and highest measured irradiance throughput by F4 and F6 respectively.

The calculated $u_{I_{sc, filters}}$ in the polychromatic measurement of full size module with the Pasan system is within the uncertainty margin of STC, 2.52%. Thanks to the reasonable uniformity of throughput irradiance of Pasan illumination across measurement plane, a reliable measurement of full size PV modules can be performed. For the measurement of small size device, the $u_{I_{sc, filters}}$ is expected to be even lower.

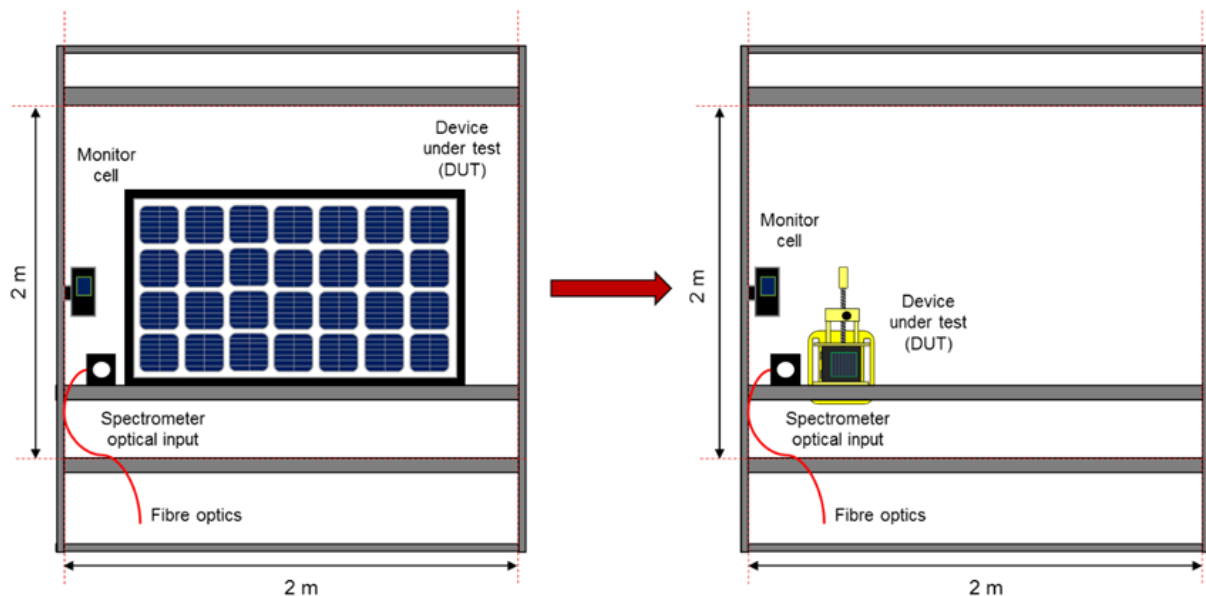


Figure 3. 14. Schematic of measurement plane showing the difference in the occupied area by a full size module and reference cell.

Reduction of occupied area from full size modules to individual cells can significantly improve the non-uniformity, hence low uncertainty in the $I_{sc, filters}$ can be achieved. Figure 3. 14. shows the difference in measurement area of the commercial modules and 2x2cm reference cell. The dotted graph on the same figure demonstrates the difference in non-uniformity measurement of the throughput irradiance against the unfiltered Pasan light source over the respective occupied area. The relatively small area taken by a 2x2cm reference cell within the measurement plane brings the non-uniformity down to less than 1%. Due to this, the calculated $u_{I_{sc, filters}}$ of small area devices using Pasan simulator for all filters can be as low as 1%.

3.4.2 Uncertainty in spectral irradiance measurement

Prior to the spectral measurement, a few adjustments are made to the spectroradiometer. It is necessary to leave the detector switched on for a period before the measurement sufficient that the temperature of the device will stabilise. Taking a small number of “blank” measurements is also recommended as a warm-up for the device to meet the requirement of the electronics target operating temperature between 32°C and 34°C. The integration time is pre-set to 7.5ms with 2ms internal delay to ensure that the stable plateau within the 10ms pulse duration of the Pasan simulator can be captured.

The optimum integration time is chosen based on non-linearity effects of the detector. Discussion regarding the non-linearity of CCD detector in respect of irradiance and correlated stray light effects has been detailed in [66]. Non-linearity and stray light effects of the Avantes spectroradiometer used in CREST have been tested through a series of measurements with varying integration times and irradiance levels using a FEL lamp with stable power supply. The results show a significant non-linearity outside the raw counts range of 8000 to 50000. In consideration of this, the spectral measurement procedure using the Avantes is restricted to 50000 counts.

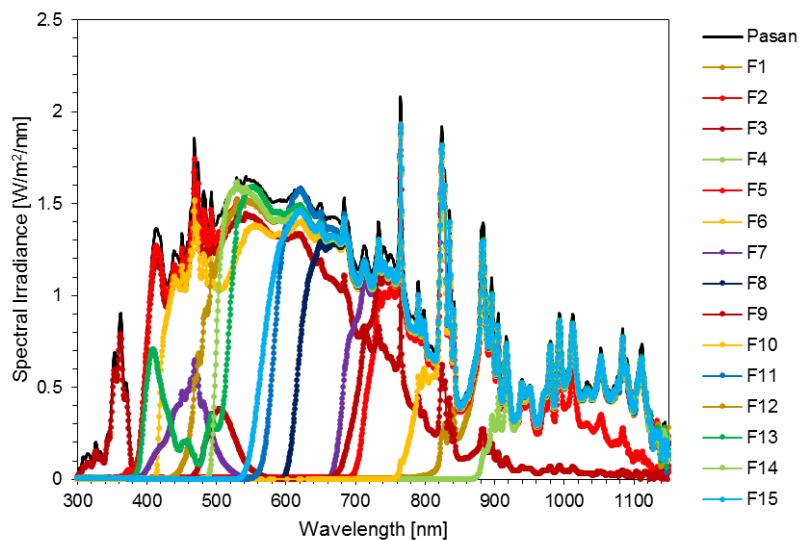


Figure 3. 15. Spectral measurement of throughput irradiance of all filters in the measurement setup.

Uncertainty contributions in $E_{\lambda, filters}$ measurement mostly depends on the calibration of the Avantes spectroradiometer. The detector is calibrated against a standard lamp as measured by the PTB using a high precision spectroradiometer. The spline interpolation method is used to transfer the standard lamp measurement into the Avantes spectroradiometer. The calculation of absolute spectral irradiance ($W/m^2 /nm$) from the raw counts measurement allows for correction of the non-linearity effect, stray light effect and transfer function during the calibration (Figure 3. 16). High uncertainty can be seen to

remain in the spectral measurement of the Pasan light source in the UV and NIR regions – higher than 30% in total uncertainty (k=1) due to the issue regarding the spectral non-uniformity (Figure 3. 16) [66].

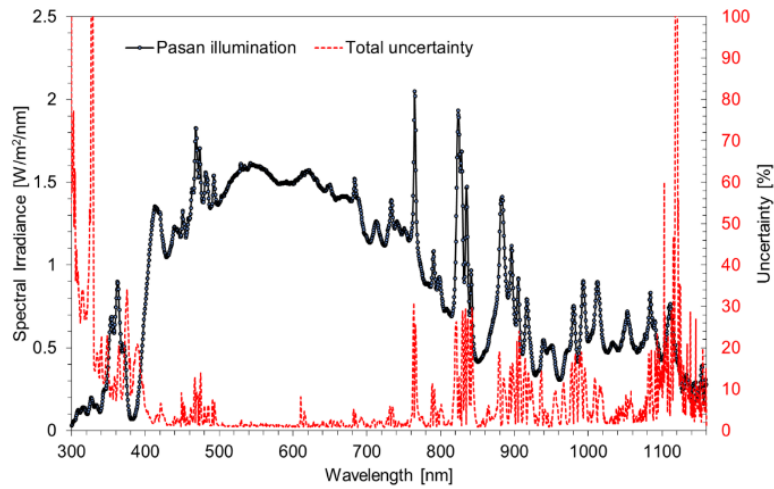


Figure 3. 16. Spectrally resolved measurement of unfiltered Pasan with corresponding total uncertainty per pixel array.

Figure 3. 17 shows the difference in spectral measurement of filter F3 in the UV region and F10 in the NIR region, against the spectral measurement of the unfiltered Pasan light source. From the graphs it can be seen that the variation in measurement of throughput spectral irradiance is relatively low despite the corresponding low signal in the UV region and high in the NIR region with the value of ± 0.25 and ± 1 respectively. This observation is in accordance with the calibration of the spectroradiometer with regard to with high non-linearity effects in the corresponding pixel, thus reducing the repeatability of measurement in this region.

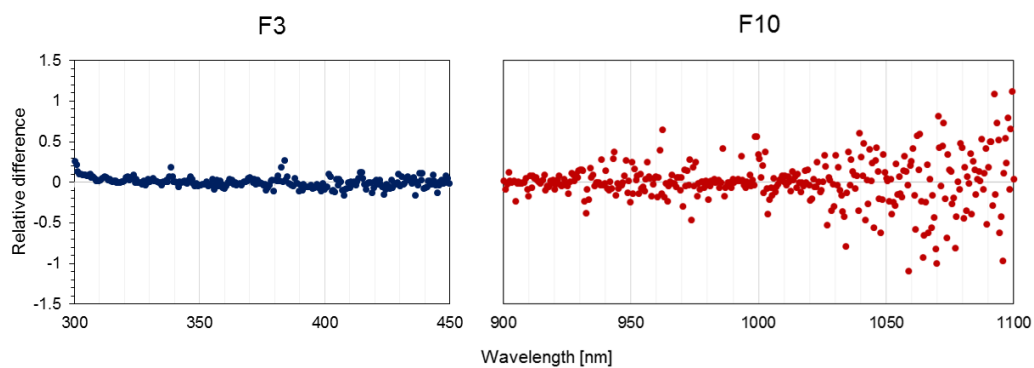


Figure 3. 17. Blue dotted graph shows the relative difference in spectral measurement of filter F3 and red dotted graph shows the measurement of F10 against the spectral the unfiltered Pasan.

3.5 Conclusions

This chapter presented review on the current methods used by various PV labs to characterise the spectral responsivity of PV devices, including the standard method, DSR [40]. The SR measurement of small area PV devices has demonstrated high accuracy where uncertainty of less than 5% in the UV and NIR region have already been reported. Low uncertainty in the SR measurement of PV cells contributes to a better calibration of measurement setups employing simulator for the performance measurement of PV devices. However, in the case of large device measurements, the importance of a reliable SR measurement is to achieve high accuracy in the performance calculation of PV modules under real operating condition.

Currently, the partial monochromatic illumination SR measurement method as reported in [59, 58] is regarded as the most precise method for SR characterisation of PV modules. However, due to the technical burden of the measurement apparatus, it is only limited to only a handful of PV labs worldwide. In this work, a practical SR measurement method for large area PV devices is developed, aiming to contribute to a reliable module energy rating assessment. The development of this method is based on the typical Pasan 3B simulator in CREST. The method is based on the novel polychromatic measurement method, which utilises broadband polychromatic illumination to measure the photoresponse of the module under test.

The polychromatic method combines results from the polychromatic measurement pairs of device short-circuit current and spectral irradiance and numerical fitting to determine the SR characteristic. Analysis of filter selection and its relation to the throughput irradiance non-uniformity has proven the suitability of the application of the coloured plastic sheets in the setup. Combination of the plastic sheets with a small number of colour band glass filters also adds an economic advantage to the method.

Uncertainty contributions from the measurement of $I_{sc, filters}$ under $E_{\lambda, filters}$ illumination are analysed from the evaluation of measurement setup. While the non-uniformity effect in the measurement depends on the dimension of the DUT, it is found that it is the predominant factor in the measurement of $I_{sc, filters}$. The measurement of non-uniformity of throughput irradiance have shown that the application of the coloured broadband filters effect the uniformity of Pasan illumination by only 0.5%. The relatively slight variation in the non-uniformity effect translate to about 1.5% - 2.5% calculated $u_{I_{sc, filters}}$ for the measurement of full size modules with the Pasan system.

Analyses of uncertainty in the spectral measurement using the Avantes spectroradiometer have been performed and reported in [66]. Using the calibration profile of the instrument, the absolute spectral irradiance is calculated, taking into account the stray light effect, non-linearity, and transfer function per pixel (wavelength). It is found that the uncertainty in spectral measurement of Pasaan illumination is mostly influenced by the non-linearity of the detector. High non-linearity of the CCD array corresponding to the NIR region result in uncertainty in the spectral measurement higher than 30%. At visible, the uncertainty is found to be relatively low at about 5%.

From the evaluation of polychromatic measurement setup, it is established that low uncertainty in $I_{sc, filters}$ measurement of the DUT is achievable while employing the broadband filters in the measurement setup. Consideration of the accuracy in the measurement of $I_{sc, filters}$ and corresponding $E_{\lambda, filters}$ is essential in the polychromatic measurement as this is the main input in the fitting algorithm for the determination of the SR characteristic of PV device. This subject will be further explored in the next chapter.

4 Spectral response measurement of full size photovoltaic modules

The development of a polychromatic SR measurement method for PV modules in this thesis is aiming for an exhaustive characterisation, to include uncertainty evaluation. The practicality of polychromatic measurements allows for the SR characterisation of PV devices of all sizes to be performed. The method requires 2 steps, i.e. optical/electrical measurement of the DUT and a data fitting algorithm. Discussion regarding the evaluation of measurement setup and uncertainty contribution into each measured element has been presented in the previous chapter. Here, the focus of discussion is on the integration of measurement data into the fitting algorithm for the final determination of the SR characteristic of the DUT.

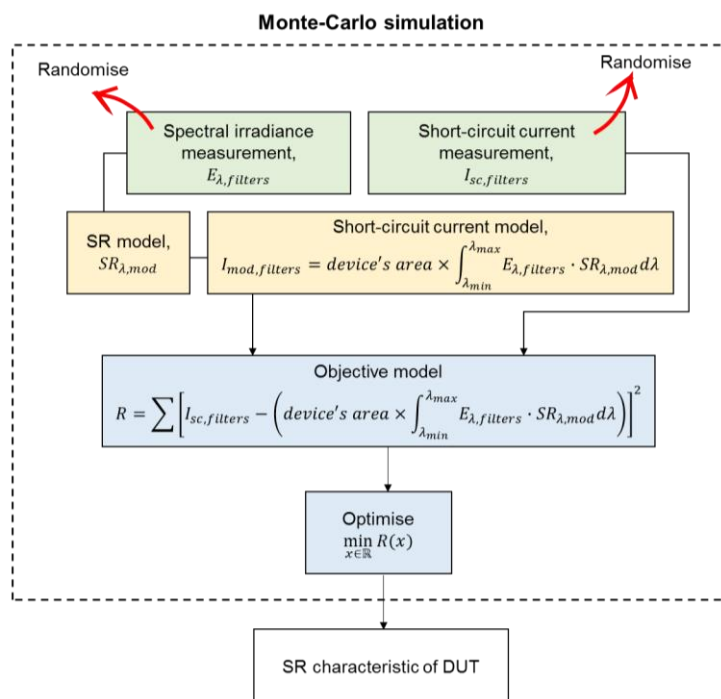


Figure 4. 1. Flow-chart of SR polychromatic measurement method.

The Monte-Carlo simulation method (MC) is used to combine the uncertainties in measurement into an integrated value, where a high number of simulation cycles are run using different input combinations, randomly varied in each cycle (Figure 4. 1) [67]. The development of the SR model to be used in the simulation and the analyses of factors affecting the polychromatic fitting algorithm will be detailed in this chapter. The validation of the SR polychromatic measurement method developed in this work is carried out by comparing measurement results of PV devices which have been previously measured using the conventional monochromatic method under an SR measurement inter-comparison campaign. Finally,

discussion regarding the practicality and optimisation of the SR polychromatic measurement method will draw this chapter to an end.

4.1 Introduction

4.1.1 Uncertainty propagation in the polychromatic SR method.

MC simulation is a type of probabilistic analysis used to calculate the impact of randomised inputs on the output of a system or process. The simulation can be used to propagate uncertainty in measurement data with complex distributions, for example in the calculation of PV device spectral MMF [46]. In the polychromatic method, since uncertainties associated with the required input measurements are different in size and vector, MC simulation is adopted to allow for a meaningful integration of measurement and data fitting parts of the process.

In this simulation, both spectral irradiance and electrical current measurements ($I_{sc, filters} - E_{\lambda, filters}$) are varied repeatedly within the corresponding uncertainty margin, producing $SR_{\lambda, mod}$ with fitted parameters at each iteration. As a result, a large sample of $SR_{\lambda, mod}$ will be generated. The median from the sample will be considered as the final SR value for the corresponding wavelength, while its uncertainty is derived from the standard deviation of the sample. In this way, the correlation between output from the simulation and uncertainty in measurements is preserved.

4.1.2 Varying input data

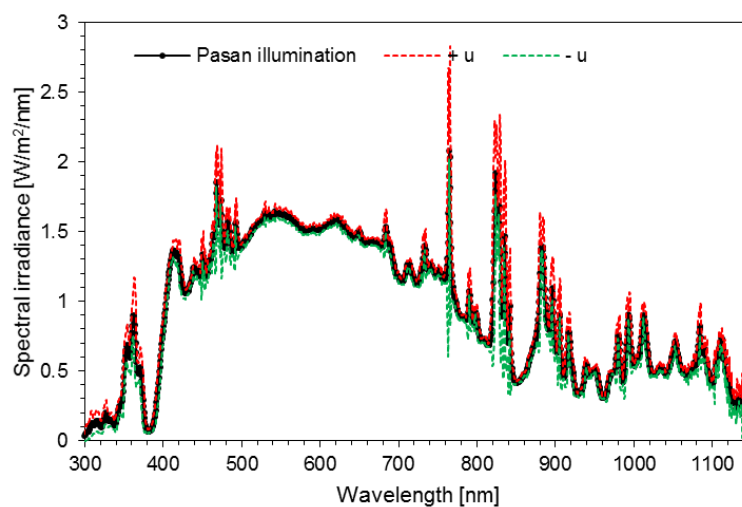


Figure 4. 2. Uncertainty envelope of the spectral measurement of the Pasan simulator irradiance.

The $I_{sc, filters}$ measurements are randomly varied within the corresponding $u_{I_{sc, filters}}$ envelope while a genetic algorithm - the random walk approach - is employed to sample the $E_{\lambda, filters}$ measurements. This more complex approach is adopted because randomly sampling the spectral measurement at individual wavelengths leads to underestimation of wavelength correlated uncertainty. Besides, it will also result in an excessive noise in the sample which will be cancelled out when integrated [46]. The random walk approach is used to shift the shape of $E_{\lambda, filters}$ within the permitted uncertainty envelope (Figure 4. 2) at each iteration in the simulation.

A random walk is a process to randomise a movement of an object by changing its direction at each turning point as it moves away from the starting point [68]. Although the number of steps from one point to another, magnitude and vector in which the object is moved are chosen randomly, the correlation between the turning points remains. Previously, this approach has been adopted in PV related research for the estimation of uncertainty of a wavelength-continuous integrated value such as the MMF as demonstrated in [46] and [69]. In the implementation of the polychromatic method, a random walk is generated and applied to each $E_{\lambda, filters}$ based on the corresponding total uncertainty at each iteration in the MC simulation. Figure 4. 3 shows an example of generated random walks that are used in this simulation.

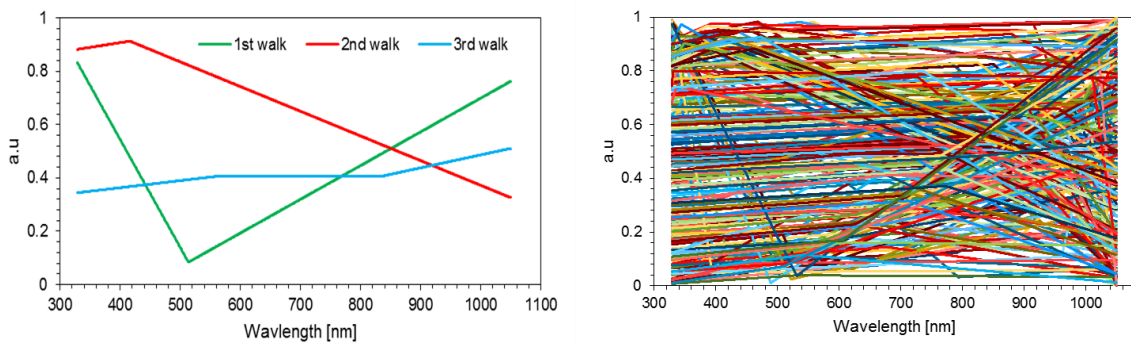


Figure 4. 3. Examples of random walks generated from 3 (left) and 250 (right) iterations.

4.2 Spectral response model

SR characteristics derived from this method are heavily dependent on the fitting algorithm (Figure 4. 1). The selection of spectral response model ($SR_{\lambda, mod}$) plays an important role in the fitting algorithm as it defines the type of relationship between the function and variables. Depending on the type of model used as $SR_{\lambda, mod}$, the convergence rate of fitted parameters will be different. The initial report on the polychromatic method [48, 62] employed a Gaussian summation function for the representation of SR characteristics. While the Gaussian function has a high degree of flexibility for the replication of curvy

graph shapes such as for a SR curve, the suitability of this function in the overall process still requires further evaluation.

4.2.1 Evaluation of continuous function as spectral response model

Replication of spectral response curves

The MC simulation calls for a high number of simulation cycles to obtain a robust selection of SR characteristics of the DUT from which the standard deviation can be derived. The simulation is first tested using the Gaussian summation model as $SR_{\lambda,mod}$ as in [48]. The Gaussian is a bell-shaped continuous function which consists of 3 parameters that represent the amplitude (h_i), its centre position (c_i), and its full width at half maximum (FWHM) (w_i) (Figure 3. 5).

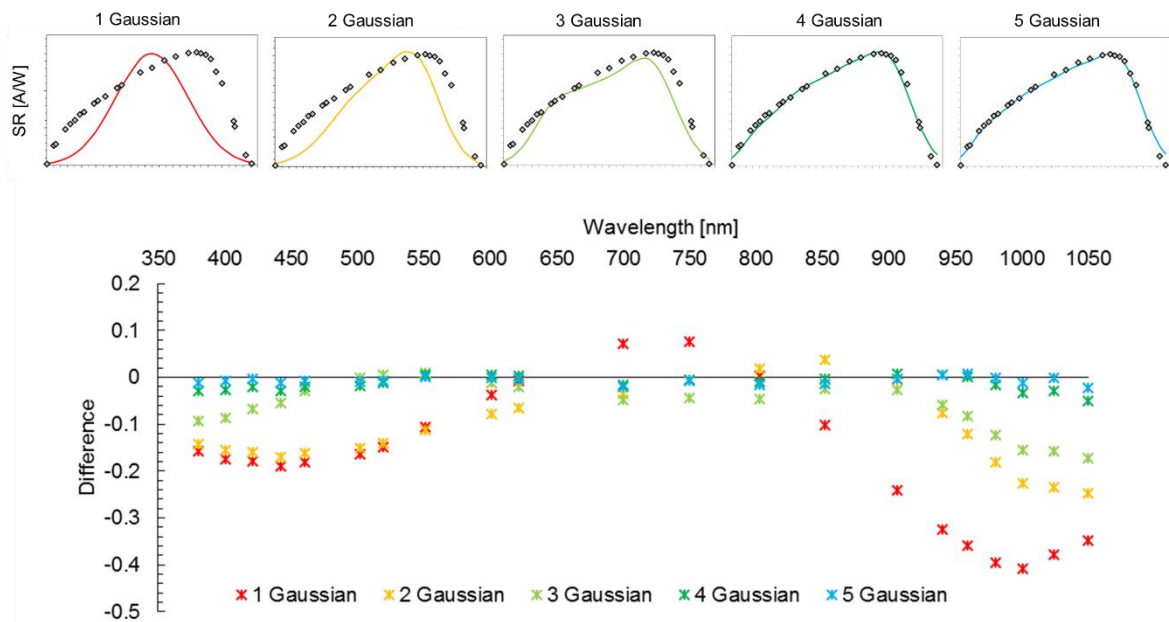


Figure 4. 4. The evolution of regression analysis using different Gaussian models to fit the measured SR points of a c-Si device (top). The graph shows the improvement of difference between the Gaussian models to the measurement of SR of the device at individual points as the number of Gaussians in the sum increases (bottom).

Summation of multiple Gaussian functions increases the parameters by 3 for each additional Gaussian. Figure 4. 4 shows direct regression analysis using different degrees of Gaussian summation to fit the measured SR characteristic of a c-Si device. It can be seen from the same figure that the relative difference between the modelled and measured curve gradually approaches 0 value as the number of Gaussians in the sum is increased. From this analysis, it is observed that high summation of the Gaussian function is able to replicate the shape of the SR curve quite precisely thanks to the flexibility provided by a large number of parameters [48, 69] (Figure 4. 4).

4.2.2 Gaussian summation function and Monte-Carlo simulation

Mathematical expressions with such a high flexibility can be a drawback when used with the MC simulation due to the increased sensitivity in the parameter convergence towards uncertainties and errors incorporated in the input data. Slight deviation in the input will divert the direction in the parameter convergence path greatly. The varying non-linearity effects across the detector pixels in the spectral measurements and irradiance non-uniformity in current measurements could result in parameter misconvergence during the optimisation of R (goodness-of-fit indicator). This is reflected in extreme values of fitted parameters or premature termination during the fitting. In both cases, the solutions will still be accepted by the optimiser because while the $SR_{\lambda,mod}$ is in a function of wavelength, integrated $I_{sc,mod}$ value is used as a key decision to optimise R (Figure 3. 7). This results in an output curve for $SR_{\lambda,mod}$ that is not representative of the typical SR characteristic of a PV device even though the area under the curve produces a value that satisfies the objective of optimisation process i.e. $R \approx 0$.

Figure 4. 5 shows the result of MC simulation of the polychromatic SR method applied to a c-Si device with 50 iterations and using a 5-Gaussian sum for the SR model (line graphs with different shades of grey). It can be seen from the figure that a very high degree of variation in the output curves is observed in comparison to the monochromatically measured SR. High uncertainty in the spectral irradiance measurement in the NIR region due to a non-linearity of the detector have led to the significant variation observed from the graph (Figure 3. 16). The gradient approach adopted in the optimiser to solve the non-linear Gaussian function as explained in the previous chapter, adds to starting values dependency related problems which further increase the uncertainty in the optimisation of R .

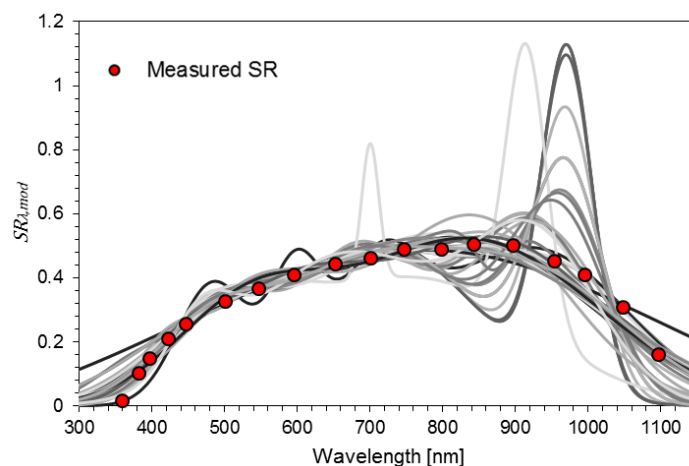


Figure 4. 5. Result comparison between 50 modelled SR curves generated through the MC simulation and the measured SR of a c-Si device.

Convergence of parameters in the fitting process however can be restricted by applying constraints in the optimiser, which is subject to knowledge of the type of DUT as reported in [69]. Adding constraints

in the fitting algorithm is not ideal because it will increase the element of uncertainty and limit the implementation of the method only to certain types of PV devices. For this reason, a mathematical expression based on a piecewise function approach has been developed so that the issues related to high complexity and flexibility such as in the continuous function can be minimised.

4.2.3 Development of spectral response model

Step function as spectral response model

One way to reduce the sensitivity of parameter convergence in the gradient approach to noise and uncertainties in the polychromatic measurements is by restricting the moving direction of parameters to one dimension. This can be done employing the step function in $SR_{\lambda,mod}$. The step function is a type of linear piecewise function, defined by a constant within an interval that makes a segment of horizontal line [70]. Increasing the number of segments with very narrow intervals in the step function will result in similar properties to the continuous function such as the Gaussian summation with regards to the capability to replicate curved graphs (Figure 4. 6).

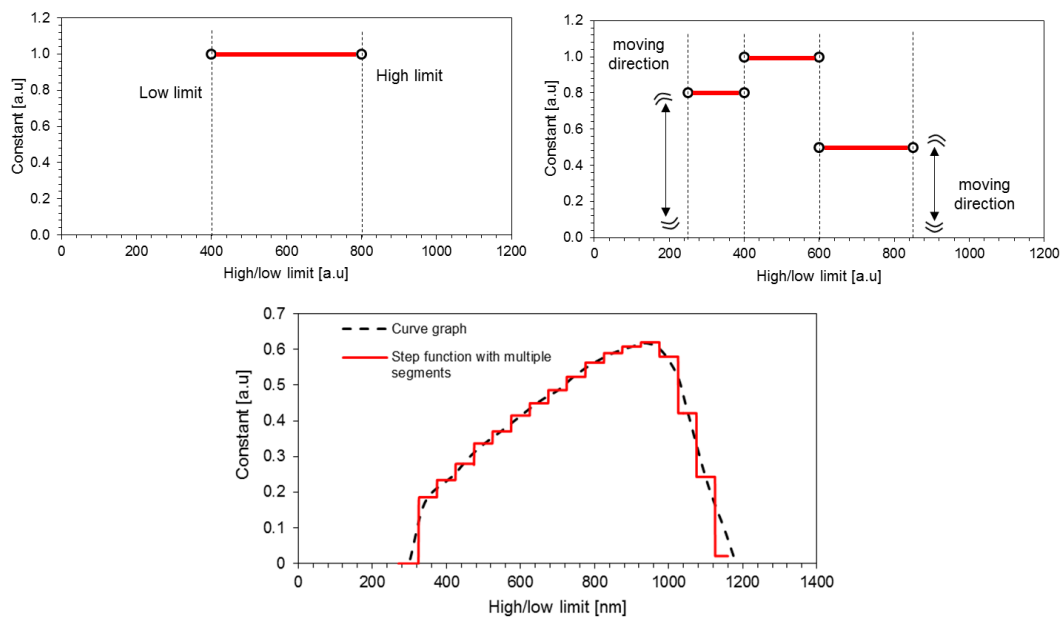


Figure 4. 6. Example of step functions showing a segment of horizontal line (left) and multiple segments (right). Replication of curvy graph by the increased steps in the step function (bottom).

In this development to the polychromatic data fitting algorithm, the constant values (heights) for each segment are set as the parameters to fit. The resolution of $SR_{\lambda,mod}$ is determined by the number of segments in the step function, which is chosen by the user. High/low limits of the function are set prior to the fitting so that the distribution of the steps will cover the range of usable wavelength in typical SR

characteristics of PV devices. In this work, the same size of interval is applied to all segments in the function to not pre-suppose any particular SR curve shape, although this could be altered as required. The central wavelengths of each segment are taken as the discrete points in the final representation of $SR_{\lambda,mod}$. The mathematical expression for the step function used in the polychromatic data fitting is as below:

$$SR_{\lambda,mod} = \begin{cases} x_1; & \lambda_{min} < \lambda < \lambda_{min+y} \\ x_2; & \lambda_{min+y} < \lambda < \lambda_{min+2y} \\ & \vdots \\ x_n; & \lambda_{max-y} < \lambda < \lambda_{max} \end{cases} \quad \text{Eq. 4. 1}$$

Where x is the parameter, n is the number of segments, y is the size of interval, and λ_{min} and λ_{max} are the lower and the upper limits of the step function.

A curve fitting simulation is performed to evaluate the validity of using the step function in $SR_{\lambda,mod}$ modelling. A step function with 18 parameters (segments) is used to fit the monochromatically measured SR curve of a c-Si device. For comparison, the same analysis is performed using a continuous function (Gaussian summation) with an identical number of parameters. Results from this simulation show good agreement between the step function and measured points is achieved, with percentage differences within $\pm 1\%$ for wavelengths from 400nm to 1100nm. Similar results are also observed in the simulation using the Gaussian summation model, although this shows more wavelength-localised variability (Figure 4. 7).

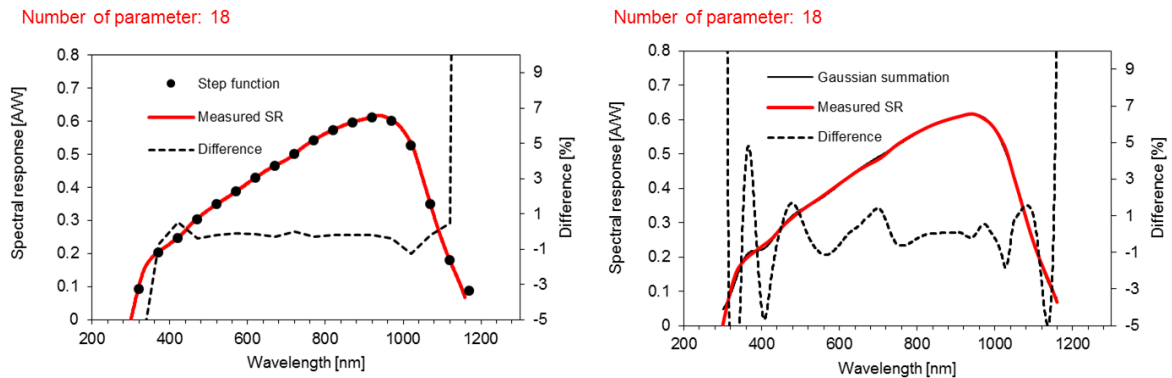


Figure 4. 7. Comparison of regression analysis results using step (left) and Gaussian summation (right) functions as the SR model fit to measured SR data points.

The suitability of the step function in the modelling of $SR_{\lambda,mod}$ has been validated through this simulation. The restriction of the direction of parameter convergence is expected to contribute to increased stability of the optimisation process while the flexibility to model spectral response of arbitrary shape is

maintained. Application of a linear model in the optimisation of R will eliminate also the starting value sensitivity which is raised in the optimiser as a result of solving a non-linear model. This will improve the speed in parameter convergence while increasing the repeatability of results and the probability of success in finding a solution.

Pre-set condition of step function in polychromatic method

The degree of flexibility of the step function used in $SR_{\lambda,mod}$ is dictated by the predetermined number of segments, n (Eq. 4. 1). High flexibility in the step function introduced by using a larger number of segments can lead to instability if taken to a point at which noise elements in the input data are being over-fitted, while at the other extreme too few segments will result in low wavelength resolution in the output $SR_{\lambda,mod}$ and poor shape match. To determine the right balance between flexibility and stability in the optimisation of R , a controlled simulation of the polychromatic method is performed using the monochromatic calibration SR of a c-Si device.

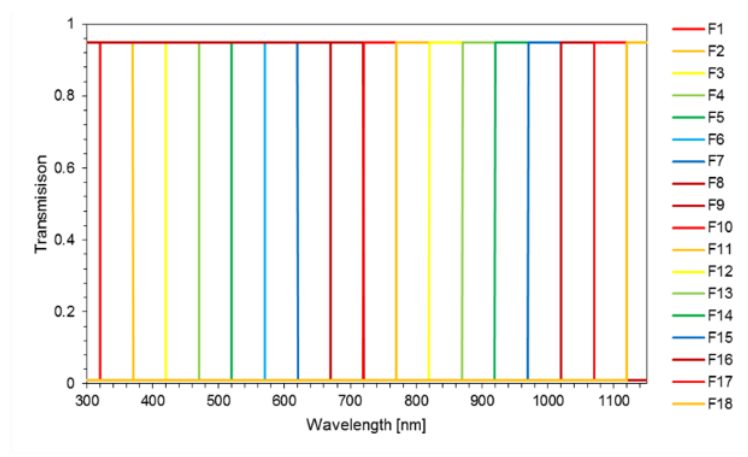


Figure 4. 8. Light transmittance profile of the combined artificial edge filters

The simulation employs a set of artificial (ideal, modelled) edge filters (a combination of low pass and high pass filters), consisting of 18 filters with 50 nm gap between the cut-off wavelengths (Figure 4. 9). Throughput spectral irradiance ($E_{\lambda,mod,simulation}$) for the filters is calculated using the (actual, measured) spectral distribution of the Pasan light source as reference. Eq. 2. 5 is used to calculate the modelled current ($I_{sc,mod,simulation}$) where $SR_{\lambda,mod}$ is the calibration SR of the c-Si reference cell. Five step functions with various numbers of segments, n are used in a MC simulation to analyse the effect on the output $SR_{\lambda,mod}$. The MC simulation is performed with 100 repeated counts using the $E_{\lambda,mod,simulation}$ - $I_{sc,mod,simulation}$ as inputs for the fitting of each of the step functions. The variation of $E_{\lambda,mod,simulation}$ in the MC simulation simulates error of up to 5% for wavelengths from 400nm to 1150nm and 10% outside this range. Error of up to 1% is applied to all $I_{sc,mod,simulation}$.

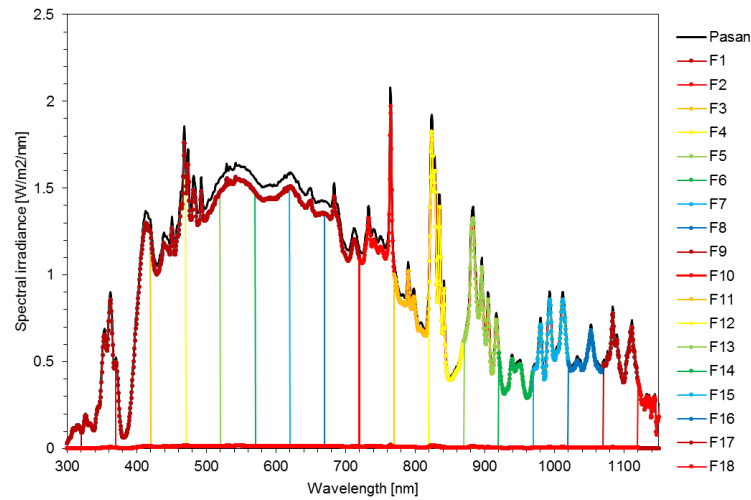


Figure 4. 9. Calculated spectral irradiance distribution used in the simulation based on the transmission profile as shown in Figure 4. 8 .

Results from randomly varied elements (19 from $E_{\lambda,mod,simulation}$ and $I_{sc,mod,simulation}$ in 100 cycles) in the MC simulation are compared to the calibration SR used in the calculation of $I_{sc,mod,simulation}$. Figure 4. 10 shows the relative difference between output $SR_{\lambda,mod}$ modelled with different n (8 and 18 segments) to the calibration SR at each of the monochromatic measured wavelengths. Good agreement between the output $SR_{\lambda,mod}$ and calibration SR can be observed from the MC simulation with fewer segments in the step function (within $\pm 2\%$). On the other hand, larger difference, up to 10%, are generally observed when the SR is modelled with a higher number of segments across the measurable wavelength range.

The $SR_{\lambda,mod}$ obtained from this simulation is the median of the 100 samples generated through the MC simulations. A large uncertainty margin (derived from the standard deviation of the samples) indicates that parameter convergence is unstable which results in great variation in the final output. As can be seen in Figure 4. 10, the $SR_{\lambda,mod}$ using an 8-segment step function shows a small uncertainty while that with 18 segments shows a larger uncertainty. This result implies that the stability in the parameter convergence has a correlation with the number of steps/parameters applied in the $SR_{\lambda,mod}$. In other words, reducing the number of parameters in $SR_{\lambda,mod}$ will result in reduced uncertainty in the optimisation process, and vice versa.

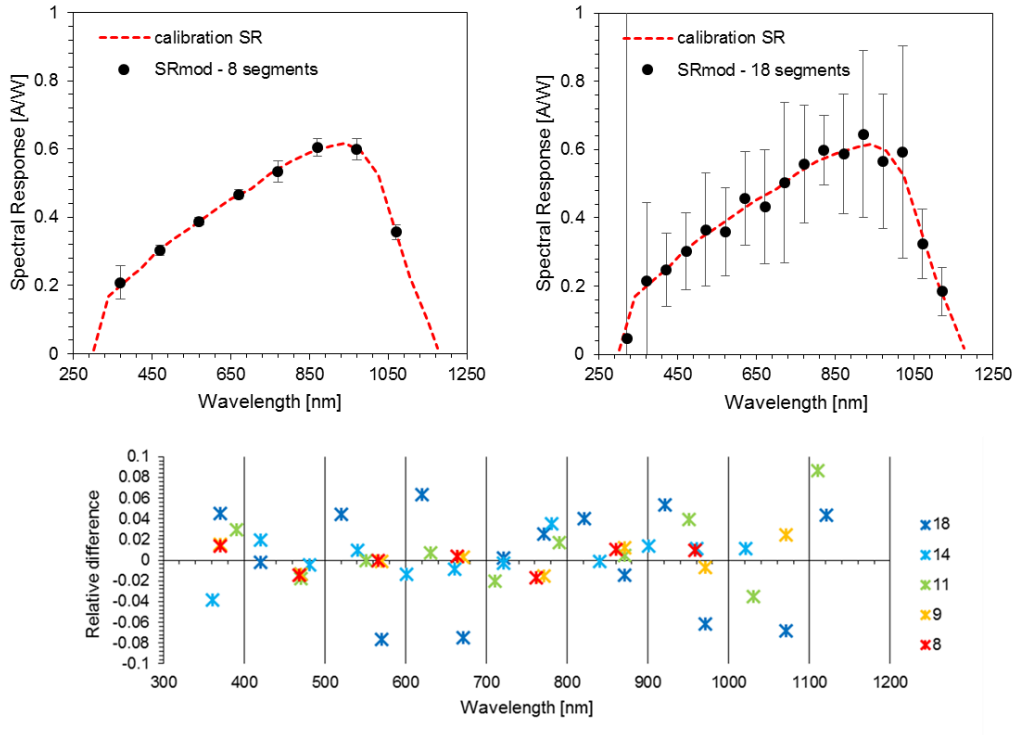


Figure 4. 10. Relative difference between the output $SR_{\lambda,mod}$ of different numbers of segments and the calibration SR.

4.3 Validation of polychromatic spectral response measurement

4.3.1 Reference cell

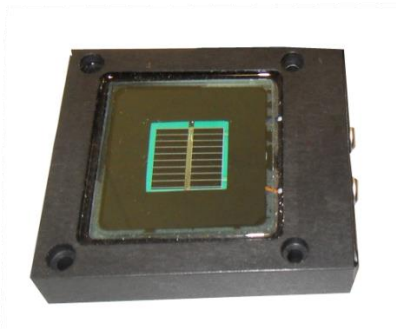


Figure 4. 11. Photograph of the reference cell used in the polychromatic measurement method.

From the simulation engaging artificial edge filters, it is realised that a reliable parameter convergence using the step function can be achieved by reducing the number of steps in the function. Pre-set conditions with 8 segments in the step function have been applied in the determination of SR characteristics of 2 reference cells of c-Si technology using the polychromatic method. Both devices have an active solar cell area of 2x2cm but different types of glass are used as the top cover. Device A

employs a clear glass cover while device B has a KG3 short pass filter glass cover, which results in a distinct difference in the SR characteristics between the devices. The SR characteristic of both devices have been measured by the JRC-ESTI, employing the DSR method in accordance with the standard procedure (IEC 60904-8). Uncertainty in SR measurements as reported by JRC-ESTI are approximately 2.5% and 3% for device A and B, respectively.

Results from the polychromatic measurement method are shown in Figure 4. 12. With uncertainty in short-circuit current measurement calculated at about 1.1% and uncertainty in spectral measurement as shown in Figure 3. 16, the output $SR_{\lambda,mod}$ is estimated from the 1000 iteration of fitting process. Point-by-point comparison between the measurements obtained via the polychromatic method and DSR shows agreement within $\pm 10\%$ for both devices. However, a striking difference regarding the uncertainty between the two measurements is apparent.

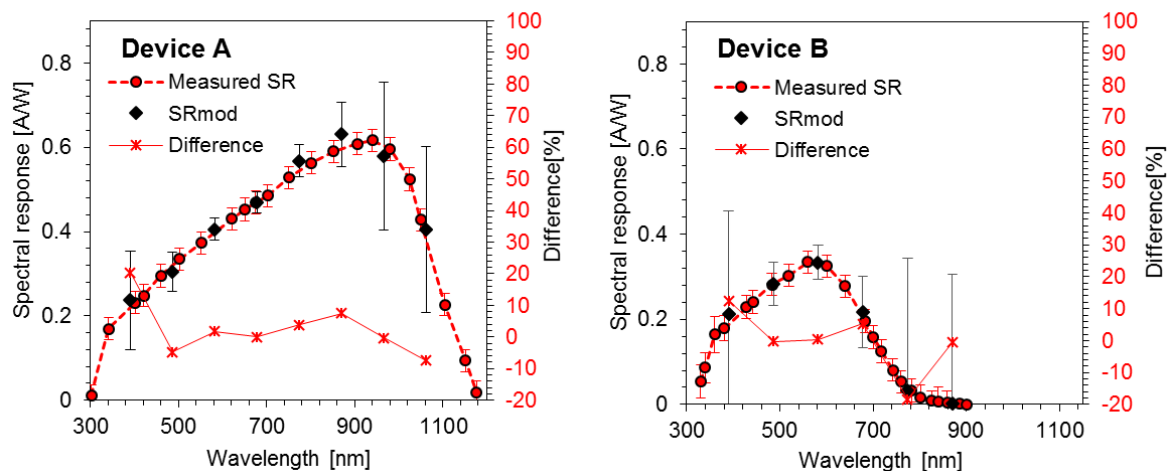


Figure 4. 12. Comparison of SR measurement obtained by the polychromatic method and the DSR method for unfiltered c-Si Device A (left) and filtered c-Si Device B (right).

Uncertainty in the SR curve of device B is generally higher than that of device A. The application of short pass (KG3) filters combined with the small active cell area, have led to the smaller $I_{sc, filters}$ generation per incident throughput irradiance. Small values that go into the optimisation process as inputs will raise the issue regarding the rounding error – type of quantization error, which eventually leads to the reduced accuracy in parameter conversion [71]. Effects of this error become more apparent in the UV and NIR regions, where non-linearity and non-uniformity issues already exist – as discussed in the previous chapter.

4.3.2 Effect of spectral variability in measurement uncertainty of the polychromatic method

Another factor that contributes to this result is lack of sufficient variation in spectral irradiance in these regions that is possible to attain with the real filters in the laboratory, rather than the idealised edge filters simulated in the preceding section. For visualisation, the measured throughput spectral irradiance of the set of filters used in this work and the simulated spectral irradiance through the ideal edge filters are shown in Figure 4. 13. The simulated spectral irradiance is an example of the ideal set of spectral measurements for the polychromatic method, yet the difference in the UV and NIR bands is obvious when compared to the real polychromatic filters. The highlighted region in the graph of the measurements shows more spectral variation compared to the UV and NIR, which results in the imbalance of inputs to the polychromatic method from the respective wavelength regions.

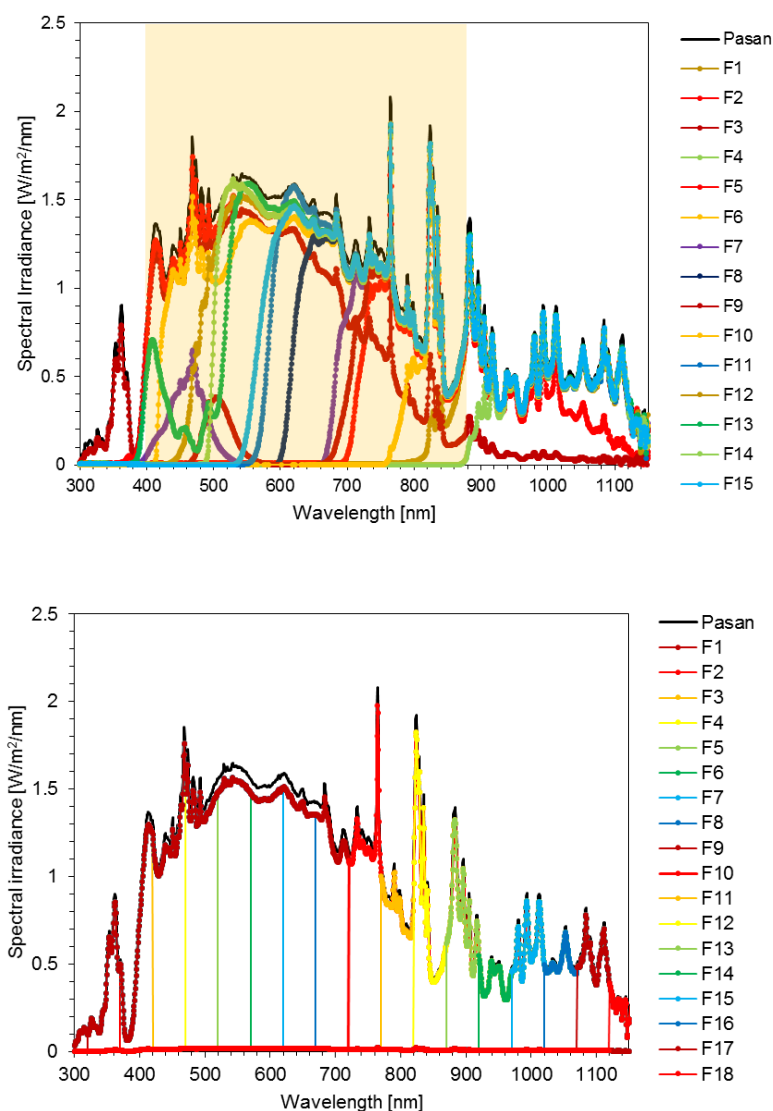


Figure 4. 13. Throughput spectral measurement (top) and the ideal case of spectral measurement data (bottom).

To test this hypothesis, polychromatic method simulations are performed with two artificial filters added in the mix of the polychromatic filters (Figure 4. 14). The artificial filters are designed to increase the variation in spectral irradiance in the 900nm to 1100nm region. The simulation incorporates the calculated throughput irradiance of the artificial filters and corresponding modelled current calculated using Eq. 3. Using the calibration SR of device A and B. The optimisation of R is done for two different measurement setups, one with and one without the two additional artificial filters. A pre-set step function of 16 segments with 50 nm interval is chosen for the $SR_{\lambda,mod}$ so that the effect of increasing the spectral variability in the NIR can be seen.

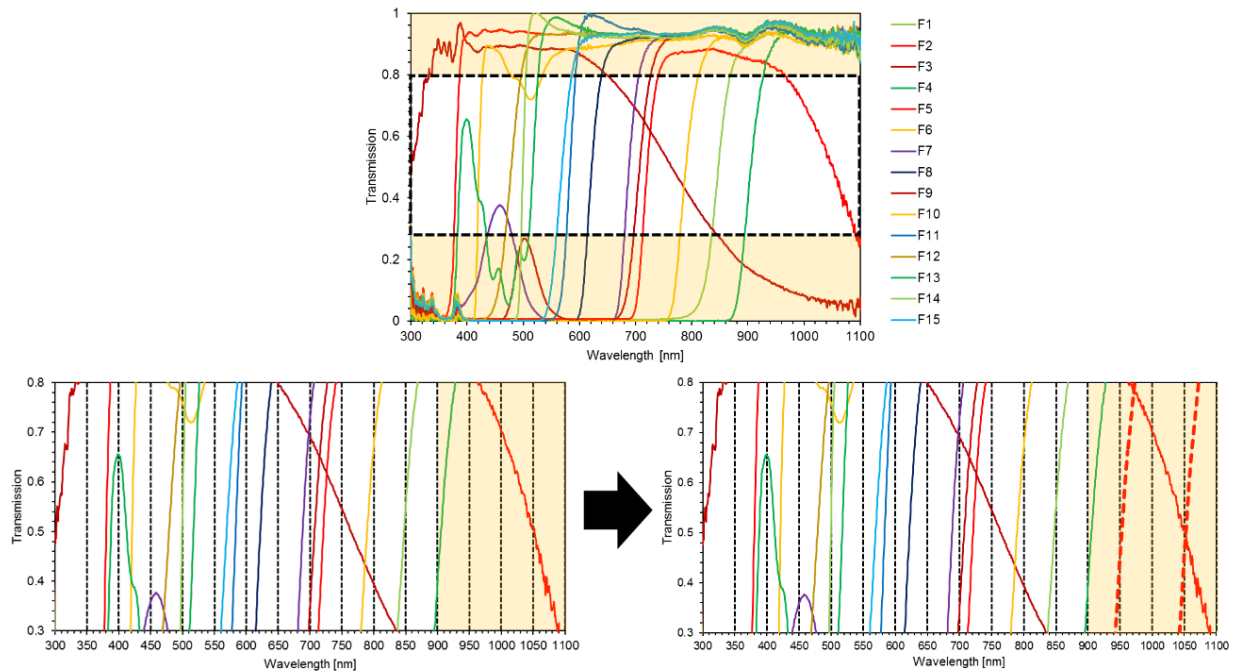


Figure 4. 14. Top Image shows the set of transmission profiles used in the current measurement setup. Bottom graph shows the improvement of spectral variability in the NIR region by the addition of 2 artificial filters in the mix (red dotted lines).

Results from the simulations are shown in Figure 4. 15. The dotted graphs show the point-to-point difference between the polychromatic measurements and the calibration SR characteristics of the c-Si devices. Significant improvements can be seen in the wavelength region 900 to 1050 nm which corresponds to the coverage of the additional artificial filters. This implies that high variability in the spectra of the filter set throughout the usable wavelength will contribute to better accuracy in the output $SR_{\lambda,mod}$.

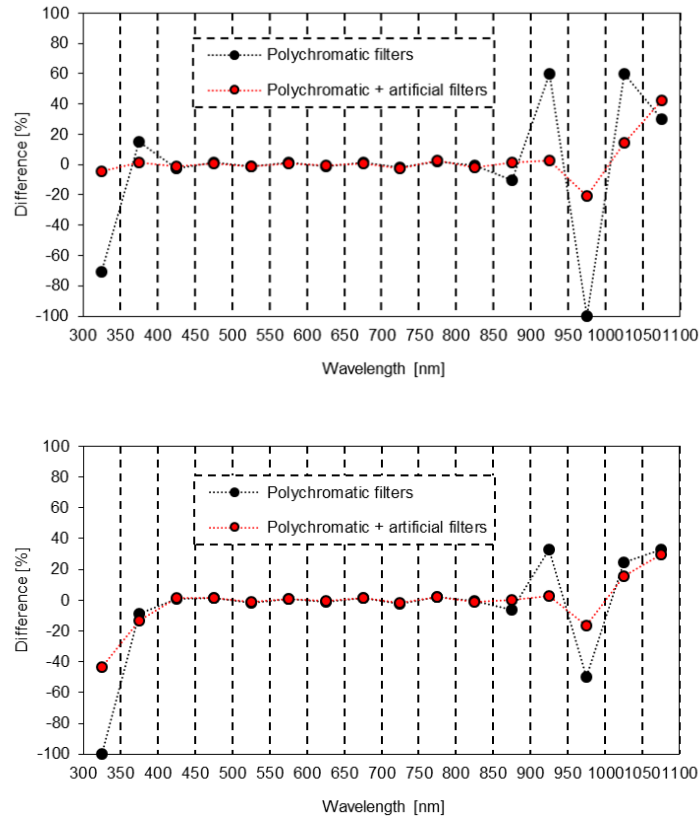


Figure 4. 15. Relative difference between the output $SR_{\lambda,mod}$ using different sets of filters for device A (top) and device B (bottom).

4.3.3 Commercial area cells

The validation of the polychromatic method in the determination of spectral responsivity of large area PV devices is performed through comparison of measurements by various labs using various facilities. This was conducted as a measurement intercomparison campaign in part of the EURAMET project “PhotoClass”. SR measurements of PV devices from cells to modules were performed using conventional (monochromatic) methods by the PTB, Fraunhofer (FhG-ISE), and CREST, employing different measurement setups. Figure 4. 16 shows the photographs of the devices used in the measurement campaign. The dimensions of PV cells most commonly used in modules are approximately 15.6×15.6cm. This is usually the maximum sample size in SR measurement systems that employ a steady state light source due to the limitation of maintaining a high irradiance uniformity over larger areas. SR measurements of the encapsulated PV cell and the 6-cell mini-module require a broad illumination system for the measurement to be carried out in its entirety (according to IEC 61853-2) [25]. In this campaign, results of such measurements have only been delivered by the PTB.

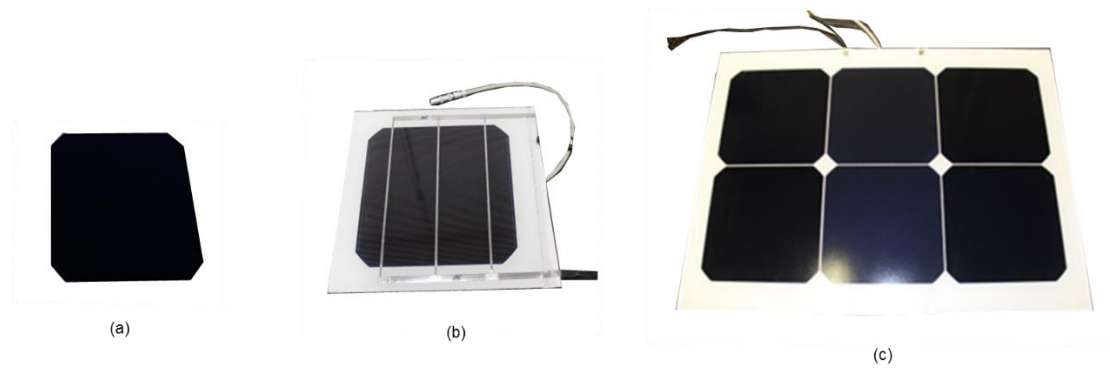


Figure 4. 16. Photograph of large area devices used in the validation of the polychromatic method; (a) non-encapsulated IBC c-Si cell, (b) encapsulated mono c-Si cell, (c) 6 series module of IBC cells.

The polychromatic spectral response measurement is performed in a fully automated mode, using a set of computer controlled motor to push/pull the filters in the filter cassette to/away from the front of the light bulbs. 4 set of $I_{sc,meas} - E_{\lambda,meas}$ (flashes) per filters are taken for each devices. Similar pre-set condition of step function $SR_{\lambda,mod}$ is applied in the fitting algorithm i.e: $n=8$, $y=96$, $\lambda_{min}=400nm$, $\lambda_{max}=1072nm$. Results from the polychromatic measurements are compared to the monochromatic measurements carried out by the PTB, FhG-ISE and CREST (Figure 4. 17). It can be seen that all measurement points, including those from the polychromatic method, agree to within their stated uncertainties. One point however, corresponding to wavelength 880nm, shows weaker agreement and shows a consistently high value deviation in comparison to the other points in the polychromatic measurements of all devices. The same was also observed in the measurements of the 2x2cm reference cells (Figure 4. 12). Issue with the lack of variability in the spectral measurement is likely to cause this result, therefore this is treated as a systematic error in the measurement.

In the measurement of the non-encapsulated cell, it can be seen from Figure 4. 17 that the monochromatic measurement uncertainties from PTB and CREST fall within the same margin, i.e. 2-3% in the visible light region and up to 8% in the NIR ($k=2$). Despite the spectral variability issue in the current polychromatic method, a relatively good agreement with the polychromatic measurement results to that of monochromatic measurement is observed in the NIR region for all devices (falls within the uncertainty envelope). Outside this region, uncertainty in the polychromatic measurement appears to be a reasonable value, up to 5%, which validates the feasibility of the method for SR characteristic determination of 15.6x15.6cm PV devices.

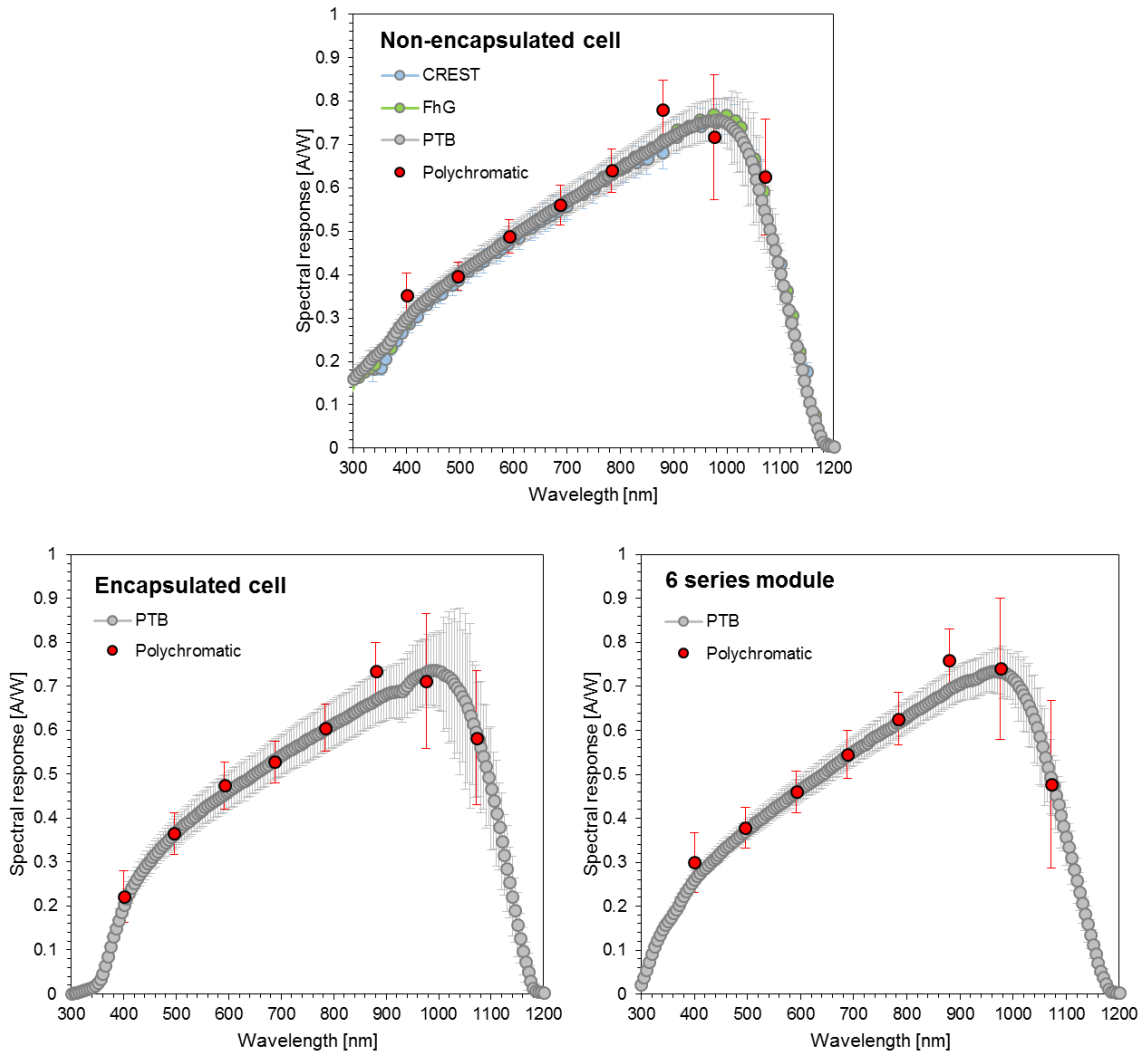


Figure 4. 17. SR measurement comparison between various labs with different measurement facilities of a bare PV cell (top), encapsulated PV cell (bottom left) and 6 series cells mini-module (bottom right).

Uncertainty in SR measurement of the encapsulated cell by PTB is approximately 5% in the visible region, while for the mini-module it is slightly lower with a maximum value of 3.6%. Uncertainty in the NIR for both measurements is about 10%. The same pattern is observed in the polychromatic measurements of both devices, where the uncertainty for the mini-module is slightly lower than that of encapsulated single cell (with 1% difference). The comparable measurement uncertainty in SR measurements by the polychromatic and standard methods implies that it is feasible to measure the spectral responsivity of large area devices with a fairly simple measurement setup by applying the polychromatic method.

4.4 Determination of spectral response curve

4.4.1 Interpolation of measurement points

Although satisfactory results have been achieved with regards to the uncertainty in the measurement of large area devices, the shortcoming of low wavelength resolution in the polychromatic method remains. Calculation of the weighted spectral sum i.e. I_{sc} generation, from the SR curve requires a higher resolution to avoid error from fine detail variation within the SR model segments. The interpolation approach is usually adopted in experimental data to join discrete points to a finer grid [72]. Here, the Hermite interpolation method is used to connect measurement points obtained from the polychromatic method. Hermite interpolation is a line smoothing algorithm which employs a collection of polynomial segments attached end-to-end [73, 74]. The wavelength points of the polychromatic measurements are interpolated to match the monochromatic measurement wavelengths in the PTB data for easy comparison, with the exclusion of the polychromatic point at 880nm (Figure 4. 18).

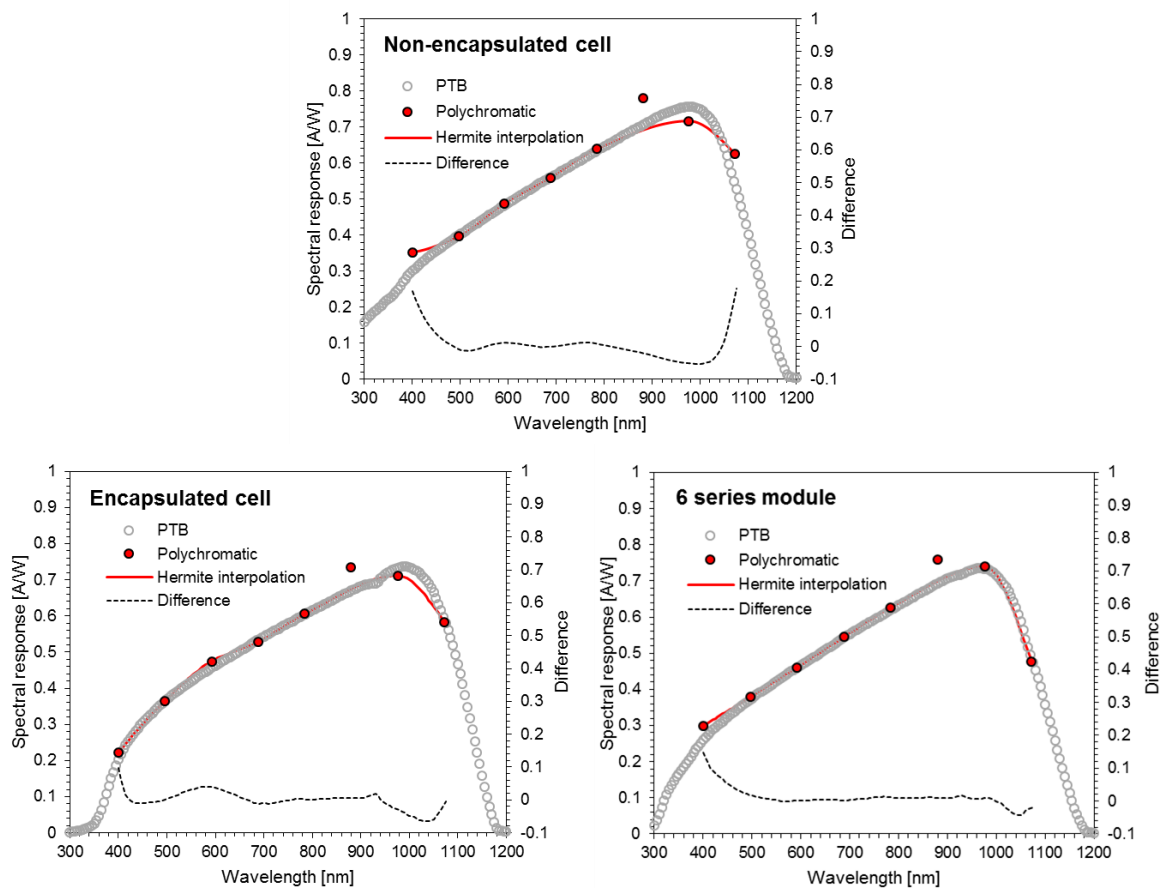


Figure 4. 18. Wavelength-by-wavelength comparison between SR measurement by PTB and Hermite interpolation curve of polychromatic measurement points of a single encapsulated cell, and 6-cell mini-module.

While differences between the interpolated data points and the measurement from PTB generally demonstrate a high value in the UV region (more than 10%), differences of less than 2% are observed

over most of the response range. The lack of SR info at each end of the curve however does not pose a major issue in the energy rating as well as energy modelling of PV modules. This is because the incorporation of SR measurement result into the calculation of effective irradiance G_{eff} (Eq. 2. 13) (to account for the usable wavelength in photocurrent generation of PV modules) requires the spectrally resolved irradiance data. Such a data is only broadly available within the range of 350nm – 1050nm as this is the specification of the widely used instrument for outdoor application, the EKO MS-700 spectroradiometer [75].

4.4.2 Application of Polychromatic SR measurement to large area modules

SR measurements of two full size modules of different technologies are performed using the polychromatic method with the same procedure as described previously. Details of the modules are shown in Table 4. 1. Similarly, measurement results are interpolated using the Hermite interpolation method, excluding the point at 880nm. Output $SR_{\lambda,mod}$ from the measurement of each module are shown in Figure 4. 20, with the uncertainty derived from a total of 1000 iteration of MC simulation.

Table 4. 1 Information of PV modules used in the polychromatic measurement method.

Module type	Module area [m ²]	Cell area [m ²]	Num. of series connection
Mono-Si	1.60	0.023	60
Back contact	1.65	0.015	96



Figure 4. 19. Photographs of the commercial PV modules used here in the polychromatic SR determination.

For PV devices under illumination, the incident photon will be absorbed by the material so that the photon can travel within the material to reach the p-n junction where the photocurrent generation occur. For silicon material, the photon absorption efficiency against the incident high energy photon (UV) is lower compared to that of low energy photon – NIR (Eq. 2. 7). For this reason, the incident NIR can travel further through the material, hence the SR peak corresponding to the NIR region in the silicon-based PV technology (Figure 2. 8). High photon energy beyond the band gap of material will not be

used in the photocurrent generation as it cannot be absorbed by the material. The SR measurement results of both mono-Si and back contact modules is shown in Figure 4. 20. Since both modules are of silicon-based technology, SR curves with peaks at the NIR region is observed in the measurement. It can also be seen from the graphs that the cut-off wavelength at about 1100nm, which corresponds to the band gap of silicon, is correctly determined in both cases.

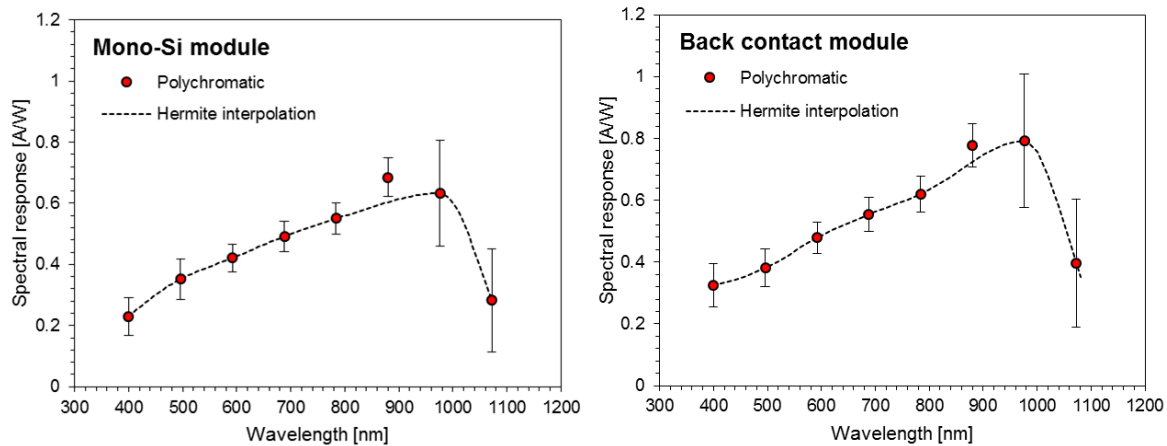


Figure 4. 20. SR curve result obtained by the polychromatic measurement method of mono-si (left) and back contact (right) modules.

While the usable wavelength range in the photocurrent generation of PV devices determined by the band gap of the material, the shape of the SR curve (gradient and peak) depends on the manufacturing method of the cell. p-n junction that is formed close to the surface of the material such as the traditional c-Si technology will cause the absorbed photon to travel a longer path than the thickness of the material thus result in energy loss in the photon when it reaches the junction. In the case of back contact technology, since the p-n junction is formed close to the rear of the material, the path in which the absorbed photon have to travel will be shorter in comparison to that of c-Si technology. As a result, photon with high energy (no loss) will be used in the photocurrent generation. Due to this effect, measurement between the mono-Si and back contact modules (Figure 4. 20) shows that the difference in peak value between both devices is obvious, with the peak observed in the back contact module 0.15 A/W higher than that of the standard mono-Si module.

4.5 Optimisation of the polychromatic spectral response method

4.5.1 Current status of the polychromatic method as implemented

The polychromatic measurement method for the determination of SR characteristics of large area PV devices has been validated against measurements made with the conventional monochromatic method. Uncertainty associated with the measurement also shows a reasonable value, i.e. less than 7% for full size modules in the visible range, which demonstrates the considerable improvement in reliability of the

method (Figure 4. 21). Nevertheless, there are some matters which still require further evaluation to fully optimise the method. These are:

- 1) High uncertainty in the measurement points corresponding to the NIR region.
- 2) Low wavelength resolution and narrow wavelength coverage in the output SR.
- 3) Systematic bias error in the measurement point at 880nm.

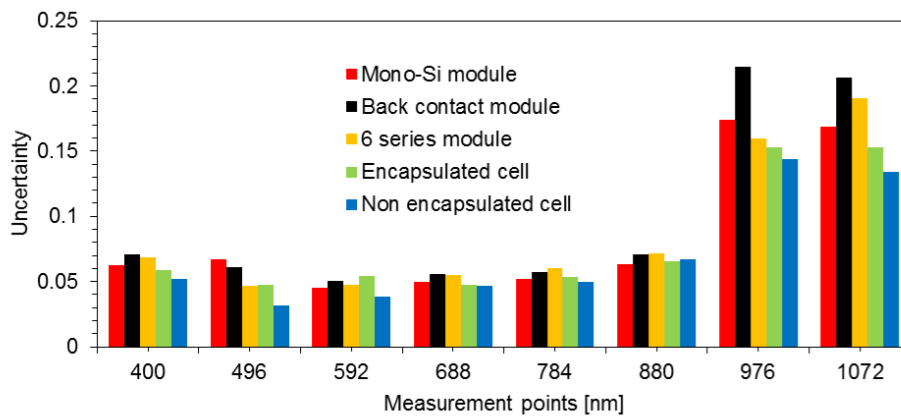


Figure 4. 21. Comparison of uncertainty in polychromatic SR of various large area devices.

The optimisation problem in the polychromatic data fitting algorithm is quite complex. While the objective function R is built based on spectrally integrated information of filtered polychromatic irradiance and corresponding photocurrent, i.e. $I_{sc, filters} - E_{\lambda, filters}$, the ultimate output of the process is the SR characteristic as a function of wavelength, modelled as $SR_{\lambda, mod}$.

Imagine a DUT which has an SR characteristic the shape of a perfectly symmetrical triangle. Employing only a single pair of $I_{sc, filters} - E_{\lambda, filters}$ measurements of the DUT in the objective function R will result in an enormous standard deviation from the MC uncertainty simulation because each solution in the optimisation will always be accepted as a valid result. Each MC cycle can produce any kind of different shape of $SR_{\lambda, mod}$, not even necessarily a triangle. Increasing the number of elements input into R , results in each incorporating a different set of wavelength functions which adds a filtering element to the decision making. The solutions that do not satisfy the objectives in each element in R , will be rejected. Eventually, the final parameter solutions from the MC simulation, i.e. variables in the step function of $SR_{\lambda, mod}$, will be left with those that represent the actual SR characteristics of the DUT.

The high uncertainty in the measurement points corresponding to the NIR region is due to lack of spectral variability in this region from one filter to another (Figure 4. 13). The uncertainty (standard deviation from the samples generated by the MC simulation) reflects the sensitivity in the parameter convergence to the varying inputs. The lack of measurement inputs incorporating the spectral data corresponding to the NIR region in the current measurement setup results in less restriction of the optimiser engine compared to the other regions, hence the high uncertainty in the final SR points. Adding more filters to the current setup with uniform wavelength cut-off variation is expected to greatly improve the result from polychromatic measurement, especially in the NIR region (Figure 4. 15).

Due to the limited number of measurement inputs into R , the number of segments/variables in the step function is reduced to 8 with the low and high limits of the function of 400nm and 1072nm, respectively. This optimum pre-set condition is chosen by balancing the flexibility of the step function with the sensitivity of the parameter convergence, tested against a high cycle count MC simulation (Figure 4. 10). Increasing the number of measurement inputs, i.e. the number of filters in the setup, would allow for a higher number of segments in the step function which also means that higher wavelength resolution and broader overall range in the output $SR_{\lambda,mod}$ could be achieved. Again, the validation of the optimum pre-set conditions using a setup with more filters in the mix can be performed against the calibration SR of a reference cell.

4.5.2 Simulation of polychromatic method in an optimised state

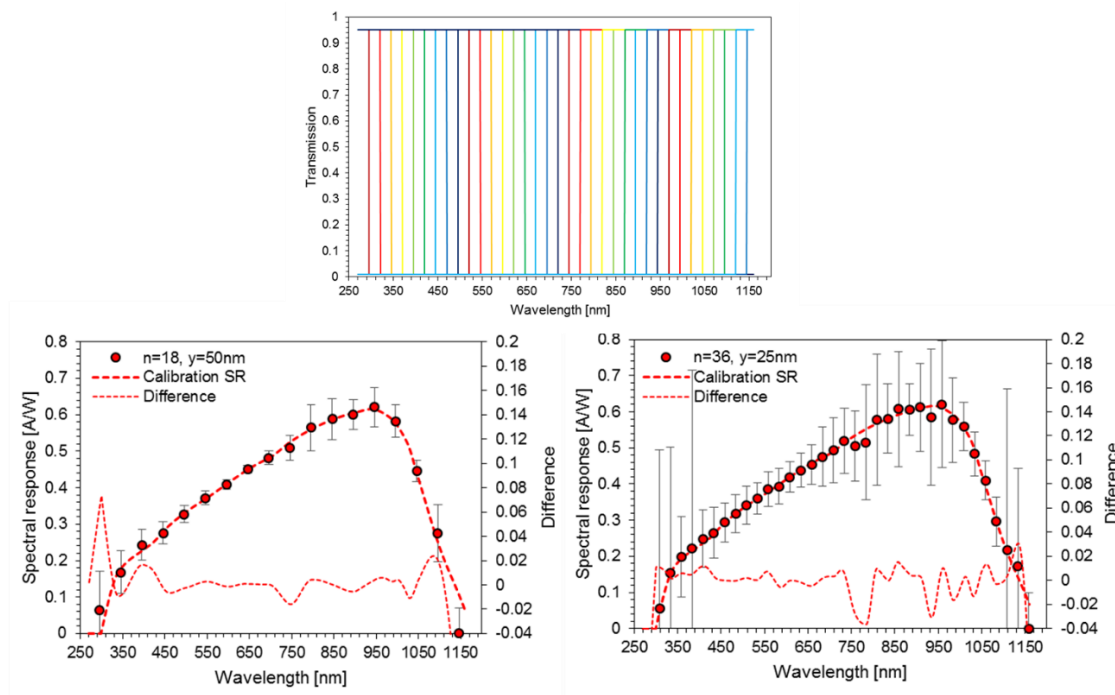


Figure 4. 22. Comparison of simulation polychromatic SR results with the calibration SR using 18 segments (left) and 36 segments (right) in the step function and an optimised set of irradiance filters (top).

Full coverage of the step function over the usable wavelength of the DUT is a likely candidate to solve the systematic error at 880nm as observed in all measurements of c-Si based technologies, with the exclusion of the reference cell with short pass filter glass (Figure 4. 12). This error is likely to be raised by the discrete sum approximation in the calculation of $I_{sc,mod}$ during the optimisation of the objective function due to the broad interval of the step function.

A simulation similar to Figure 4. 14 is performed to verify these assumptions made regarding the optimisation of the polychromatic SR method. Figure 4. 22 shows results employing 36 artificial edge filters with 25nm gap between the cut-off wavelengths and uncertainties derived from MC simulation. Different pre-set conditions are chosen in the simulation (see Eq. 4. 1) with 18 and 36 segments, n in the step functions with narrowed intervals, y for a full coverage over the usable wavelength of a c-Si device. Output $SR_{\lambda,mod}$ from the simulation is compared to the calibration SR as used in the calculation of $I_{sc,mod,simulation}$. Results from the comparison show that while good agreement between the output $SR_{\lambda,mod}$ and calibration SR are achieved for both pre-set conditions ($\pm 4\%$), the difference in the uncertainty is obvious with higher values observed in the simulation with 36 segments. The simulation demonstrates conclusively that determination of the SR characteristic of PV modules of high wavelength resolution and high accuracy can be obtained using the polychromatic method by optimising the filter selection used in the measurement setup. Realising such an optimised design with available and affordable filters remains a challenge however.

4.6 Conclusions

This chapter presented the assessment of uncertainty propagation in SR characterisation of PV devices by the polychromatic measurement method. The method which combines measurements and a fitting algorithm has the advantage of high practicality thanks to the application of broadband filters in the setup. It has been realised that the determination of SR characteristics through this method relies heavily on the inputs of the fitting algorithm. MC simulation method has been applied to analyse the uncertainty in the SR characteristic determination by the polychromatic method.

It has been concluded that the continuous Gaussian summation function (as used in the initial work on the polychromatic method) could restrict the automation of the fitting algorithm. To ensure reliable parameter convergence, a SR model based on the piecewise step function has been developed. The evaluation of pre-set condition of the function to be used in the MC simulation shows that 8 is the optimum number of steps, considering the set of broadband filters currently employed in the measurement setup and the Pasan solar simulator light source. It is also demonstrated that the standard deviation derived from the MC simulation reflects the stability of the parameter convergence of the fitting

algorithm, where a low number of parameters, i.e. segments in the step function, results in a lower uncertainty and vice versa. Nevertheless, large standard deviation is always calculated for the measurement points in the NIR region, which has been shown to be caused by the lack of spectral variation in the inputs in this region, due to lack of filters of suitably varying transmittance.

SR characterisation of a set of PV devices of large area have been measured using the polychromatic measurement method. These results have been compared to measurements of the same devices made by different laboratories, employing the monochromatic DSR method. Uncertainty in the DSR method ranges from 2%-8% depending on the wavelength region. Uncertainty in the polychromatic measurement demonstrated a comparable value of 5% in the visible and 10% in the NIR regions for the measurement of 15.6 × 15.6 cm PV devices.

Hermite interpolation is used to fill in between the SR measurement points obtained through the polychromatic measurement method. Polychromatic SR measurement of PV module of 6 series connected cells and the DSR measurement exhibited agreement within 10%, thus validating the polychromatic method developed in this thesis. A reliable measurement of SR characterisation of full size PV modules has also been performed using this method with uncertainty of less than 7% in the visible.

Through simulation of the optimisation of the polychromatic method, it has been shown that the improvement of the method will require additional broadband filters while considering their cut-off wavelengths. For the ideal is a uniform spectral variation throughout the usable wavelength range of the DUT. By doing this, the number of segments in the step function used as the SR model can be increased, yielding better coverage of measurement points over the wavelength range and higher wavelength resolution.

The SR measurement procedure described in the current standard for the SR measurement of PV modules (IEC 61853-2) cannot be applied in the measurement of full size PV modules without some difficulties in both practicality and technicality. The advantage of polychromatic method in its ability to measure the SR characteristic of full size module is a significant improvement on the current methods and this will become necessary for the energy rating standard.

5 Optical angular response measurements of full size photovoltaic modules

The proportions of direct and diffuse contributions to solar global (horizontal) irradiance are governed by the solar elevation angle (the sun vertical position above the horizon) and the weather. Higher latitude locations and those with cloudy climates will experience more diffuse radiation, while higher direct radiation ratios can be found under clear skies in the summer, especially at low latitude locations. The convention for PV modules operating outdoors is erection at a fixed optimal tilted angle, to maximise incident irradiation on the modules over the full year. This is typically 10-20° lower than the site latitude, depending on climate. Since the diffuse component is much weaker than the direct, the impact of the view-factor reduction in incident diffuse radiation on the module plane due to this orientation is not significant. Tilting the module from the horizontal does however introduce a third influence on the direct/diffuse ratio – the angle of incidence of the sun to the module. For example, at higher latitudes the sun may pass behind a tilted module plane even when it is still reasonably high above the horizon and the sky is cloud free.

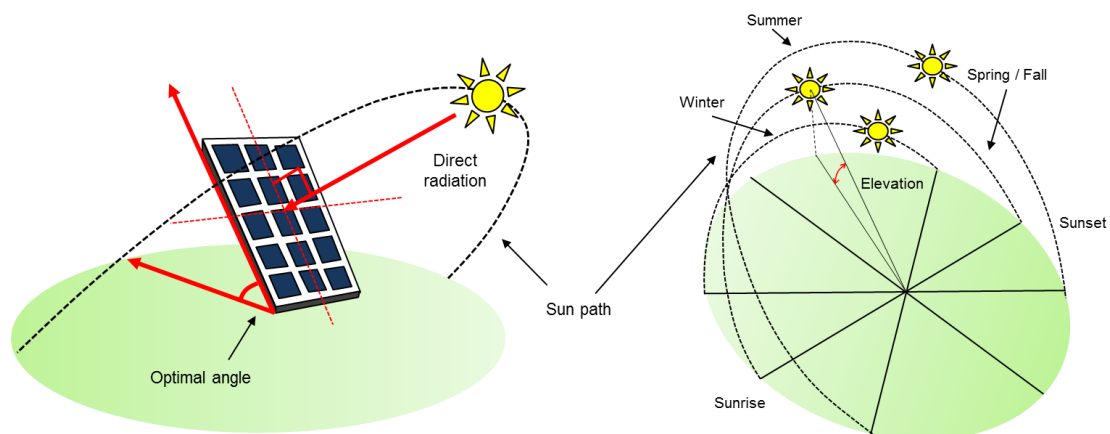


Figure 5. 1. Schematic of optimal orientation angle of a PV module operating outdoors and seasonal sun path geometry with respect to a point on earth at a latitude of about 50° N.

The optimal orientation of a PV module is generally when the surface of the modules is perpendicular to the direction of the direct beam (irradiance incident at 0°), unless it is cloudy and there is no direct component, in which case maximising the view factor to the sky is optimal (Figure 5. 1). Careful calculation of the optimal angle, incorporating sun path information and typical weather patterns, maximises the overall annual in-plane irradiation. However, the apparent sun position varies continuously and as the angle of incidence increases, the efficiency of a PV module decreases due to the increased reflection. The impact of angular losses in PV module performance over a long period of

time, i.e. energy yield, can be significant [76], therefore the incorporation of this effect in the performance calculation is crucial and it is also included in the IEC 61853-2 standard.

The quantification of angular losses of PV modules is achieved by the measurement of optical transmittance of the module encapsulation against varying AoI. According to Snell's law, the reflection at a planar air/glass interface becomes significant at incident angles higher than 45°, thus it is recommended that this data is used in the energy performance calculation for modules with flat uncoated front glass [25]. Nevertheless, as the technology in PV manufacturing matures, there are many different methods introduced in glass manufacturing for PV encapsulation to reduce optical loss such as anti-reflective coated glass (ARC) [77].

Furthermore, it is known that soiling can affect the efficiency of PV by up to 80% [78, 79]. Considering this, anti-soiling coatings are also being incorporated into the encapsulation [80, 81]. Variation of coating deposition methods adopted by PV manufacturers leads to variation in the optical properties of the finished modules and so the angular response cannot be estimated reliably by simple modelling. On account of this, the IEC 61853 includes the standard procedure to perform the angular response measurement of PV modules directly, as for other PV device characteristics, in part 2 of the series, as this information will be required in PV energy rating assessment.

From the literature, it is noticeable that research with regards to outdoor angular response measurement methods is more advanced than that of indoor methods due to the limitations of simulated light sources (particularly collimation for large areas) [82, 83, 84, 85]. The application of the ideal natural sunlight allows for the measurement of angular response characteristic of large area PV devices without the concern of reduction in irradiance uniformity even in tilted orientations.

A typical indoor measurement method employs a light source that is far from ideal regarding the angular distribution of the light beams, which results in high volume non-uniformity in the setup. The evaluation of the lab-standard Pasan 3B solar simulator as the basis for an angular response measurement setup will be described in this chapter, with an uncertainty analysis of the measurement. Short-circuit current measurement of the full-size PV modules with many series connected cells (and bypass diodes) is performed using a partial illumination method. Results from the angular response measurement of various PV devices employing the Pasan facility will be discussed.

Application of the same facility for both spectral and angular response measurements allows for further evaluation regarding the angle-dependent SR characteristic of PV modules to be carried out. The potential for this characterisation method is achieved by simulation which is presented in the last section. Research with regard to the spectral-angular characterisation method on large PV devices has not been reported to date, making the presented work the first of such.

5.1 Introduction

The final aim for angular response measurement of PV modules is to model angular losses accurately as part of an energy yield estimation or energy rating method. There are different models that can be used to quantify this loss but all require measured inputs in the form of modules technology-specific. These models have been developed by various institutes and PV researchers analytically. The theoretical values can yielded through this modelling helps PV researchers to understand the factors that need to be taken into consideration in the characterisation of angular response of PV module.

5.1.1 Existing methods for angular response measurement of photovoltaic modules

Analytical models of photovoltaic devices

It has been realised that the angular dependence of encapsulated PV devices under normal operating conditions is almost exclusively determined by the optical loss due to reflection at the air/glass interface [86]. Various modelling approaches have been developed by PV researchers to account for the angular effect losses in PV module performance estimation, but all calculate the overall angular transmittance $\tau(\theta)$ through the glass to the active PV layer, as a function of angle of incidence.

Physical models to account for angular losses on the glass surface are reported in [87] and [88]. The former employs a relatively simple transmittance model called the angle of incidence modifier $IAM(\theta_s)$ (Eq. 5. 1). The model has been adopted by the American Society of Heating, Refrigerating and Air-Conditioning Engineers (ASHRAE), hence it is also known as the ASHRAE model. Its main benefit is that it contains only a single parameter:

$$IAM(\theta_s) = 1 - b_0 \left(\frac{1}{\cos\theta_s} - 1 \right) \quad \text{Eq. 5. 1}$$

Where θ_s is the angle of incidence, and b_0 is an empirical coefficient of the type of PV device. A default b_0 coefficient value of 0.05 is usually used for standard PV modules [89].

The physical model reported in [88] requires the calculation of the angle of refraction θ_r of the glass/air interface (Snell's law). This is also known as the Fresnel model. The model can be written as,

$$\tau(\theta) = e^{-\left(\frac{KL}{\cos\theta_r}\right)} \cdot \left[1 - \frac{1}{2} \left(\frac{\sin^2(\theta_r - \theta)}{\sin^2(\theta_r + \theta)} + \frac{\tan^2(\theta_r - \theta)}{\tan^2(\theta_r + \theta)} \right) \right] \quad \text{Eq. 5. 2}$$

Where K and L are the extinction coefficient of the glass and its thickness respectively.

Sandia National Laboratories has long experience in the evaluation of PV performance in the field. Based on analytical analysis, a 5th order polynomial fitting approach has been suggested by Sandia to model the angular losses in I_{sc} of PV modules, denoted as $f2(\theta_{AOI})$ [83].

The model reported in [90] is based on experimental and theoretical results and yields the angular losses ($AL(\theta_{AOI})$). The model takes into account the optical properties of the front glass cover i.e. reflectance, transmittance and absorptance, hence there is increased confidence regarding its validity. The simplified model can be written as,

$$AL(\theta_{AOI}) = 1 - \frac{\exp\left(\frac{-\cos\theta_{AOI}}{a_r}\right)}{\exp\left(\frac{-1}{a_r}\right)} \quad \text{Eq. 5. 3}$$

Coefficient a_r describes the angular losses of the glass, determined by means of experimental data fitting.

These analytical models are used in the calculation of PV module performance to account for the angular loss effect in various performance modelling software. The evaluation of analytical models for this purpose in [86] and [91] have reported that the models demonstrated good agreement at low angular response with more divergence for Aoi beyond 60°. The energy rating method requires measurement of angular response due to the module-to-module variation of such a characteristic, depending on various glass treatments which generally are not disclosed by manufacturers. The IEC standard for the characterisation method has only been recently published [25] and is reviewed in the following.

Main considerations in angular response measurement

A “cosine response” describes the angular response of an ideal optical device, in which its response is proportional to the cosine of the angle of incidence [92], i.e.: the response is unaffected by any factors other than the geometrical projection of the light source onto the receiver plane. The AoI dependency of a real PV module performance is influenced by the combination of cosine effect and additional optical losses due to the orientation of the modules with respect to the light source, predominantly angle-dependent reflectance. The angular response characterisation of a PV device measures its light transmission property at various AoI, which is dictated largely by the optical properties of the outer glass used in the device, but may also be affected by internal layers in front of the PV active components. This is calculated by normalising the measurement of short-circuit current at different AoI ($I_{sc}(\theta)$) to that when the AoI is 0° ($I_{sc}(0^\circ)$). The cosine effect in the measurement is removed by dividing the normalised short-circuit current measurement by the cosine of AoI ($\cos \theta$):

$$\tau(\theta) = \frac{I_{sc}(\theta)}{I_{sc}(0^\circ) \cos \theta} \quad \text{Eq. 5. 4}$$

The measurement of the angular response can be performed using both natural and artificial light. While the concept is straightforward, there are a number of practical considerations to be accounted for in the measurement setup. This is to ensure that the measurement of electrical parameters at various AoI is not affected by other factors besides the light source. The main requirements for angular response measurement are visualised in Figure 5. 2 and discussion of each is described as follows:

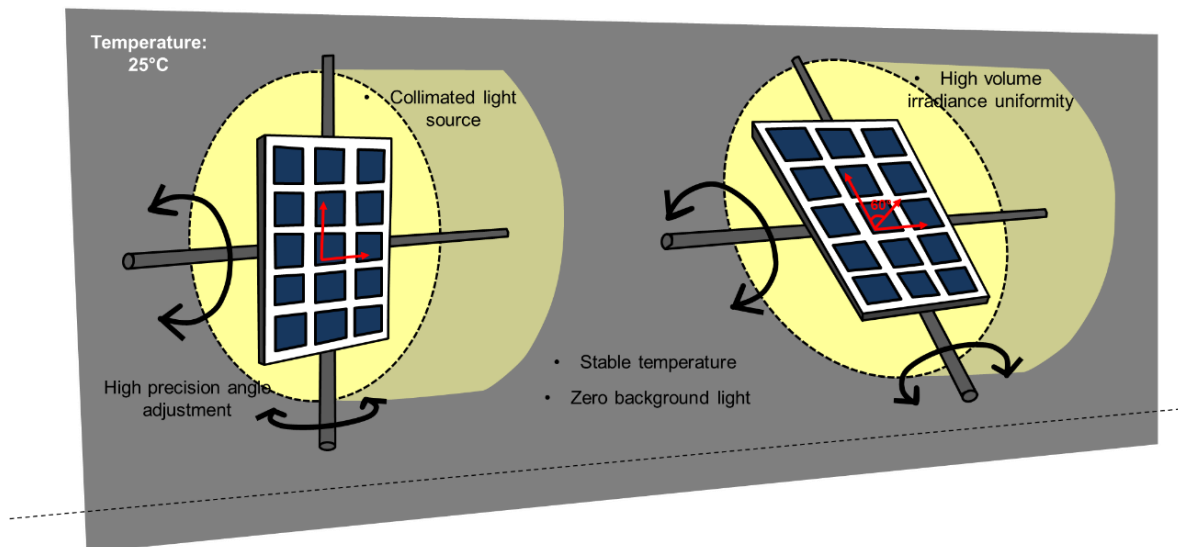


Figure 5. 2 Schematic of an ideal measurement setup for the angular response characterisation of PV modules.

1) Reduced background light

To measure the true response of DUT in respect to AoI from the light source alone care must be taken in the measurement setup to ensure that any irradiance other than the intended light source is minimised as much as possible. Means to prevent reflection from surfaces around the DUT such as the ceiling, floor, and nearby objects has to be incorporated in the measurement setup. If the measurement takes place outdoor, there may be reflected light from neighbouring buildings and trees and also the ground.

2) Minimal divergence of light source

A perfectly collimated light is ideal in the application to angular response characterisation to eliminate the error in the measurement due to light divergence. In the application to PV measurements, this effect will cause variations in the AoI across the DUT even in “normal” position. Further to this, as the device is rotated the intensity of light will also vary between the parts of the device closer to the light source and those further away. In practice, having a perfectly collimated light source is not possible for a full-sized module area measurement setup employing a solar simulator, therefore the magnitude of the uncertainty contributed by this effect has to be incorporated in the measurement.

For outdoor measurements, it is necessary that the measurement takes place when the sky is clear to ensure so far as possible that only the direct normal irradiance (DNI) is used in the measurement. The solar DNI is the closest to a perfectly collimated light, considering the very large distance to the light source, approximately 149 million km away.

3) High irradiance volume uniformity

This requirement especially applies to the indoor measurement setup due to the variation of divergent light source. While the non-uniformity of the projected illumination in xy dimension can be quite high for the standard solar simulator, irradiance measured at different distance from the light source (z direction) vary. This volume non-uniformity is what caused the “simulator effect” [93] in the angular dependence measurement of series connected PV modules. The non-uniformity effects will result in a systematic error in the measurement, though this can be corrected for using details of 3 dimensional irradiance uniformity of the measurement area.

4) Accurate angle adjustment

An accurate adjustment of tilt angle is crucial. A goniometric stage is usually employed in the angular response measurement setup to introduce controlled variation of Aol for both indoor and outdoor measurements. In the case of indoor measurement, the DUT is typically fixed to the centre of the stage, aligned to the centre of light source so that the Aol shift will be symmetrical in both directions (normal to +90°/normal to -90°). The thickness of the DUT also has to be taken into account while making this adjustment, to make the axis of rotation pass through the front surface.

5) Stable temperature

Electrical parameters of PV devices are temperature dependent [94] and angular response measurement can be time consuming. Performing such a measurement in a controlled temperature environment is ideal. The IEC 61853-2 standard includes a correction procedure to be applied for the outdoor measurement method.

Outdoor measurement method

Angular response characterisation under natural sunlight only considers the contribution in current generation by the DNI. For this reason, a correction procedure to eliminate the contribution from the diffuse irradiance component (G_{diff}) in the measurement has to be applied. G_{diff} is calculated using Eq. 5. 5, therefore the measurements of direct beam irradiance (G_{DNI}) by a pyr heliometer mounted on a sun-tracker and in-plane irradiance (G_{POA}) by a pyranometer are required.

$$G_{diff}(\theta) = G_{POA}(\theta) - G_{DNI}(\theta)\cos(\theta) \quad \text{Eq. 5. 5}$$

A two-axis tracker is usually used to adjust the Aol to the DUT(s) and instruments for irradiance measurement with respect to the position of the sun. The electrical and temperature measurements of the DUT (I_{scm} and T_m) are taken at various Aol under a short period of time (up to 1 hour) to minimise the error due to varying spectral distribution. Strict requirements during the measurement period regarding the ratio of G_{DNI} to the global normal irradiance (G_{GNI}) must be more than 85% in a clear sky condition is also specified in the IEC 61853-2. The measurement of G_{GNI} is taken using a pyranometer, mounted on sun-tracker.

The I_{scm} obtained during the measurement will subsequently be translated to a module temperature of 25°C using Eq. 5. 6.

$$I_{sc}(\theta) = \frac{I_{scm}(\theta)}{1 + \alpha_{I_{sc}}[T_m(\theta) - 25]} \quad \text{Eq. 5. 6}$$

Where $\alpha_{I_{sc}}$ is the temperature coefficient of the DUT I_{sc} in units of /°C [85]. The angular transmission of the DUT at different AoI is calculated using the equation below,

$$\tau(\theta) = \frac{I_{sc}(\theta) \cdot G_{POA0} - I_{sc0} \cdot G_{diff}(\theta)}{I_{sc0} \cdot G_{DNI}(\theta) \cos(\theta)} \quad \text{Eq. 5. 7}$$

Where $I_{I_{sc0}}$ and G_{POA0} are the measurements of short-circuit current and G_{POA} at $\theta = 0^\circ$ respectively.



Figure 5. 3. Photograph of two-axis tracker for outdoor angular response characterisation of PV modules as used by Sandia National Laboratories [95].

The measurement method outlined in IEC 61853-2 has been evaluated by the PV reliability laboratory of Arizona State University [86]. The results obtained from the evaluation confirmed earlier advice from the IEC that devices with glass superstrate structure have very similar AoI characteristics, even among different PV technologies. Another explicit measurement method has also been developed by Sandia [84]. The difference between the Sandia and IEC 61853-2 methods is that the air mass during the measurement period is incorporated into the Sandia model, due to the nature of the energy yield modelling developed by the institution (Eq. 5. 8) [82].

$$f_2(\theta) = \frac{\left[\frac{I_{sc}}{I_{scr}} \right] \left[\frac{E_0}{f_1(AM)[1 + \alpha_{isc}(T_c - T_0)]} \right] - f_d E_{diff}}{E_b} \quad \text{Eq. 5. 8}$$

Where I_{scr} is the short-circuit current measurement at normal incidence, E_0 is the reference irradiance (1000 Wm^{-2}), $f_1(AM)$ is a dimensionless empirical correction function based on the air mass, T_0 and T_c are the reference temperature (25°C) and module temperature, E_b is the direct irradiance, and $f_d E_{diff}$ is the fraction of the contribution by the diffuse irradiance component in the current generation of the DUT.

The IEC 61853-2 takes different approach to incorporating the spectral effect into the estimation of PV performance which is by the calculation of effective irradiance (AM1.5G equivalent) based on the SR characteristic of the DUT (Eq. 2. 13). Spectral correction is applied at a different stage to reduce the complexity in the measurement procedure, and hence increase the practicality of the standard PV energy rating method.

Recent developments in the outdoor measurement method by Sandia mean that the uncertainty in the measurement can be further reduced by directly measuring the in-plane diffuse irradiance component (Figure 5. 4) and optimising the tracker system [82], enabling a full range of AoI adjustment (normal to $\pm 90^\circ$). This method has been validated against the AoI measurement employing the same tracker system under different skies, performed by the CFV Solar Test Laboratory.



Figure 5. 4. Photograph of pyranometer with diffuser attachment for the measurement of diffuse in-plane irradiance reported in [82].

Although the outdoor angular response measurement of PV modules can be performed using an ideal light source, i.e. natural sunlight, there are many factors affecting the accuracy in performing such a

measurement. Despite the simple principle in terms of method, the inconsistency of irradiance/temperature conditions and significant diffuse irradiance under real environmental conditions calls for several other instruments to be employed in the measurement. The calibration and angular characterisation of pyranometers and pyrhemometers for the measurement of global in-plane and direct/global normalised irradiance contribute significant uncertainty in the final results. The accuracy in angle adjustment by the two-axis tracker and temperature measurement of the back of the DUT also contribute to the uncertainty in the outdoor measurement setup. For this reason, many researchers favour the indoor measurement method, where the irradiance and temperature conditions during the measurement can be controlled and the measurements are not weather-dependent.

Indoor measurement method

The standard indoor measurement procedure outlined in the IEC 61853-2 is rather simple compared to the outdoor method. It requires the I_{sc} measurement of the DUT to be taken at two orthogonal angular directions relative to the normal of the DUT for cases where rotationally asymmetric behaviour of the module is observed. For this, the application of a high precision rotation stage with symmetrical rotation is crucial. The AoI is varied in 10° steps between -60° to +60° while 5° step increment is recommended outside this range due to the higher rate of optical loss experienced by the DUT at high AoI. Variation in the temperature of the DUT is monitored for stability throughout the measurement to remove the need for temperature correction. The angular transmission of the DUT at each AoI is calculated using Eq. 5. 4.

There are very few published reports to be found regarding angular response measurement of full-size PV modules using the indoor method. Due to the time-consuming nature of the measurements, illuminating the modules with a steady state light source will increase the temperature of DUT over the measurement period. For this reason, indoor characterisation is usually performed using the common short-pulsed flash type solar simulator facility, combined with a rotation stage to introduce AoI variation [93, 89, 96].

Unlike the outdoor measurement method, the indoor setup suffers from high irradiance volume non-uniformity as a result of employing a non-collimated light source. Irradiance non-uniformity especially in the z-axis (optical axis from light source to module) is significant at high AoI when the horizontal edges of the DUT are moved closer to/further from the light source relative to its centre point. The influence of non-uniform irradiance is prominent in the case of electrical measurements of large area PV modules. For modules of series connected cells with bypass diodes, the I-V characteristic is affected by the least performing cell within each bypass-protected block (referred to as “strings” below), according to Kirchhoff’s law. For an otherwise good quality module, this would be the cells that are the

furthest from the light source due to the divergence of the rays and subsequent reduction in irradiance further from the lamps. A study regarding this factor in indoor angular response measurement setup of full size PV modules has been reported in [93] and the term “simulator loss” is used to address this issue. This can be quite complex to accommodate since most module area simulators have an extended source of several individual lamps that does not follow a simple $1/r^2$ law.

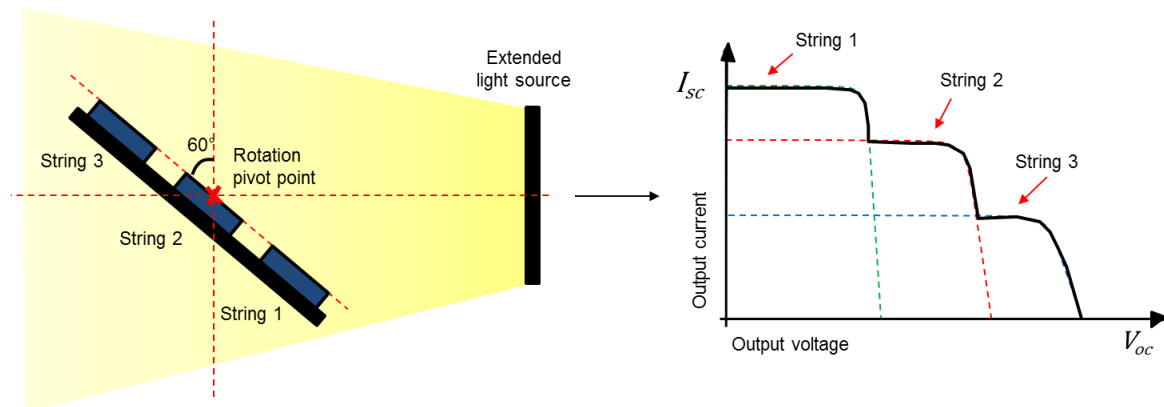


Figure 5. 5. Schematic of setup configuration for angular response measurement of a tilted PV module with 3 bypass diodes (left) and the resulting measured I-V characteristic (right).

Figure 5. 5 shows a schematic of the angular response measurement of a typical commercial c-Si PV module with 3 strings (3 bypass diodes) using an extended light source. At higher tilt angles (e.g. 60°), it can be seen that the bottom half of the module is moved closer to the source with respect to the rotation point in comparison to the top half. Due to the different irradiance incident on each string, 3 steps in the I-V characteristic measurement are observed which correspond to the distance of the string to the light source and the resulting differences in photocurrent generation. This simulator loss effect prevents the indoor angular response measurement of full size PV modules to be performed directly and corrections are required, or at least an increased uncertainty.

It has been reported in [9] that the effect of non-uniformity in the z-axis can be reduced by restricting the electrical measurement to an individual cell within the module instead of the entire module. 3 methods have been proposed to achieve this:

1) Production of a mini module with identical optical configuration to the full-size module

This method benefits from the reduced total active area so that the non-uniformity effect in the angular response measurement can be reduced. A single cell to test is manufactured with dummy (not electrically connected) cells surrounding the active one to recreate the neighbouring cell effects as

would be experienced by a cell in a full module. The drawback of this method is that it requires the manufacturer to produce bespoke samples for testing, which will be made outside of the main production lines and may not be representative, besides being impractical in terms of effort.

2) Individual cell contact through the back sheet of the module

Electrical measurement probes are attached directly to the back of a cell in the module under scrutiny. This method allows the electrical measurement of a single cell without altering the optical configuration but it is a destructive method which makes the module unusable.

3) Non-destructive method – based on partial-illumination

This is a newly developed method by TUV Rheinland to measure the angular response characteristic of PV modules. It is based on the partial illumination method as applied in the measurement of spectral response developed by AIST [59]. In this method, the target cell within the module is partially masked to reduce the effective incident irradiance on the cell. This forces the target to be the current-limiting cell in the corresponding string. As a result, the specific cell's short-circuit current can be detected, since the lowest plateau in the I-V measurement will always show the electrical performance of the target cell (for example, this would be string 3 in Figure 5. 5).

The non-destructive method has been implemented at CREST as part of this work, using the same Pasan 3B solar simulator as used for the polychromatic SR measurements. The implementation of this method and uncertainty analysis will be discussed in the following sections. Use of the same facility in the measurement of spectral and angular response characteristics opens the possibility for full measurements of angularly-dependent spectral response characteristics of full size PV modules.

5.2 Evaluation of angular response measurement setup

5.2.1 Short-pulse flash solar simulator facility as measurement setup

Indoor angular response measurements at CREST are carried out using a Pasan 3B simulator as the light source. The temperature inside the facility is controlled at $25^{\circ}\text{C} \pm 1^{\circ}\text{C}$ via air-conditioning. A motor-powered turntable that rotates 360° horizontally is attached to the existing measurement plane structures to introduce variation of angle of incidence to the DUT, which is mounted on the turntable (Figure 5. 6). The application of a computer-controlled turntable allows for the measurements to be performed in fully automated mode. Factors that affect the angular response measurement of PV

devices employing the Pasan system have been evaluated to investigate the uncertainty contributions of this setup to the final measurement.

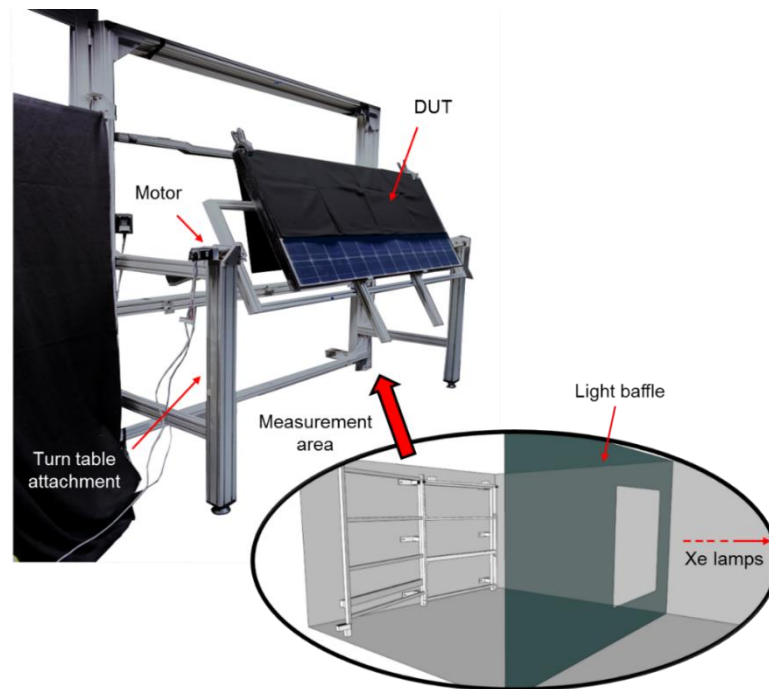


Figure 5. 6. Photograph of the angular response measurement setup and schematic image of Pasan 3B simulator at CREST.

Characterisation of the Pasan illumination over the DUT area

Every light source has a certain degree of divergence of distance from the source, except for an ideal, perfectly collimated source. In the case of the Pasan 3B solar simulator, the angular distribution due to light divergence is more complex in comparison to light sources with a single bulb (which may often be reasonably approximated as a point source, at a suitably large source-target distance) because of the unique orientation and arrangement of the four Xe lamps used in the system. The total physical extension of the lamp array is tens of centimetres. For this reason, the $I_{sc}(\theta)$ measurement of DUT at an AoI of 90° relative to the centre of the lamp housing will not be zero as there will be some remaining (although small) view factor between the DUT and part of the lamp array (Figure 5. 9).

An evaluation to investigate the variability of the angular distribution of light from the Xe lamps onto the test plane has been performed using a black tube with a rotating stage attachment inside it. A 2x2 cm c-Si reference cell is fixed on the rotation stage and measurements of the $I_{sc}(\theta)$ of the cell are taken at various tilt angles at different points A~I across the measurement plane (Figure 5. 8).

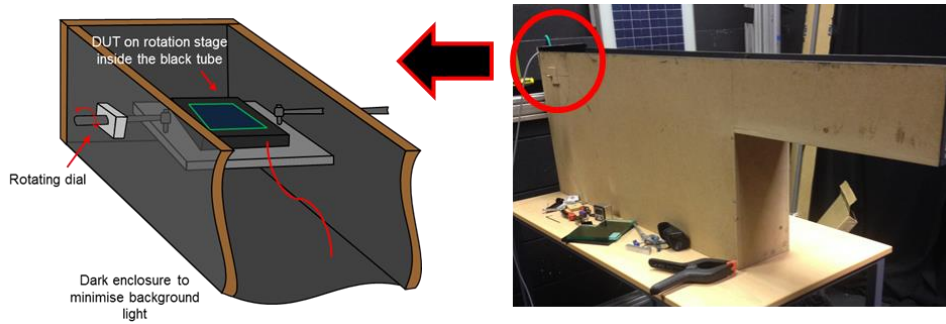


Figure 5. 7. Image of the black tube used in the evaluation of angular distribution of Pasan illumination.

Depending on the position of the tube, the amount of light i.e. divergent beams with certain angles, that enter it will be different, hence the observed variations in the $I_{sc}(\theta)$ measurement of the cell. From this evaluation, it can be seen that the $I_{sc}(\theta)$ of the cell measured at normal position i.e. tilted angle = 0° varies by 47%. Mostly low $I_{sc}(\theta)$ value is observed when the tube is not in alignment with the height of Xe lamps from the ground, at point ABC and GHI, while $I_{sc}(\theta)$ measurement at point DEF are almost identical at low tilt angle. As the tilt angle increased ($>40^\circ$), more variation in $I_{sc}(\theta)$ measurement is observed which implies the variability of angular distribution of the Pasan light source.

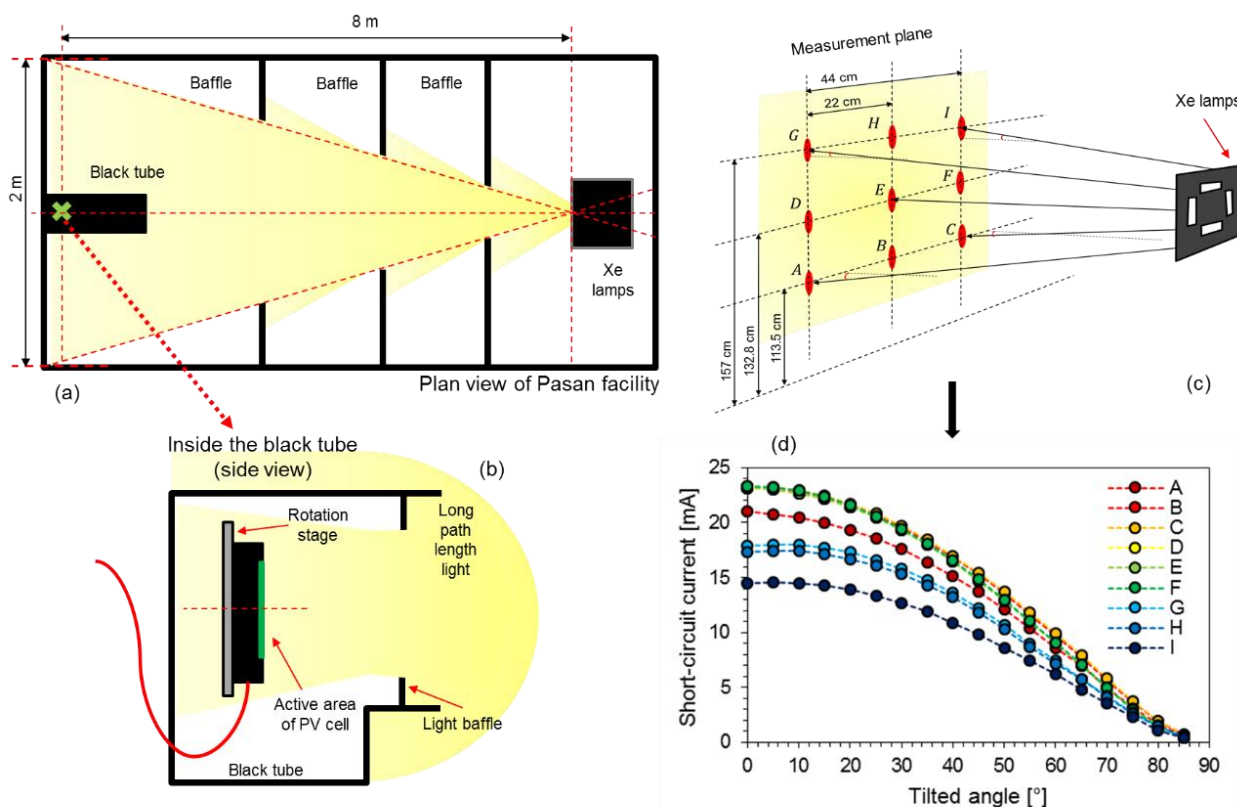


Figure 5. 8. Schematic showing the measurement setup used for evaluation of the angular distribution variability of the Pasan light source (a,b,c) and the $I_{sc}(\theta)$ measurement results from a small-area reference cell at various positions within the measurement plane (d).

Theoretically, systematic error due to light divergence in the $I_{sc}(\theta)$ measurement can be corrected for using detailed knowledge of the angular distribution from the Xe lamps. However, since this is not known, the error is estimated using a geometrical calculation and it is represented as uncertainty. Given that the Xe lamps are an extended light source and the centre of the DUT is aligned with the rotation axis, error contribution in the $I_{sc}(\theta)$ measurement due to the effect of diverging light can be approximated using geometrical considerations (Figure 5. 9). From this model, the maximum angle of the divergent light as seen by the DUT at each tilt angle (θ) can be calculated using the relationship shown in Eq. 5. 9.

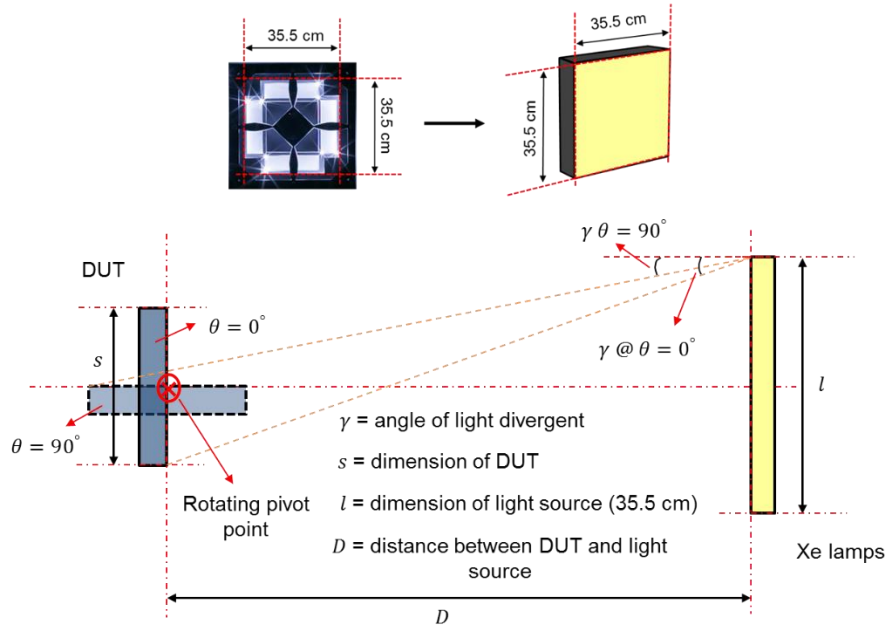


Figure 5. 9. Schematic of the approximation of Xe lamps as an extended light source (top) and the geometrical relationship of angle distributions of divergent light incident on the DUT.

$$\gamma = \tan^{-1} \left[\frac{(l/2 + s/2 \cos \theta)}{D} \right] \quad \text{Eq. 5. 9}$$

Therefore, it can be estimated that uncertainty due to divergent light (U_{DL}) in the angular response measurement has a rectangular distribution, which ranges from $\theta - \gamma$ to $\theta + \gamma$ at all tilt angles. With index of the recorded data denoted as i , U_{DL} can be calculated using the interpolated measurement result:

$$U_{DL} = 1 - \frac{\int_{\theta-\gamma}^{\theta+\gamma} \Delta I_{SC}(\theta) d\theta \cdot \Delta I_{SC \theta=0^\circ} \cdot \gamma_{\theta=0^\circ}}{\int_{\theta-\gamma}^{\theta+\gamma} \Delta I_{SC}(\theta = 0^\circ) d\theta \cdot \Delta I_{SC \theta} \cdot \gamma_{\theta}} \quad \text{Eq. 5. 10}$$

$$\int_{\theta-\gamma}^{\theta+\gamma} \Delta I_{SC}(\theta) d\theta = \left(\frac{\gamma}{\theta_{i+1} - \theta_i} \cdot \frac{\Delta I_{SC i+1} - \Delta I_{SC i}}{2} + \frac{\gamma}{\theta_{i+1} - \theta_i} \cdot \frac{\Delta I_{SC i+1} - \Delta I_{SC i-1}}{2} + 2\Delta I_{SC i} \right) \cdot \gamma \quad \text{Eq. 5. 11}$$

Depending on the size of DUT, the contribution of U_{DL} to the measurement will be different where a lower uncertainty contribution is expected for smaller device and vice versa.

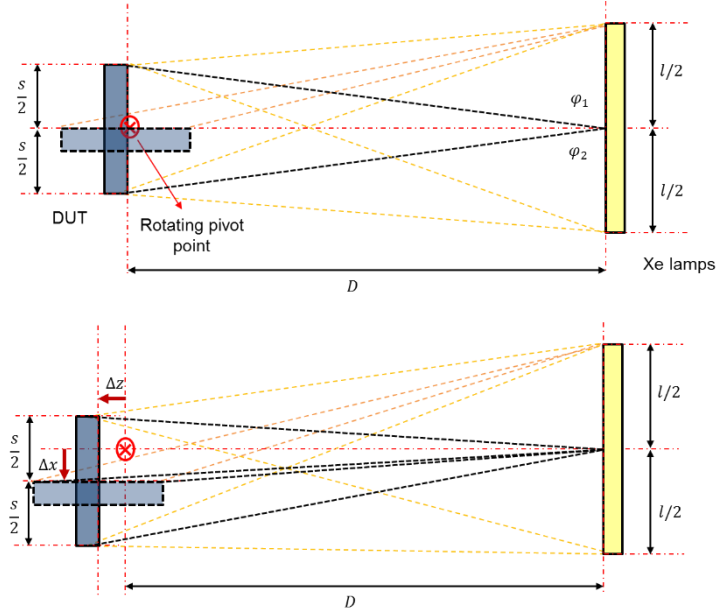


Figure 5. 10. Schematic showing the ideal condition when the DUT is aligned with the rotating pivot point (top) and the condition when there is displacement in the alignment (bottom).

Misalignment of the centre of the DUT with the centre point of the light source will result in additional systematic error because of the poor volume uniformity of Pagan light. The uncertainty due to this error is approximated from the ratio of incident power on the DUT from the divergent light (P_{DL}) to that under ideal conditions, perfectly collimated light (P_{col}). In tilted conditions, the loss in P_{col} is affected only by the cosine of the rotation angle, thus the uncertainty (U_{LS}) can be written as Eq. 5. 12, with $P_{col,\theta} = \cos \theta$.

$$U_{LS,\theta} = 1 - \frac{P_{DL,\theta} \cdot P_{col,\theta=0^\circ}}{P_{col,\theta} \cdot P_{DL,\theta=0^\circ}} \quad \text{Eq. 5. 12}$$

P_{DL} can be calculated using the tangent relationship from the angle distribution of projected divergent light from a point within the length of the light source, assuming that the intensity of the incident light is uniform over the surface of DUT. This relationship is illustrated in the schematic shown in Figure 5. 10. The top image shows the condition in which the DUT is properly aligned with the rotating pivot point and the centre of Xe lamps. At this orientation, the U_{LS} contribution in $I_{sc}(\theta)$ is estimated to be very

small, thus negligible. On the other hand, when the position of the DUT deviates from the pivot point by $\Delta x \Delta z$, P_{DL} can be written as:

$$\begin{aligned}
 P_{DL,\theta} &= \varphi_{1,\theta} + \varphi_{2,\theta} \\
 &= \tan^{-1} \left(\frac{dx + \frac{s}{2} \cos \theta - \Delta x \sin \theta - \Delta z \cos \theta}{z + \frac{s}{2} \sin \theta + \Delta z \sin \theta - \Delta x \cos \theta} \right) \\
 &\quad + \tan^{-1} \left(\frac{dx + \frac{s}{2} \cos \theta + \Delta x \sin \theta + \Delta z \cos \theta}{z - \frac{s}{2} \sin \theta + \Delta z \sin \theta - \Delta x \cos \theta} \right)
 \end{aligned}
 \tag{Eq. 5. 13}$$

Where dx is the origin point of projected light within the light source ($-l/2 < dx < +l/2$). Therefore, total U_{LS} can be expressed as the sum of contributions from light origin points over the total extension of the light source:

$$U_{LS,\theta} = 1 - \frac{\sum_{dx} P_{DL}}{\sum_{dx} P_{DL,\theta=0^\circ} \cdot \cos \theta}
 \tag{Eq. 5. 14}$$

In the angular response characterisation, the positioning of the DUT on the rotation stage (itself at 7.5 m distance from the Xe lamps) is carried out using a self-levelling rotary laser tool with precision of ± 0.08 mm/m (Figure 5. 11). Use of the level gives uncertainty in Δx and Δz of 1mm. For a 15.6x15.6 cm cell, this results in a misalignment contribution to final uncertainty below 1% at a worst-case angle of incidence of 85°. Therefore, it can be estimated that the U_{LS} contributes very little uncertainty to the overall angular response characteristic measurement.

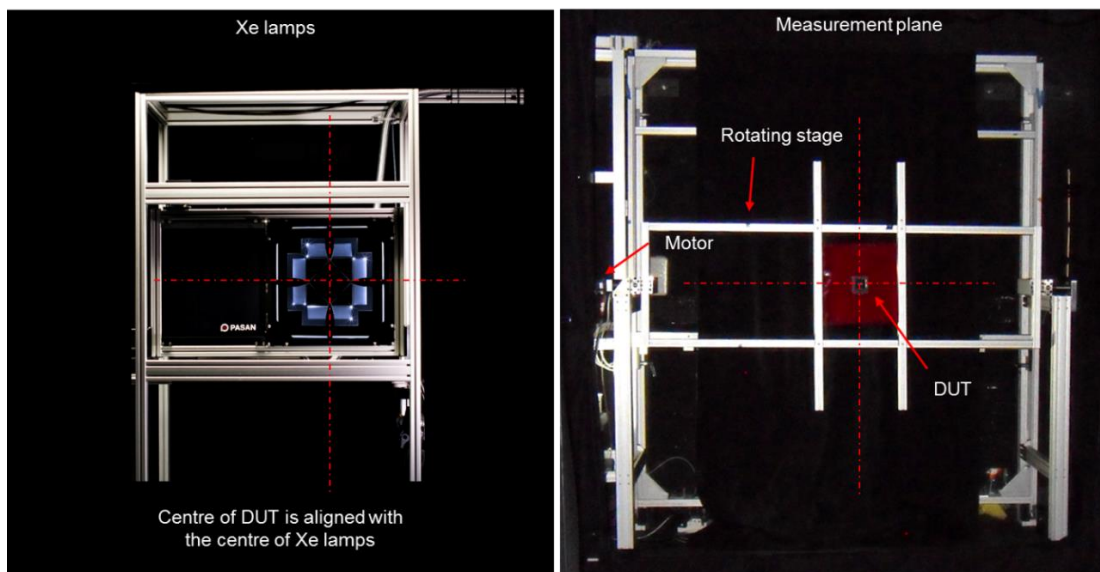


Figure 5. 11. Photograph of Xe lamps from the DUT point of view (left) and rotation stage with DUT fixed on it from the Xe lamps point of view.

Reducing background light in the measurement environment is a crucial requirement for reliable angular response characterisation. The Xe lamps used in the Pasan system are especially designed to illuminate the entire 2x2m measurement plane uniformly. When such an amount of light is projected on a small area device e.g. a standard 15.6x15.6cm c-Si cell, the amount of background light present in the measurement area becomes significant. Uncertainty due to this background light (U_{BG}) in the $I_{sc}(\theta)$ measurement is estimated using the value of relative incident irradiance when the DUT is tilted at 90° to that of when DUT is in the normal position. While $G_{BG,\theta}$ is the irradiance contributed by the background light with the assumption that the angular distribution of the background light is uniform, U_{BG} can be written as,

$$G_{BG,\theta} = \Delta I_{sc,\theta=90^\circ} - \frac{\sum_{dx} P_{div} x_{\theta=90^\circ}}{\sum_{dx} P_{div} x_{\theta=0^\circ}} \quad \text{Eq. 5. 15}$$

$$U_{BG,\theta} = 1 - \frac{G_{BG} \sin \theta}{\Delta I_{sc}(\theta)} \quad \text{Eq. 5. 16}$$

The value of U_{BG} increases with the increasing tilt angle as there will be higher amount of light incident on DUT, contributed by the light reflection within the measurement setup. The high uncertainty due to background light at high Aol can contribute to the uncertainty in angular response measurement greatly. To minimise the background light within the measurement plane, the metal structural beams are covered using non-reflective black matte cloth (Figure 5. 12). With this, the light reflection is suppressed by more than 20%.

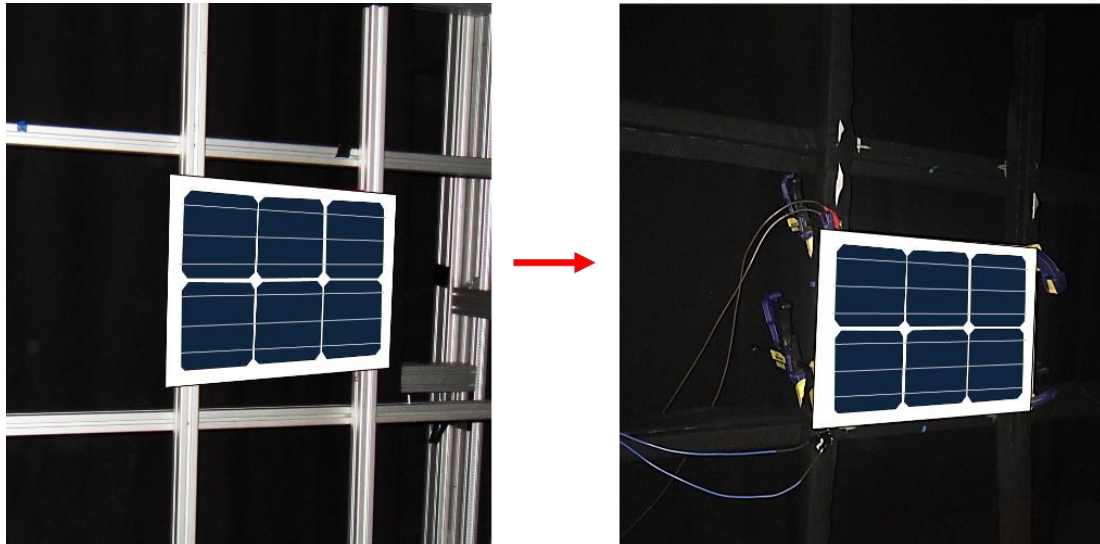


Figure 5. 12. Photograph of rotation stage before (left) and after (right) the beams are covered using black matte cloth to reduce background light effect.

Angle adjustment of the DUT

Apart from the optical factors, the mechanics of the rotation stage also contribute to uncertainty in the angular response characterisation in the context of angle adjustment. Figure 5. 13 shows a photograph of the tilted rotation stage attachment in the Pasan facility with reference cell fixed on it. Calibration of the stage angle is performed using a digital gauge with precision of 1° on a flat surface that is parallel to the floor/wall. The shifting of angle of the stage is influenced by the combined factors of motor control, gear mechanics and the flexing of the beams due to the load of the DUT. The variability of the angle readout (U_A) is measured from the standard deviation of multiple load tests, performed using various DUT of different dimensions and weights and is approximately 0.5°. The uncertainty in regard to angle adjustment (U_C) is estimated using the relationship between the expected tilt angle of the stage and U_A . This can be calculated using an interpolation equation written as,

$$U_{C,\theta_i} = \max \left| 1 - \frac{\left[\frac{U_A}{\theta_{i+1} - \theta_i} \cdot (\tau_{\theta_{i+1}} - \tau_{\theta_i}) \right] + \tau_{\theta_i}}{\tau_{\theta_i}} \right|, \left| 1 - \frac{\left[\frac{U_A}{\theta_{i-1} - \theta_i} \cdot (\tau_{\theta_{i-1}} - \tau_{\theta_i}) \right] + \tau_{\theta_i}}{\tau_{\theta_i}} \right| \quad \text{Eq. 5. 17}$$

Where the i notation is referring to the sequence of tilt angles during the measurement and τ_{θ_i} is the optical transmission of the DUT (Eq. 5. 4). The contribution of U_C in the angular response characterisation is device dependent, hence it is calculated separately for each DUT.

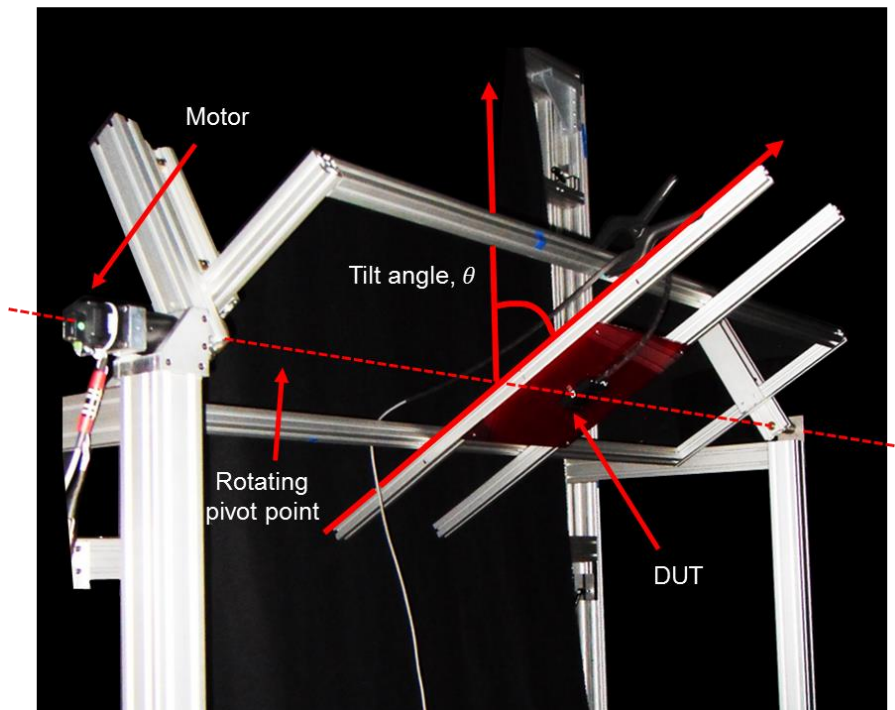


Figure 5. 13. Photograph of the rotation stage attachment in tilted position around the pivot point axis with DUT attached.

5.3 Angular response measurement of cell area PV devices

The combined uncertainty in the angular response characterisation of PV devices employing the Pasan system and rotational stage attachment is analysed individually per DUT. Other uncertainty contributions in the characterisation include the non-linearity of the device, temperature variability, irradiance uniformity and those related to the electrical components in the Pasan system. These uncertainties are found to be relatively small in comparison with the optical and mechanical factors as discussed above. An uncertainty value of 0.1% is applied for extraction of the $I_{sc}(\theta)$ parameter from the raw I-V curve data and the figures reported below are formed from the average $I_{sc}(\theta)$ values from 4 measurement runs.

Table 5. 1. List of devices used in the angular response measurement.

PV technology	Dimension	Configuration
c-Si 1	2x2 cm	Encapsulated
c-Si 2	2x2 cm	Non-encapsulated
c-Si 3	15.6x15.6 cm	Encapsulated
Poly-Si	15.6x15.6 cm	Encapsulated
Back contact 1	12.5x12.5 cm	Encapsulated
Back contact 2	12.5x12.5 cm	Non-encapsulated
CIGS	30x30 cm (67 cells)	Encapsulated

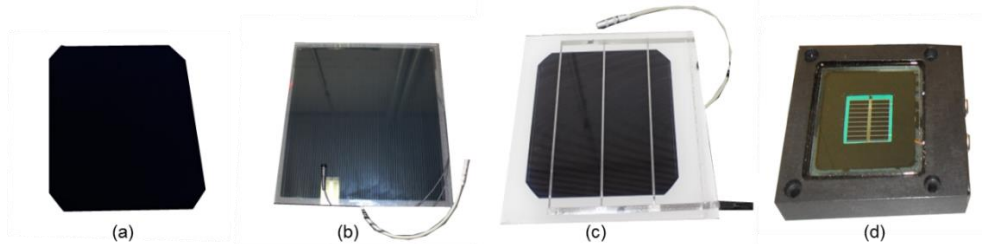


Figure 5. 14. Photograph of samples used for the angular response measurements using the Pasan facility; (a) Non-encapsulated back contact cell, (b) Encapsulated CIGS module, (c) Encapsulated c-Si cell, (d) Encapsulated c-Si reference cell.

The angular response characteristics of 7 PV devices of different technologies have been measured using the Pasan system setup (Table 5. 1). As shown in the table, the devices used in this measurement have different dimensions and configurations. 5 of the cells are encapsulated with clear glass on top while the other 2 are not. Assuming that the angular response characteristic of PV devices with encapsulation across all technologies agrees with the Fresnel model (Eq. 5. 2) with index of refraction, $n=1.3$ (solar glass) [97], the measurements are carried out with 2 objectives:

- 1) To evaluate the variability of Aol dependency of the encapsulated devices.
- 2) To compare the angular response characteristics of the non-encapsulated and encapsulated PV cells of the same technology.

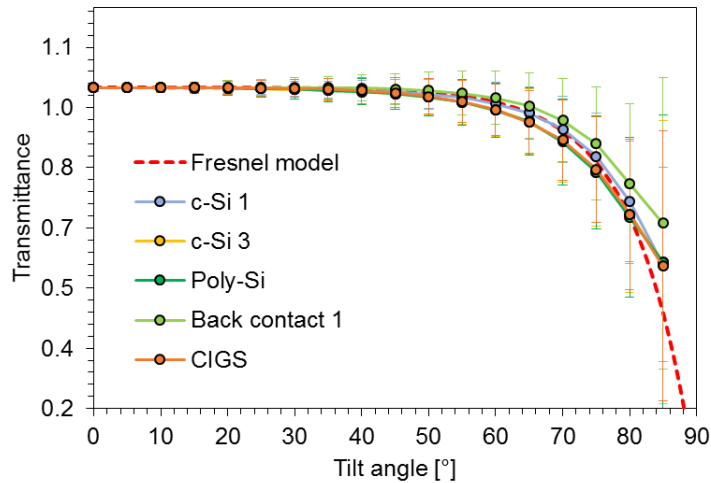


Figure 5. 15. Measurement results of the encapsulated PV devices and Fresnel mode.

Results from the angular response measurements of encapsulated PV devices and comparison to the Fresnel model are shown in Figure 5. 15. The first noticeable finding is that the uncertainty in the measurement of each device shows the same trend i.e. gradual increase from low to high tilt angle. The combined uncertainty ($k=2$) in the angular response increases from about 0.6% at 0° angle to a maximum value of 25% at the highest tilt angle. The predominant uncertainty contribution in the measurement employing the Pasan setup is from the background light reflection, U_{BG} , with a calculated value of 10%. Next to this is the uncertainty in the angle adjustment of the DUT, U_A , with a contribution of about 7%. This result confirm the hypothesis that the theoretical Fresnel model agrees with the angular response characteristic of encapsulated devices.

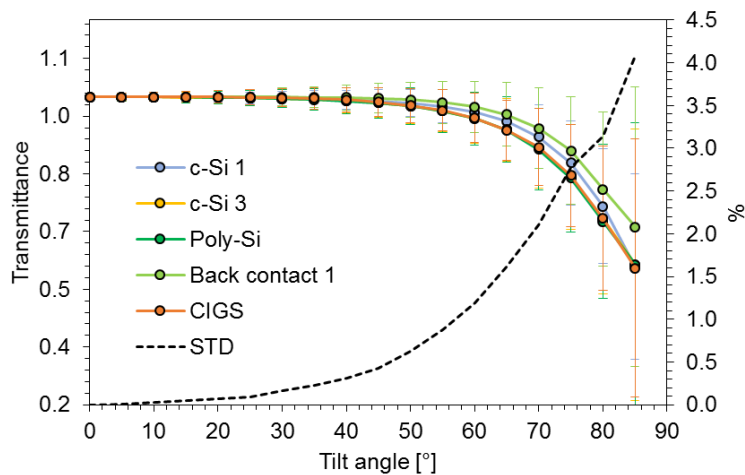


Figure 5. 16. Variability of angular response characteristics of encapsulated PV devices of different technologies.

The variability of angular response characteristic is quantified from the standard distribution of the measurement results (Figure 5. 16). From the graph, it can be seen that variation of the angular response for every device becomes more pronounced from tilt angles of 45°, which is in agreement with Snell's law. The variability between the different encapsulated devices is relatively small with standard deviation of values of 4% even at high tilt angle. This variation in angular response characteristic at high tilt angle translate to about 1.5% difference in the annual yield simulation of PV modules installed at 22° tilt angle, south-facing (typical orientation at Loughborough), under the same environmental conditions.

The Aol dependency of PV devices is largely governed by the reflection loss which occurs at the air/glass interface. As a result, the angular response of a PV device will depend on the optical properties of the top glass used in the encapsulation. These properties vary from device to device due to differences in the materials and methods used for the application of anti-reflection coatings on the top glass by PV manufacturers, hence the variation in the angular response measurement as presented earlier. The angular loss modelled using the Fresnel model have shown that the Aol dependency of encapsulated devices of solar glass without coating have higher sensitivity against varying incident angle compared to those without encapsulation (Figure 5. 17). Measurement of angular response of 2 different PV technologies with/without encapsulation of the same dimensions i.e. c-Si 1/c-Si 2 and back contact 1/back contact 2 are compared (Figure 5. 18) to validate this theory.

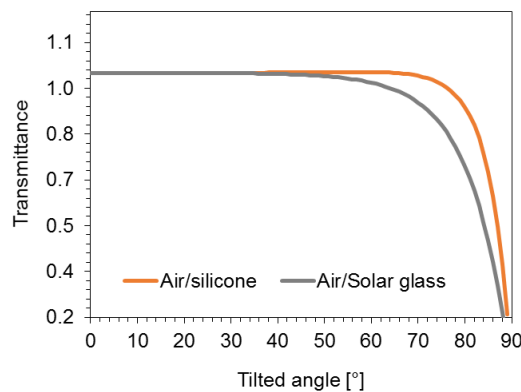


Figure 5. 17. Graph of Fresnel model of different refractive index.

The measurement results shown in Figure 5. 18 shows that both c-Si and back contact devices without encapsulation show a noticeable difference in Aol dependency trends in comparison to those of the corresponding encapsulated devices. The light transmittance of c-Si 2 is lower at tilt angle between 25° to 60°, compared to c-Si 1 but maintains a more stable transmittance before abruptly dropping at the high angle of 85°. On the other hand, results from the measurement of back contact devices demonstrate an Aol dependency that is almost identical to each other for tilt angles up to 60°, while slight variation is observed with increasing angle. From this observation, it can be said that the device

with encapsulation has a higher Aoi dependency at high tilt angle compared to the one without, thus confirmed the theoretical angular loss of Fresnel model.

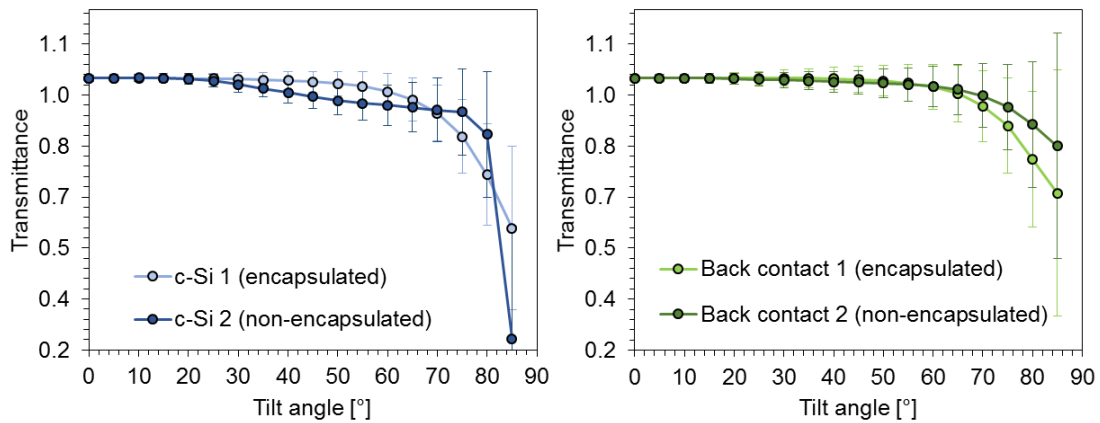


Figure 5. 18. Comparison of angular response of encapsulated/non-encapsulated c-Si (left) and back contact (right) devices.

The encapsulation of PV devices not only function as protection but also to reduce the variability in the angular loss at varying Aoi due to the physical factors, i.e different surface treatment method by manufacturers. The unique angular response shift observed in the measurement of non-encapsulated c-Si 1 device is likely to be caused by this physical factors.

5.4 Partial illumination method in I-V curve measurement of photovoltaic modules

Angular response characterisation of full size PV modules is carried out using the non-destructive partial illumination method to minimise the volume non-uniformity effect in the $I_{sc}(\theta)$ measurement [93, 9]. The method introduces a mismatch effect to PV devices with series cell connection by the application of a partial mask on the target cell within the device. The current this cell generates – the operating current, will then be detectable in the measured I-V curves of the module even at tilted angles, hence a reliable angular response characterisation is possible.

The positioning of the DUT on the rotation stage is crucial in the characterisation of full size modules. The usual (although not universal) physical arrangement of series-connected cells within c-Si PV modules is oriented to the longer side of the module frame. In any case, it is important to orient the module so that the cells strings are parallel to the axis of rotation. This ensures that the number of steps appearing in the I-V measurements corresponds to the number of cell sub-strings within the module (due to the change in irradiance in the z-axis) and that the photocurrent of the target (current-limiting) cell can be extracted [98]. 50% of the target cell area is masked using black tape. This high degree of

shading is to ensure that the current limit is set by the target cell, not by any other cell that happens to receive the least incident light (i.e. one that is rotated further from the light source, string 3 in Figure 5.5) [89].

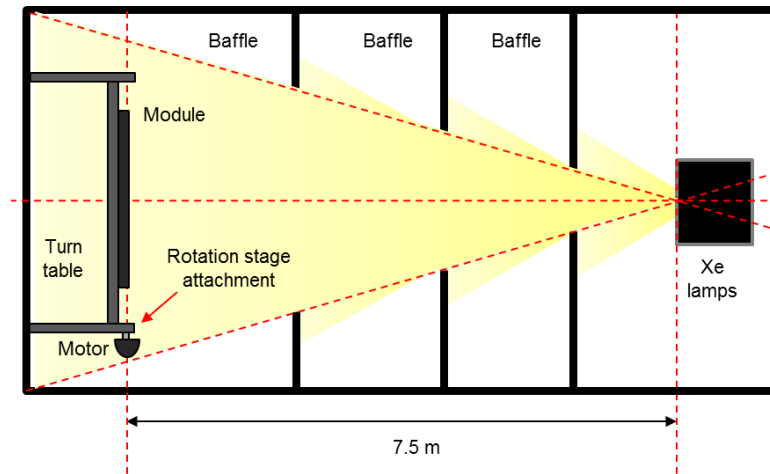


Figure 5.19. Plan view of the orientation of a module in respect to the centre point of the Xe lamps in the Pasan facility at CREST.

To reduce systematic errors due to the divergence of the Pasan light source, the target cell within the module is aligned with the centre point of the Xe lamps. For a module with 3 sub-strings, the target cell can be any cell in the middle string (actually of any string, but it is practical to use the centre one for mechanical balancing of the load on the rotation stage motor). For modules with different numbers or orientations of sub-strings, the placement is adjusted accordingly – just following the key principles that the cell strings should be parallel to the rotation axis and the target cell should align with the centre of the light source.

5.4.1 Extraction of target cell photocurrent from module I-V curves

In the partial illumination method, the extraction of operating current is performed by locating the intersection point between 2 I-V measurements of the same module, one with the tape shading applied to a cell and one being a voltage-scaled copy of the full, unshaded module I-V curve. Under the string mismatch condition caused by the partial shading of the target cell, in a module of n strings (bypass diodes) the total voltage of the remaining, unshaded strings (V_{n-1}) can be calculated by Eq. 5.18 [99]:

$$V_{n-1} = \left(\frac{n-1}{n}\right) \cdot V \quad \text{Eq. 5.18}$$

Where V is the full module voltage without shading. The voltage of the unshaded I-V curve is scaled by $\left(\frac{n-1}{n}\right)$ to remove the voltage contribution from the string containing the shaded target cell.

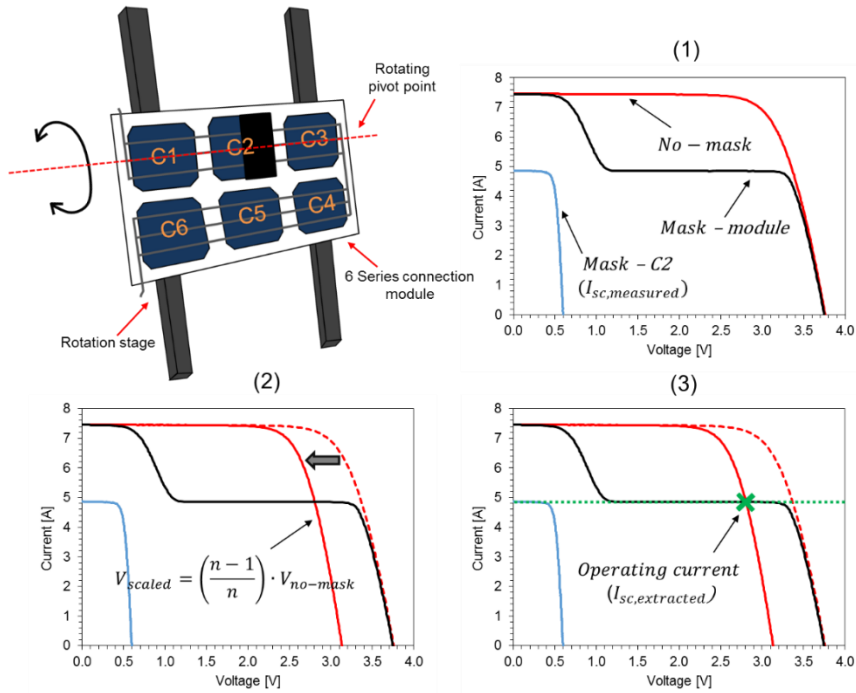


Figure 5. 20. Schematic of the 6 series-connected cells module in the validation of the algorithm for photocurrent extraction using the mismatch theory (top left) and graphs of I-V measurements showing the flow of the algorithm (1)-(3).

An algorithm to detect the intersection point of the 2 curves has been developed to automate the process of operating current extraction ($I_{sc,extracted}$). This algorithm is validated against the direct measurement of a custom 6 series-connected cells c-Si module. The module has accessible terminals attached to each cell, thus the direct measurement of I-V curves of individual cells is possible ($I_{sc,measured}$). Figure 5. 20 shows a simplified graph showing the flow of the algorithm (1-3).

Firstly, an I-V curve is measured without any shading in place. With the cell configuration in the module as shown above, opaque tape is applied over half of cell C2. The cell is bypassed by connecting two diodes across the terminals (C1-C2-C3 & C4-C5-C6). I-V measurements under both conditions are taken 4 times at each tilt angle. Each unshaded I-V curve is scaled down in voltage by a factor 5/6. Where these curves intersect their corresponding shaded I-V curve measurements, the current is read off and is taken as the photocurrent of the (half-shaded) target cell ($I_{sc,extracted}$).

These are compared to the photocurrents from the direct cell I-V measurement using the accessible terminals ($I_{sc,measured}$). The comparison between the normalised $I_{sc,measured}$ and $I_{sc,extracted}$ at different AoI is shown in Figure 5. 21. From the graph, it can be seen that the difference between the characteristics are less than 1%, even at a high angles of incidence, which is within the direct

measurement uncertainty. This value is adopted as an estimation of the additional uncertainty contribution for characterising modules, for which this operating current extraction method will be used.

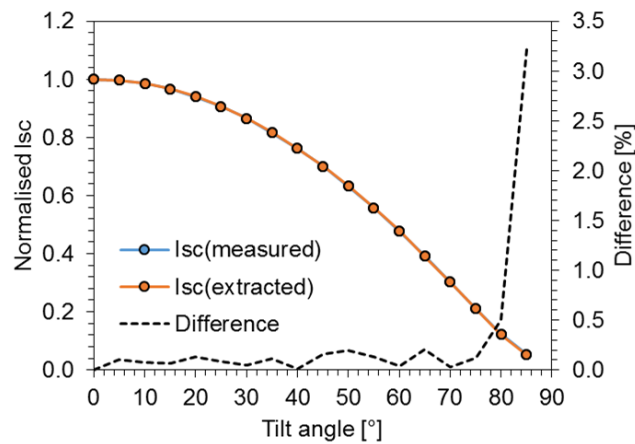


Figure 5. 21. Comparison of normalised short-circuit current measurements taken directly at the target cell's terminals to that extracted from an I-V measurement taken at the module's terminals.

5.4.2 Angular response measurements of full size photovoltaic modules

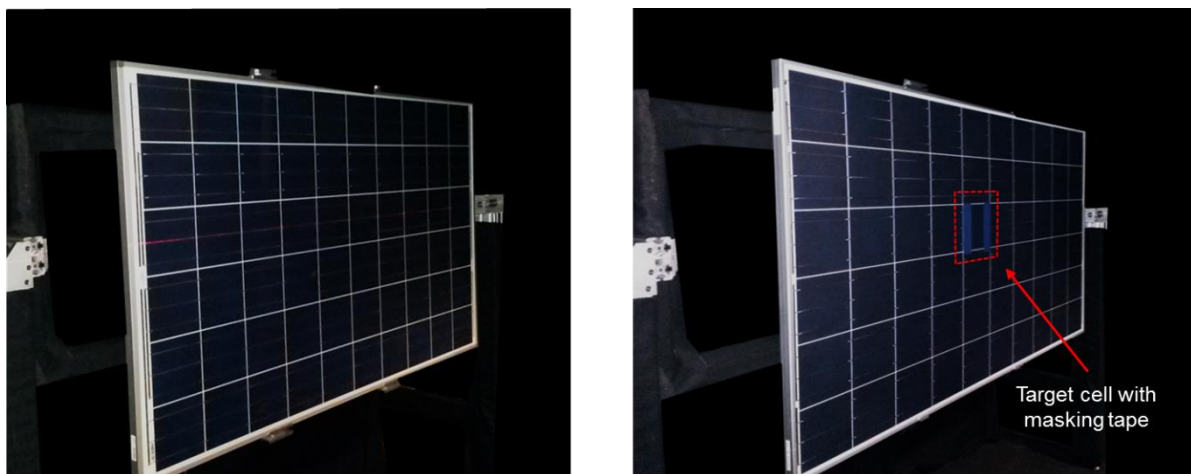


Figure 5. 22. Photograph of a PV module mounted on the rotation stage for I-V curve measurements with (right) and without (left) opaque tape applied to target cell

The partial illumination method has been applied to measure the angular response of two modules of different technologies, a mono-Si and a back contact module. These are the same sample modules which were used in the measurement of polychromatic spectral response in the previous chapter (Figure 4. 20). Results from these are plotted in Figure 5. 23.

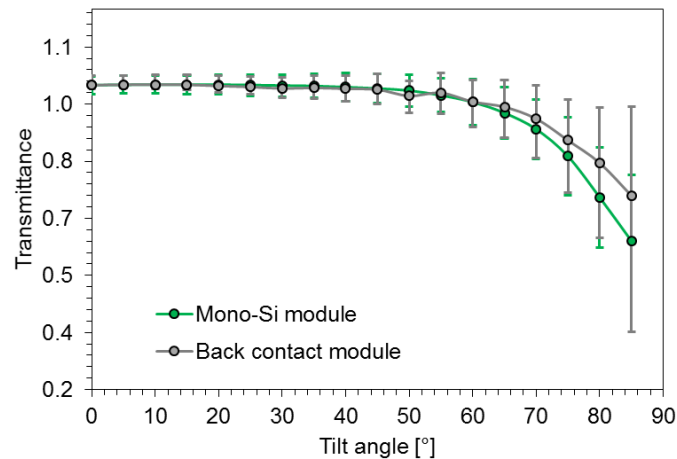


Figure 5. 23. Transmittance of mono-Si and back contact modules against varying tilt angle in the measurement of angular response using the modified Pasan solar simulator.

From this measurement, it is apparent that the AoI dependency of the mono-Si module is higher than that of the back contact module. The identical result in measurement of both full size modules and encapsulated individual cells of the same technologies strongly supports the successful upscaling of the characterisation technique.

5.5 Angle-dependent spectral response measurements of photovoltaic devices

Knowledge of the angular response characteristic of a PV device is important to determine the reflection losses experienced by the device under the non-standard operating conditions of the outdoor environment. It enables a more accurate performance prediction of the device under different conditions and so the overall energy yield over longer timescales. The angular response characterisation described in the previous sections provides information of the total irradiance loss due to reflection at given incident angles. However at a more detailed level, the transmittance/reflectance can be expected to vary by different wavelengths also, depending on the type of glass and coating used in the PV encapsulation system and any treatment of the cell surface [100, 101]. Therefore, to fully maximise accuracy in energy yield estimation, the full angle-dependent SR characteristic of the device will be necessary.

5.5.1 Angular/spectral effect on the performance of photovoltaic modules

Method for angle-dependent spectral response characterisation of PV devices

Very recently, research into characterisation methods of the angle-dependent spectral responsivity of PV devices has been conducted on the single cell scale by the FhG-ISE and PTB [102, 103]. The

characterisation is carried out using a monochromatic system with a rotation stage. The monochromatic illumination setup in PTB is a tuneable laser-based system while FhG-ISE use a more traditional narrow-band filter-based system. The former paper investigates the angular dependency of spectral response of PV devices with/without encapsulation, and the latter explores the effect of texturing of the cell on the spectral responsivity at varying angles (Figure 5. 24). Significant angular-spectral variation by wavelength is noticeable in all the measurements.

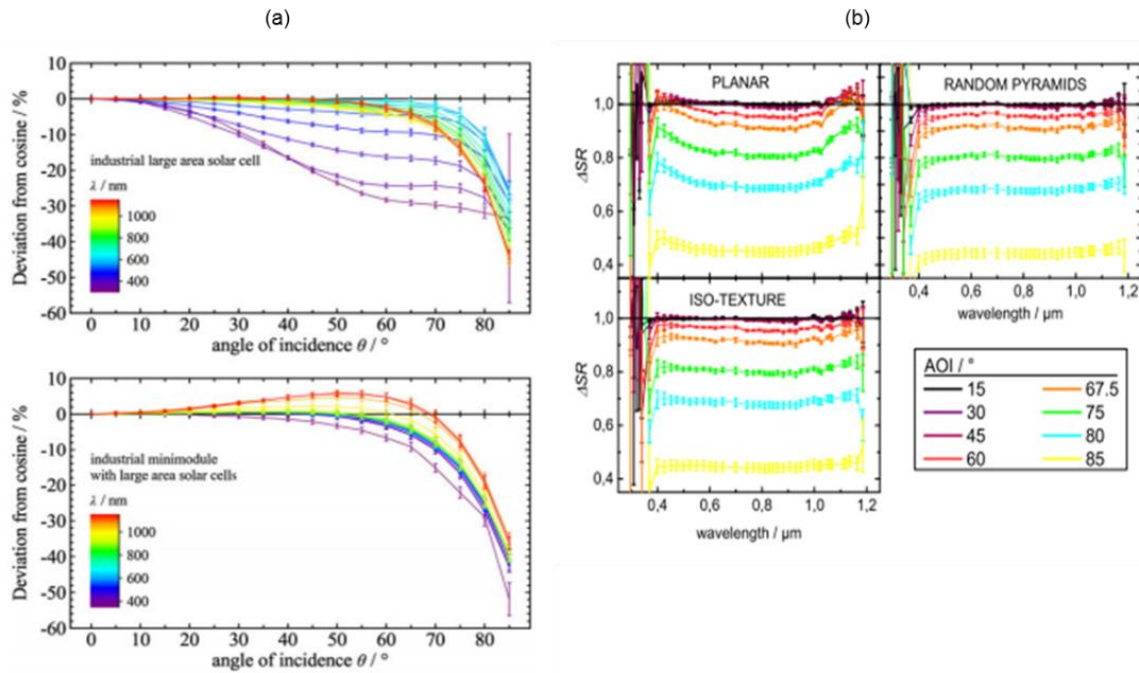


Figure 5. 24. Image of the angular spectral response curve of various PV devices determined using the DSR method with rotation table as developed by PTB (left) [103] and FhG (right) [102].

As can be seen in Figure 5. 24, quantification of angle-dependent spectral response performed by both institutions uses the ratio of measurement at each tilt angle to that at normal incidence. The DSR method adopted by the institutions restricts the measurement of absolute spectral response curves due to the high uncertainty contribution by the reference cell. Furthermore, the same inherent limitations of the monochromatic measurement setups employed makes the application of such characterisation to full size PV modules difficult (as described in the previous chapters).

Simulation of angle-dependent spectral response measurements using the polychromatic fitting method

Both the spectral response (polychromatic) and angular response (partial illumination) measurement methods described in this thesis are developed around the same facility of a standard large-area solar simulator and a few additional measurement tools, i.e. spectroradiometer and broadband filters for the spectral response measurement, and custom-built rotation stage attachment for the angular response

measurement. The combination of these measurement tools for the complete characterisation of angle-dependent spectral responsivity of full size PV modules using the Pasan facility in CREST would seem feasible.

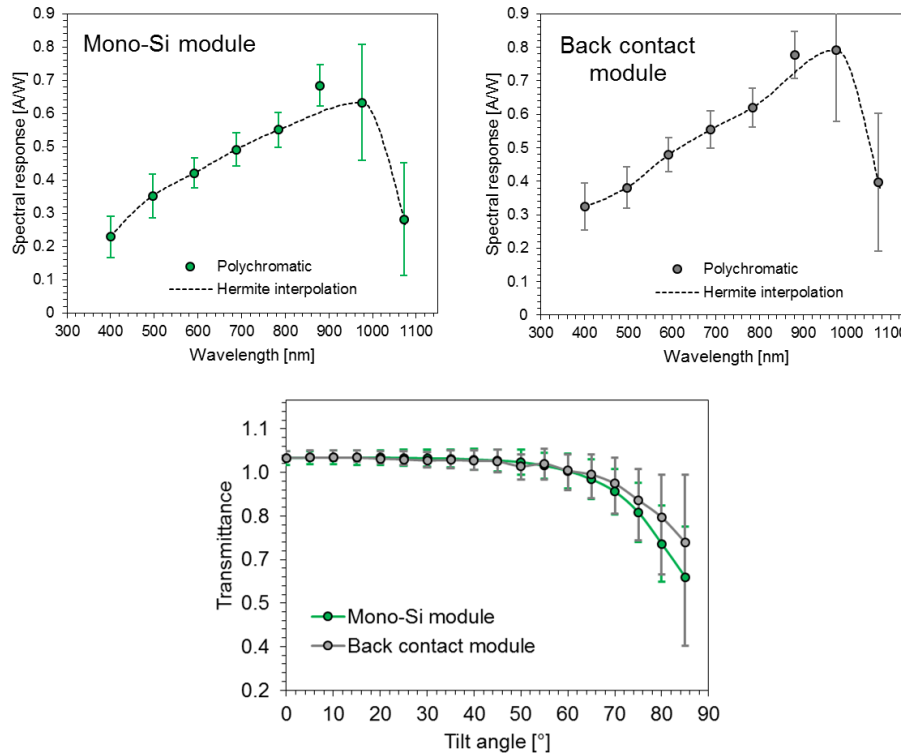


Figure 5. 25. Spectral response at normal incidence and broadband angular response of two full size modules determined using the polychromatic method and partial illumination method respectively.

To test the idea, simulations of this characterisation process have been performed using the results from the polychromatic and partial illumination measurement of two PV modules, one mono-Si and one back contact module (Figure 5. 25). Light transmittance data for both devices is used to modify the $I_{sc,filter}$ measurements of the corresponding device to account for their optical loss at tilted angles ($I_{sc,filter,\theta}$). The polychromatic fitting is then performed using the $I_{sc,filter,\theta}-E_{\lambda,filter}$ pairs as input for the determination of the absolute spectral response curves of the modules at each tilted angle. Results from this simulation are shown in Figure 5. 26.

The polychromatic method developed in this research has been established to be feasible, in that a comparable result to the measurements by the FhG-ISE (Figure 5. 24b) can be observed. It can be seen from the simulation result that the ratio between the spectral response curves at varying angles to the normal position shows slightly higher values in the response curves corresponding to 400nm and 1070nm at low tilt angles. At higher tilt angles, the difference in ratio values across the wavelength

points become less pronounced which implies the low angular dependency of spectral responsivity of the modules simulated here.

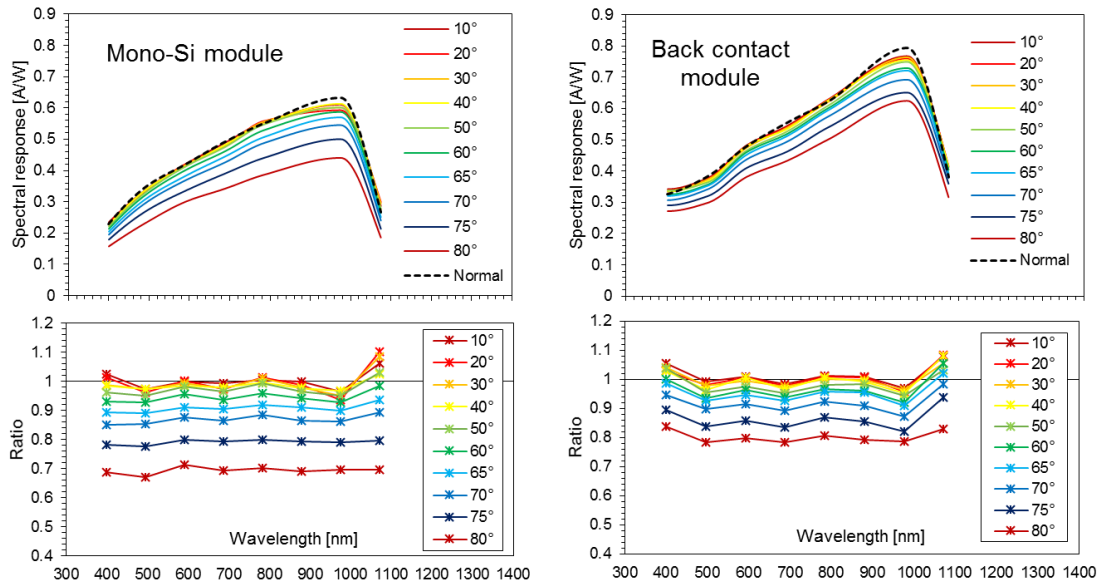


Figure 5.26. Simulation result of angle-dependent spectral response curves of mono-Si and back contact modules (top) and the ratio of the shift in spectral response curve at varying angle to the normal position (bottom).

The feasibility of employing the Pasan facility for the characterisation of angular dependent spectral response of full size PV modules has been demonstrated through this simulation. Research into this characterisation method will lead to a more complete characterisation and improved accuracy in the energy yield calculation of PV modules operating under real environments.

5.6 Conclusions

In this chapter, the methods to quantify the angular loss behaviour of PV modules was discussed. The absence of specific angular response measurement data contributes to uncertainty in the calculation of PV energy yield. Through the energy yield simulation using the widely used PVsyst software, it is found that 4% different in angular response dependency between PV modules against high tilt angle (<60°) will result in about 1.5% different in annual energy yield under the same orientation and environmental conditions. High uncertainty in existing outdoor methods due to the meteorological dependency, equipment calibration and the constant shift in spectrum and temperature of outdoor conditions led to the development of the indoor angular response measurement method.

In this work, the Pasan facility in CREST with its custom rotation stage attachment was used to develop an indoor angular response measurement setup. Evaluation of the setup has been performed through direct experiment and excessive background light due to divergence of the light source is found to be the major uncertainty contributor in the measurement – up to 52% at high tilt angles. Measurement of the Aol dependency of full size PV modules is carried out using the non-destructive method introduced by TUV Rheinland. This method allows for the $I_{sc,\theta}$ measurement of a single cell within the module with minimum volume non-uniformity effect to be performed even at high tilt angle.

Angular response measurements and uncertainty analyses have been performed with various PV devices, of different types, scales and encapsulation and the results are compared to measurements by other laboratories and to angular loss modelling. The angular response of encapsulated PV devices demonstrates 4% variability at high tilt angle. It is evident that the back contact technology has a lesser sensitivity to varying Aol, most likely thanks to an undisclosed cell treatment by the manufacturer. The same trend is also observed in the measurements of full size PV modules.

The characterisation of angle-dependent spectral response of PV devices improves knowledge of the behaviour of the devices in real environments, which will result in the improved accuracy in the calculation of energy yield from different modules. The possibility of full characterisation using the combination of indoor angular response and polychromatic spectral response methods introduced in this thesis is demonstrated through the simulation using measurement results of two full size PV modules.

6 Thesis conclusions

Improvements to energy yield modelling, including for standardised energy rating, call for more detailed characterisation of PV modules. Specifically, this should include the spectral and angular response functions to more accurately model the effects of varying spectrum and sun position on module performance. The measurement of these characteristics for large area (full commercial size) PV modules is challenging, mostly due to the limitations of measurement setup. Despite being published as a standard (IEC 61853-2), only a handful of reports can be found on the measurement methods to acquire spectral and angular response characteristics at module scale and even fewer describing their uncertainties. It has been the aim of this thesis to contribute to the standardisation and improvement of the PV energy rating method through the development of practical and simplified measurement methods, with accuracy and uncertainty validated against other procedures.

6.1 Spectral response characterisation

Preliminary development work on SR characterisation of PV modules, based on the concept of the polychromatic method has been described previously. The polychromatic method combines both measurement and fitting processes in the determination of SR characteristics and relies on wideband (polychromatic) filtering of a white light source, modelling of the spectral response and a parameter fitting/optimisation process. The spectral response work of this thesis has contributed a complete overhaul of the method, replacing and substantially improving hardware and software elements and the core model and fitting engine. Furthermore, an extensive evaluation of the uncertainties has been undertaken for the first time, including the inputs and propagation to the output result. The final uncertainty in the determined spectral response has been tested as part of a first-of-its-kind intercomparison of spectral response measurements between leading laboratories in Europe.

Measurement of SR characteristics of PV devices by the new polychromatic method has shown good agreement to that of the DSR method with $\pm 10\%$ difference across the usable wavelength range. Uncertainty in SR polychromatic measurement of full size PV modules corresponding to the UV and visible light ranges has shown that uncertainty within 7% is achievable. Although SR determination by the polychromatic method is obtained indirectly, the incorporation of detailed information of the uncertainties in incident spectral irradiance and corresponding short-circuit current measurements into the SR model throughout the process yields a low and validated uncertainty in the final result. The specific improvements developed as part of this work are described as follows:

6.1.1 Coloured broadband filters

The fundamental idea of the polychromatic method is to maximise the incident filtered irradiance for the measurement of SR characteristic of PV devices. The preliminary work on this method utilised a set of paper-thin gel-type coloured broadband filters to modify the light source spectrum. Unreliability regarding the physical fragility of such filters restricted their application in the solar simulator for the measurement of large area PV devices. In this work, a new set of hard plate coloured broadband filters has been assembled and employed to significantly improve the polychromatic measurement. Thorough evaluation of the target plane irradiance non-uniformity has demonstrated that the throughput irradiance is only weakly affected by the filters, with maximum increase of only 0.5% as compared to the unfiltered irradiance. The lowest total throughput irradiance measured from the set of filters is 150W/m^2 , still higher than the minimum irradiance value specification for the power measurement G-T matrix of the IEC energy rating standard. This high incident irradiance contributes to low uncertainty in the measurement of short-circuit current ($I_{sc,filter}$) of full size commercial modules, where the estimated standard uncertainty ($u_{I_{sc,filter}}$) ranges from 1.5% to 2.5% (within the uncertainty margin of I_{sc} at STC).

The set of filters currently employed in this work has a total of 15 filters with unique wavelength cut-off profiles. It has been demonstrated through simulation that increasing the number of filters with consideration of uniform distribution of cut-off wavelengths across the full band would further improve the result of the SR curve determination by the polychromatic method (although may be cost-prohibitive).

6.1.2 Spectral irradiance measurement

A substantial portion of the polychromatic measurement data points is made up of spectral irradiance data. In this work, the spectral measurements have been performed using an Avantes CCD-array based spectroradiometer in the raw unit of incident counts per array pixel. Translating this measurement into an accurate absolute spectral irradiance value in $\text{W/m}^2/\text{nm}$ requires an extensive evaluation of the instrument. Effects of stray light on each of the pixels and their linearity have been evaluated as part of the detailed calibration process of the spectroradiometer. A transfer function has been incorporated into the equation of absolute spectral irradiance to compare the spectroradiometer measurement to the calibration curve of a traceable standard lamp. Correction of wavelength mapping by the peak detection method have been performed using pencil line lamps. The evaluation of uncertainty in spectral measurement is a complex task where the relative uncertainty in each of the sources mentioned are propagated and combined in accordance with the GUM [43]. The uncertainty in spectral measurement corresponding to the visible/UV and NIR is 5% and 30%, respectively.

The incorporation of uncertainty associated with the spectral measurement into the polychromatic measurement reliably is a challenge in itself. Currently there are no standardised guidelines for the propagation of spectral measurement uncertainty into other parameters such as the MMF, etc. In this work, a random walk method has been adopted to perform this task where measurement of spectral irradiance is varied randomly within the limits of the uncertainty envelope for each wavelength to preserve the correlation between the neighbouring wavelengths throughout. Through this method, the uncertainty in spectral measurement is successfully propagated into the final result of polychromatic SR measurement.

6.1.3 Fitting algorithm

In this work, the polychromatic fitting algorithm, based on a gradient descent method, has been developed for integration of measurement data and the numerical based SR curve model. The reported preliminary work of the polychromatic method employed a non-linear Gaussian summation function in the fitting algorithm. While the function is able to replicate the typical SR curve of PV devices, the flexibility of the function and high number of parameter in the function gave rise to instability in parameter convergence. Simulation of the SR model demonstrated that a continuous function would often result in failure in parameter convergence due to the complex relationship between variables of the function. This resulted in extreme sensitivity of the algorithm to starting input values, with the high number of parameters in the SR curve model increasing the risk of failure in parameter convergence. As a result, the fitting process was often unstable and thus had limited scope for reliable application as a characterisation method.

To allow for stable parameter convergence, a piecewise linear step function has been evaluated for use in the polychromatic fitting algorithm. Robust statistical analysis proved that optimal balance between the availability of spectral data and number of parameters is the factor that influences stability in parameter convergence. High spectral variation will contribute to increased certainty of output and better coverage of measurement points over the usable wavelength range.

6.2 Angular response characterisation

Standard methods for the angular response characterisation of PV modules have only been published recently. Research into outdoor measurement methods is more common than indoor, as evidenced by the number of reports on such work. The indoor measurement method in this thesis has been developed using a standard module-area solar simulator for reasons of practicality. The angular distribution effect, also called the simulator loss, in such a measurement setup can be a major drawback in the accuracy of angular response measurements, especially for series connected modules. In this work, current

measurements of such modules have been performed using a partial illumination method to minimise the volume non-uniformity effect of the setup. The effect of systematic errors on the measurement of the short-circuit current of the DUT at different angles has been investigated and incorporated in the propagation of uncertainty to the final characteristic.

A set of PV devices with dimensions ranging from reference cells to full size PV modules has been measured and compared to results from other laboratories. The measurement setup consists of a custom rotating stage attachment and Pasan solar simulator for the determination of light transmittance dependency against varying angle-of-incidence (AoI). The devices can be categorised as encapsulated/non-encapsulated. Results from the measurement of encapsulated PV devices demonstrated 4% variation at a large tilt angle of 80°.

6.2.1 Measurement setup

Optical factors in the measurement setup govern the accuracy of angular response measurements of PV devices. Electrical factors in the measurement uncertainty mostly cancel out in this calculation, due to the normalisation approach. Ideally a fully collimated light source would be used for the measurement of the angular characteristic. High variation of angular distribution of the Pasan light source resulted in increased uncertainty with regard to the true angle of incidence to the DUT. This has been realised as a map of measurements of the short-circuit current of a PV cell in a restricted field-of-view tube at various points across the measurement plane. This enabled a definition of suitable area in the test plane to conduct angular response measurements with minimal influence from the non-ideal source.

The significance of the light divergence effect in angular response measurement was evaluated. The estimation of this effect as uncertainty in the measurement has been performed using a geometrical approximation. It was established that excessive background light, resulting from reflection of divergent light, is the predominant factor in the uncertainty of the angular response measurements. Improvement to reduce background light within the specific measurement setup of this work have been achieved by careful suppression of localised reflectance in the test chamber (a 20% reduction in measured current distortion at high angles of incidence).

6.2.2 Measurement of photovoltaic modules

The simulator loss effect contributes to uncertainties in measurement of short-circuit current of series connected multi-cell modules as the tilt angle is increased. This is caused by uncertainty in the detection of operating currents of individual sub-strings within the module. To control operating current extraction,

a mismatch condition is forced on the target cell of the module by the application of deliberate shading on half of the cell. The current limiting behaviour demonstrated by the target cell allows for reliable operating current detection. Hence, there is an increase in confidence in the current measurement of the module even at high incident angles. An algorithm to automate operating current extraction has been developed with accuracy to 1%. The comparison between angular response measurements of standard mono-Si and back contact devices demonstrated variation at high tilt angles, with the latter being less sensitive against varying angle of incidence – results in line with other published characteristics.

Angular response measurements of various commercial size PV cells have shown that the angular response characteristics of PV devices varies by 4%. This translates to approximately 1.5% difference in the simulation of annual energy yield under the same array orientation and weather data (Loughborough used as an example).

6.3 Potential future research

The development of the SR polychromatic measurement method has demonstrated the significance of quantity of measurement data points in improving the uncertainty in the output of the fitting algorithm. Research regarding the type of filters and the distribution of cut-off wavelength of filters for application of the polychromatic measurement setup would be very useful for optimisation of the method. Strong correlation between the SR model and success in the parameter convergence has been established through the evaluation of sensitivity of the fitting algorithm. Exploration of other models for SR characteristic representation would open up possibilities for the development of a more efficient fitting algorithm.

Detailed knowledge of the optical factors i.e. angular distribution of divergent light, details of light reflectivity around the measurement setup and volume non-uniformity of the illumination, could extensively reduce uncertainty in angular response measurement. Although the unique orientation of light bulbs in the Pasan light source results in high irradiance uniformity over the 2x2 m measurement plane at the distance of 8 m, the complexity of light projection makes the evaluation of optical factors in depth quite challenging. A branch of research dedicated to exploring these effects on this commonly used facility would be beneficial in assisting PV energy rating standardisation.

Development of spectral and angular response characterisation methods around the same solar simulator facility creates the potential for the measurement of full angle-dependent spectral response

characteristics of PV modules (an “SR-AR matrix”). Comprehensive characterisation of PV modules as such would substantially contribute to improvements in accuracy of PV energy rating assessment and would be congruent with the approach taken by the IEC in other parts of the energy rating standard so far. The possibility of such characterisation has been demonstrated through the simulation of polychromatic fitting using the measurements of both spectral and angular response characteristics of the same module as inputs and could form the basis of a practical implementation.

Publications and achievement

Journal publication (plan):

Authors: Husyira Al Husna, Tom Betts.

Title: Effect of Spectral Response Measurement of PV Modules in Energy Yield Modelling.

Target journal: Progress in Photovoltaics.

Conferences:

- 1) Influence of spectral variations on photovoltaic module energy rating; 13th Photovoltaic Science, Application & Technology, (PVSAT-13), Oral presentation, 2017.

- 2) Uncertainty in spectral response measurement of photovoltaic modules; 26th International Photovoltaic Science and Engineering Conference (PVSEC-26), Poster presentation, 2016.

- 3) Validation of spectral response polychromatic method measurement of full size photovoltaic modules using outdoor measured data; 12th Photovoltaic Science, Application & Technology (PVSAT-12), Poster presentation, 2016.

- 4) Spectral response measurements of photovoltaic devices using a pulsed source solar simulator; 11th Photovoltaic Science, Application & Technology (PVSAT-11), Oral presentation, 2015.

- 5) Spectral response measurements of photovoltaic modules using a flash solar simulator; 25th International Photovoltaic Science and Engineering Conference, (PVSEC-25) Oral presentation, 2015.

Award:

Best Student Poster Prize by the Institute of Physics (IoP) at the 12th Photovoltaic Science, Application & Technology (PVSAT13).

References

- [1] Paris: REN21 Secretariat, "Renewables 2017 Global Status Report," Renewable Energy Policy Network for the 21st Century, 2017.
- [2] International Finance Corporation; World Bank Group, "Utility-Scale Solar Photovoltaic Power Plant," International Finance Corporation, Washington, 2015.
- [3] Y. Poissant, S. Pelland and D. Turcotte, "A comparison of energy rating methodologies using field test measurements," in *23rd European Photovoltaic Solar Energy Conference and Exhibition*, Valencia, Spain, 2008.
- [4] J. Roy, T. R. Betts, R. Gottschalg, S. Mau, S. Zamini, R. P. Kenny, H. Mullejans, G. Friesen, S. Dittmann, H. G. Beyer and A. Jagomagi, "Validation of proposed photovoltaic energy rating standard and sensitivity to environmental parameters," in *European Photovoltaic Solar Energy Conference and Exhibition*, Valencia, Spain, 2008.
- [5] R. P. Kenny, D. Vigano, E. Salis, G. Bardizza, M. Norton, H. Mullejans and W. Zaaiman, "Power rating of photovoltaic modules including validation of procedures to implement IEC 61853-1 on solar simulators and under natural sunlight," *Prog. Photovolt: Res. Appl*, vol. 21, pp. 1384-1399, 2013.
- [6] D. Dimberger, B. Muller and C. Reise, "PV module energy rating: opportunities and limitations," *Prog. Photovolt: Res. Appl*, vol. 23, pp. 1754-1770, 2015.
- [7] T. Huld, E. Salis, A. Pozza, W. Herrmann and H. Mullejans, "Photovoltaic energy rating data sets for Europe," *Solar Energy*, vol. 133, pp. 349-362, 2016.
- [8] I. D. Sara, "Polychromatic Determination of Spectral Response of PV Devices (Unpublished thesis)," Loughborough University, 2013.

- [9] W. Herrmann, M. Schweiger and L. Rimmelspacher, "Solar simulator measurement procedures for determination of the angular characteristic of PV modules," in *29th European Photovoltaic Solar Energy Conference and Exhibition*, Amsterdam, 2014.
- [10] National Renewable Energy Laboratory, "Research cell efficiency record," [Online]. Available: <https://www.nrel.gov/pv/assets/images/efficiency-chart.png>.
- [11] National Center for Photovoltaics, "Cell efficiency explanatory notes," [Online]. Available: https://www.nrel.gov/pv/assets/pdfs/cell_efficiency_explanatory_notes.pdf.
- [12] L. M. Fraas, "History of Solar Cell Development," in *Low-cost Solar Electric Power*, New York, Springer International Publishing, 2014, pp. 1-10.
- [13] L. M. Fraas, "Types of Photovoltaic Cells," in *Low-cost Solar Electric Power*, New York, Springer International Publishing, 2014, pp. 31-41.
- [14] M. A. Green, K. Emery, Y. Hishikawa, W. Wilhelm, E. D. Dunlop, D. H. Levi and A. W. Ho-Baillie, "Solar cell efficiency tables (version 49)," *Progress in Photovoltaics: Research and Applications*, vol. 25, pp. 3-13, 2017.
- [15] Kaneka Corporation, "World's Highest Conversion Efficiency of 26.33% Achieved in a Crystalline Silicon Cell," Kaneka Corporation, Tokyo, 2016.
- [16] D. Chiras, "An Introduction to Solar Electricity," in *Power from the Sun*, Gabriola Island, New Society Publishers, 2009, pp. 1-21.
- [17] Fraunhofer Institute for Solar Energy Systems, ISE & PSE AG, "Photovoltaics report," Fraunhofer Institute for Solar Energy Systems, ISE, 2017.
- [18] R. Fu, D. Feldman, R. Margolis, M. Woodhouse and K. Ardani, "U.S. Solar Photovoltaic System Cost Benchmark: Q1 2017," National Renewable Energy Laboratory, 2017.
- [19] Solargis, "The World Bank, Solar resource data: Solargis," 2017. [Online]. Available: <https://solargis.com/maps-and-gis-data/download/world>.

- [20] M. Bliss, "Measurement System for Fast Power and Energy Rating of Photovoltaic Devices (Unpublished PhD Thesis)," 2011 .
- [21] M. Wiesenfarth, S. P. Philipps, A. W. Bett, K. Horowitz and S. Kurtz, "Current status of concentrator photovoltaic (CPV) technology," Fraunhofer & NREL, 2017.
- [22] Sandia Natinal Laboratories, "PV Performance modelling collaborative : Spectral Response," [Online]. Available: <https://pvpmc.sandia.gov/modeling-steps/2-dc-module-iv/effective-irradiance/spectral-response/>.
- [23] S. R. Williams, T. R. Betts, R. Gottschalg, D. Neumann, M. O. Prast and A. Nositchka, "Evaluating the outdooe performance of PV modules with different glass textures," in *26th EUPVSEC*, Hamburg, 2011.
- [24] J. H. Fatehi and K. J. Sauer, "Modelling the incidence angle dependence of photovoltaic modules in PVsyst," in *Photovoltaic Specialists Conference (PVSC), 2014 IEEE 40th*, Colorado, USA, 2014.
- [25] IEC 61853-2, "PV module performance testing and energy rating - Part 2: Spectral responsivity, incidence angle and module operating temperature measurements," 2016.
- [26] D. L. King, "Photovoltaic module and array performance characterization methods for all system operating conditions," *AIP Conference Proceedings*, vol. 394, no. 347, 1997.
- [27] D. Anderson, T. Sample and E. Dunlop, "Obtaining module energy rating from standard laboratory measurements," in *17th European Photovoltaic Solar Energy Conference (EUPVSEC)*, Munich, Germany, 2001.
- [28] R. Bharti, J. Kuitche and M. G. TamizhMani, "Nominal Operating Cell Temperature (NOCT) : Effects of module size, loading and solar spectrum," in *34th IEEE Photovoltaic Specialists Conference (PVSC)*, Philadelphia, 2009.
- [29] T. Candelario, S. Hester, T. Townsend and D. Shipman, "PVUSA-performance, eperience, and cost (PV power systems)," in *Photovoltaic Specialists Conference*, Las Vegas, 1991.

- [30] C. M. Whitaker and J. D. Newmiller, "Photovoltaic Module Energy Rating Procedure," National Renewable Energy Laboratory, Colorado, 1998.
- [31] A. Louwen, A. C. de Waal, R. E. I. Schropp, A. P. C. Faaij and W. G. J. H. M. van Sark, "Comprehensive characterisation and analysis of PV module performance under real operating conditions," *Prog. Photovolt: Res. Appl*, vol. 25, pp. 218-232, 2017.
- [32] IEC 60904-3, "Photovoltaic devices - Part 3: Measurement principles for terrestrial photovoltaic (PV) solar devices with reference spectral irradiance data," 2016.
- [33] IEC 60904-9, "Photovoltaic devices - Part 8: Solar simulator performance requirements," 2007.
- [34] IEC 60904-1, "Photovoltaic devices - Part 1: Measurement of photovoltaic current-voltage characteristic," 2006.
- [35] T. Huld, E. Dunlop, H. G. Beyer and R. Gottschalg, "Data sets for energy rating of photovoltaic modules," *Solar Energy* 93, pp. 267-279, 2013.
- [36] T. Huld and A. M. G. Amillo, "Estimating PV Module Performance over Large Geographical Regions: The Role of Irradiance, Air Temperature, Wind Speed and Solar Spectrum," *Energies*, vol. 8, pp. 5159-5181, 2015.
- [37] D. L. King and P. E. Eckert, "Characterizing (rating) the performance of large photovoltaic arrays for all operating conditions," in *25th Photovoltaic Specialist Conference*, Washington DC, 1996.
- [38] B. Kroposki, K. Emery, L. Mrig, C. Whitaker and J. Newmiller, "Photovoltaic module energy rating methodology development," in *25th IEEE Photovoltaic Specialist Conference*, Washington DC, 1996.
- [39] IEC 61853-1, "PV module performance testing and energy rating - Part 1: Irradiance and temperature performance measurements and power rating," 2011.
- [40] IEC 60904-8, "Photovoltaic devices - Part 8: Measurement of spectral responsivity of a photovoltaic device," 2014.

- [41] D. Faiman, "Assessing the Outdoor Operating Temperature of Photovoltaic Modules," *Prog. Photovolt: Res. Appl.*, vol. 16, pp. 307-315, 2008.
- [42] IEC 61853-4, "Photovoltaic (PV) module performance testing and energy rating - Part 4: Standard reference climatic profiles," 2016.
- [43] ISO, "Guide to the Expression of Uncertainty in Measurement (GUM)," 1995.
- [44] H. Mullejans, W. Zaaiman and R. Galleano, "Analysis and mitigation of measurement uncertainties in the traceability chain for the calibration of photovoltaic devices," *Measurement Science and Technology*, vol. 20, pp. 075-101, 2009.
- [45] D. Dimberger, G. Blackburn, B. Muller and C. Reise, "On the impact of solar spectral irradiance on the yield of different PV technologies," *Solar Energy Materials and Solar Cells*, vol. 132, pp. 431-442, January 2015.
- [46] J. Hohl-Ebinger and W. Warta, "Uncertainty of the spectral mismatch correction factor in STC measurements on photovoltaic devices," *Progress in Photovoltaics: Research and Applications*, vol. 19, pp. 573-579, 2011.
- [47] B. H. Hamadani, J. Roller, B. Dougherty, F. Persaud and H. W. Yoon, "Absolute spectral responsivity measurements of solar cells by a hybrid optical technique," *Optical Society of America*, vol. 52, no. 21, pp. 5184-93, 2013.
- [48] I. D. Sara, T. R. Betts and R. Gottschalg, "Determining spectral response of a photovoltaic device using polychromatic filters," *IET Renewable Power Generation*, pp. 467-473, 2014.
- [49] H. Field, "Solar cell spectral response measurement errors related to spectral band width and chopped light waveform," in *26th IEEE Photovoltaic Specialists Conference*, California, 1997.
- [50] J. Metzdorf, "Calibration of solar cells. I: The differential spectral responsivity method," *Appl. Opt.*, vol. 26, no. 9, pp. 1701-1708, 1987.

- [51] J. Carabe, "A new approach to measuring spectral responses of non-linear solar cells," *Solar Cells*, vol. 31, pp. 39-46, 1991.
- [52] S. Winter, T. Fey, I. Kroger, D. Friedrich, K. Ladner, B. Ortel, S. Pendsa and F. Witt, "Design, realization and uncertainty analysis of a laser-based primary calibration facility for solar cells at PTB," *Measurement*, vol. 51, pp. 457-463, 2014.
- [53] M. Mundus, D. Lill, J. Hohl-Ebinger and W. Warta, "Advanced spectral response measurement with wide range tunable laser system," in *29th European PV Solar Energy Conference and Exhibition (EUPVSEC)*, Amsterdam, 2014.
- [54] B. Hamadani, J. Roller, H. Yoon and B. Dougherty, "A large-area, LED-based spectral response measurement system for solar PV device characterization," in *Semiconductor Device Research Symposium (ISDRS)*, Maryland, USA, 2011.
- [55] P. R. Beljean, J. Roux, Y. Pelet, C. Droz, N. Peguiron and V. Fakhfour, "Module spectral response measurements using large flashers," in *25th European Photovoltaic Solar Energy Conference and Exhibition (EUPVSEC)*, Valencia, Spain, 2010.
- [56] M. Pravettoni, A. Komlan, R. Galleano, H. Mullejans and E. D. Dunlop, "An Alternative Method for Spectral Response Measurements of Large-Area Thin Film Photovoltaic Modules," *Prog. Photovolt: Res. Appl.* 2012, pp. 416-422, 2011.
- [57] Y. J. Ye, S. Guo, M. T. Walsh, Y. Hishikawa and A. R. Stangl, "On the spectral response of PV modules," *IOPScience*, no. Meas. Sci. Technol. 25 095007, pp. 1-15, 2014.
- [58] M. Schweiger, M. Ulrich, I. Nixdor, L. R. U. Jahn and W. Hermann, "Spectral analysis of various thin-film modules using high-precision spectral response data and solar spectral irradiance data," Frankfurt, 2012.
- [59] Y. Tsuno, Y. Hishikawa and K. Kurokawa, "A Method for Spectral Response Measurements of Various PV Modules," in *23rd EU PVSEC*, Valencia, Spain, Sept. 2008.

- [60] H. Schade and Z. E. Smith, "Optical properties and quantum efficiency of a-Si_{1-x}C_x: H/a-Si: H solar cells," *Journal of Applied Physics*, vol. 57, pp. 568-574, 1985.
- [61] P. Sperfeld, K. -H. Raatz, B. Nawo, W. Moller and J. Metzdorf, "Spectral-irradiance scale based on radiometric black-body temperature measurements," *Metrologia*, vol. 32, pp. 435-439, 1995.
- [62] I. D. Sara, T. R. Betts and R. Gottschalg, "Analysis of a suitable model for spectral response of a photovoltaic device," in *27th European Solar Energy Conference and Exhibition (EUPVSEC)*, Frankfurt, Germany, 2012.
- [63] K. Levenberg, "A Method for the Solution of Certain Non-Linear Problems in Least Squares," *The Quarterly of Applied Mathematics*, vol. 2, pp. 164-168, 1944.
- [64] W. H. Press, S. A. Teukolsky, W. T. Vetterling and B. P. Flannery, "Minimization or Maximization of Functions," in *Numerical Recipes 3rd Edition: The Art of Scientific Computing*, New York, Cambridge University Press, 2007, pp. 487-555.
- [65] D. E. Goldberg, "A gentle introduction to genetic algorithm," in *Genetic Algorithms in Search, Optimization & Machine Learning*, New York, US, Addison-Wesley Publishing Company, Inc., 1989, pp. 1-25.
- [66] B. Mihaylov, "Uncertainty considerations in photovoltaic measurements (Unpublished thesis)," Loughborough University, 2016.
- [67] JCGM 102:2011, "Evaluation of measurement data - Supplement 2 to the "Guide to the expression of uncertainty in measurement", 2011.
- [68] J. Klafter and I. M. Sokolov, *First Steps in Random Walks: From Tools to Applications*, New York, US: Oxford University Press Inc., 2011.
- [69] B. Mihaylov, M. Bliss, T. Betts and R. Gottschalg, "Propagation of measurement uncertainties in mismatch factor correction for photovoltaic device calibration," in *The 6th World Conference on Photovoltaic Energy Conversion*, Kyoto, Japan, 2014.

- [70] E. W. Weisstein, "Piecewise Constant Function," MathWorld - A Wolfram Web Source , [Online]. Available: <http://mathworld.wolfram.com/PiecewiseConstantFunction.html>. [Accessed 2017].
- [71] P. Aksoy and L. Denardis, *Information Technology in Theory*, Boston: Thomson Learning Inc., 2008.
- [72] W. H. Press, S. A. Teukolsky, W. T. Vetterling and B. P. Flannery, "Interpolation and Extrapolation," in *Numerical Recipes 3rd Edition: The Art of Scientific Computing*, New York, Cambridge University Press, 2007, pp. 110-154.
- [73] E. W. Weisstein, "Hermite's Interpolating Polynomial," MathWorld - A Wolfram Web Source, [Online]. Available: <http://mathworld.wolfram.com/Hermite'sInterpolatingPolynomial.html>. [Accessed 2017].
- [74] R. H. Bartels, J. C. Beatty and B. A. Barsky, "Hermite and Cubic Spline Interpolation," in *An Introduction to Spline for Use in Computer Graphics & Geometric Modeling*, California, Morgan Kaufmann Publisher Inc., 1987, pp. 9-18.
- [75] Y. Horio, M. M. Rahman, Y. Imai, Y. Hishikawa and T. Minemoto, "Impact of average photon-energy coefficient of solar spectrum on the short circuit current of photovoltaic modules," *Current Applie Physics*, vol. 17, pp. 1341-1346, 2017.
- [76] N. Martin and J. M. Ruiz, "Calculation of the PV modules angular losses under field condition by means of an analytical model," *Solar Energy Materials & Solar Cells*, vol. 70, pp. 25-38, 2001.
- [77] S. C. Pop, V. Abbaraju, B. Brophy, S. Yang, S. Maghsoodi and P. Gonsalves, "A Highly Abrasive-Resistant, Long-Lasting Anti-Reflective Coating for PV Module Glass," in *2014 IEEE 40th Photovoltaic Specialist Conference (PVSC)*, Colorado, 2014.
- [78] E. Klimm, T. Lorenz and K.-A. Weiss, "Can anti-soiling coating on solar glass influence the degree of performance loss over time of PV modules drastically?," in *28th European Photovoltaic Solar Energy Conference and Exhibition*, Paris, 2013.

- [79] R. Hammond, D. Srinivasan, A. Harris and J. Wohlgermuth, "Effects of soiling on PV module and radiometer performance," in *IEEE Photovoltaic Specialists Conference*, California, 1997.
- [80] M. Garcia, L. Marroyo and M. Perez, "Soiling and other optical losses in solar-tracking PV plants in Navarra," *Progress in Photovoltaics*, vol. 19, no. 2, pp. 211-217, 2010.
- [81] N. Martin, E. Mujeto, F. Soriano, S. Temprano and M. C. Alonso-Garcia, "Validating an angular of incidence losses model with different PV technologies and soiling conditions," in *27th European Photovoltaic Solar Energy Conference and Exhibition*, Frankfurt, Germany, 2012.
- [82] B. H. King, D. Riley, C. D. Robinson and L. Pratt, "Recent advancements in outdoor measurement techniques for angle of incidence effects," in *IEEE Photovoltaic Specialist Conference (PVSC)*, New Orleans, LA, USA, 2015.
- [83] D. L. King, W. E. Boyson and J. A. Kratochvill, "Photovoltaic Array Performance Model," Sandia National Laboratories, California, USA, 2004.
- [84] D. L. King, J. A. Kratochvil and W. E. Boyson, "Measuring solar spectrum and angle-of-incidence effects on photovoltaic modules and solar irradiance sensors," in *IEEE Photovoltaic Specialists Conference*, California, USA, 1997.
- [85] D. L. King, J. A. Kratochvil and W. E. Boyson, "Temperature coefficients for PV modules and arrays: measurement methods difficulties, and results," in *IEEE Photovoltaic Specialists Conference (PVSC)*, Anaheim, CA, USA, 1997.
- [86] B. Knisley, "Validation of draft international electrotechnical commission 61853-2 standard: Angle of incidence effect on photovoltaic modules," Solar America Board for Codes and Standards (Solar ABCs), 2013.
- [87] A. F. Souka and H. H. Safwat, "Optimum Orientations for the Double-Exposure, Flat-Plate Collector and Reflectors," *Solar Energy*, vol. 10, pp. 170-174, 1966.
- [88] W. De Soto, S. A. Klein and W. A. Beckman, "Improvement and validation of a model for photovoltaic array performance," *Solar Energy*, vol. 80, no. 1, pp. 78-88, 2006.

- [89] A. S. Shikoh, T. R. Betts, S. R. Williams, R. Gottschalg, D. Neumann, M. O. Prast and W. A. Nositchka, "Representation of optical losses in PV system yields estimates," in *27th European Photovoltaic Solar Energy Conference and Exhibition*, Frankfurt, 2012.
- [90] N. Martin and J. M. Ruiz, "A new model for PV modules angular losses under field conditions," *International Journal of Solar Energy*, vol. 22, no. 1, pp. 19-31, Jan. 2002.
- [91] G. Nofuentes, J. de la Casa, M. Torres-Ramirez and M. Alonso-Abella, "Solar Spectral and Module Temperature Influence on the Outdoor Performance of Thin Film PV Modules Deployed on a Sunny Inland Site," *International Journal of Photoenergy*, vol. 2013, pp. 1-12, 2013.
- [92] J. J. Michalsky, L. C. Harrison and W. E. Berkheiser, "Cosine response characteristic of some radiometric and photometric sensors," *Solar Energy*, vol. 54, no. 6, pp. 397-402, 1995.
- [93] M. Bui, C. Voelker, B. Li and D. M. J. Doble, "Oblique angle of incidence measurement of PV modules on a solar simulator," in *26th European Photovoltaic Solar Energy Conference and Exhibition*, Hamburg, 2011.
- [94] D. Olivier, R. Vaillon and M. Green, "Temperature Coefficients of Photovoltaic Devices," in *Thermal Behavior of Photovoltaic Devices*, Cham, Springer International Publishing, 2017, pp. 29-70.
- [95] Sandia National Laboratories, "PV Performance - Modelling Collaborative," [Online]. Available: <https://pvpmc.sandia.gov/modeling-steps/1-weather-design-inputs/array-orientation/two-axis-tracking/>. [Accessed 2017].
- [96] W. Herrmann, L. Rimmelpacher and M. Reuter, "Optical Characteristics of PV Module Front Glasses - Incidence Angle Effect of Various Glass Types and Impact of Annual Energy Yield," in *28th European Photovoltaic Solar Energy Conference and Exhibition*, Paris, 2013.
- [97] M. Shields, "PV Systems: Low Levels of Glare and Reflectance vs. Surrounding Environment," Sunpower, 2010.

- [98] S. Guo, T. M. Walsh, A. G. Aberle and M. Peters, "Analysing partial shading of PV modules by circuit modelling," in *Photovoltaic Specialists Conference (PVSC), 2012 38th IEEE*, Texas, USA, 2012.
- [99] D. Passias and B. Kallback, "Shading effects in rows of solar cell panels," *Solar Cells*, vol. 11, pp. 281-291, 1984.
- [100] H. Saha, S. K. Datta, K. Mukhopadhyay, S. Banerjee and M. K. Mukherjee, "Influence of surface texturization on the light trapping and spectral response of silicon solar cells," *IEEE Transaction on Electron Devices*, vol. 39, no. 5, pp. 1100-1107, May 1992.
- [101] P. Campbell and M. A. Green, "Light trapping properties of pyramidally textured surfaces," *Journal of Applied Physics*, vol. 62, no. 1, pp. 243-249, 1987.
- [102] I. Geisemeyer, N. Tucher, B. Muller, H. Steinkemper, J. Hohl-Ebinger, M. C. Schubert and W. Warta, "Angle Dependence of Solar Cells and Modules: The Role of Cell Texturisation," *IEEE Journal of Photovoltaics*, vol. 7, pp. 19-24, January 2017.
- [103] F. Plag, I. Kroger, T. Fey, F. Witt and S. Winter, "Angular-dependent spectral responsivity - Traceable measurements on optical losses in PV devices," *Progress in Photovoltaics: Research and Applications*, Nov. 2017.
- [104] P. K. Nayak, G. Garcia-Belmonte, A. Kahn, J. Bisquert and D. Cahen, "Photovoltaic efficiency limits and material disorder," *Energy Environ. Sci.*, vol. 5, no. 6022, 2012.